

NASA CR 51009

N63 21350

CODE-1

Space Programs Summary No. 37-22, Volume III

for the period May 1, 1963 to June 30, 1963

618 *The Deep Space Instrumentation Facility*

OTS PRICE

XEROX	\$	<u>660 pl.</u>
MICROFILM	\$	<u>2.03 mf.</u>

jpl

JET PROPULSION LABORATORY
CALIFORNIA INSTITUTE OF TECHNOLOGY
PASADENA, CALIFORNIA

July 31, 1963

Space Programs Summary No. 37-22, Volume III

for the period May 1, 1963 to June 30, 1963

The Deep Space Instrumentation Facility

C.A. JET PROPULSION LABORATORY
CALIFORNIA INSTITUTE OF TECHNOLOGY
PASADENA, CALIFORNIA

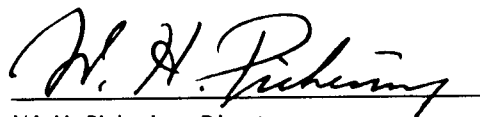
July 31, 1963

Preface

The *Space Programs Summary* is a six volume, bimonthly publication designed to report on JPL space exploration programs, and related supporting research and advanced development projects. The subtitles of all volumes of the *Space Programs Summary* are:

- Vol. I. The Lunar Program (Confidential)
- Vol. II. The Planetary-Interplanetary Program (Confidential)
- Vol. III. The Deep Space Instrumentation Facility (Unclassified)
- Vol. IV. Supporting Research and Advanced Development (Unclassified)
- Vol. V. Supporting Research and Advanced Development (Confidential)
- Vol. VI. Space Exploration Programs and Space Sciences (Unclassified)

The *Space Programs Summary*, Volume VI is an unclassified digest of appropriate material from Volumes I through V, plus the space science instrumentation studies of the JPL Space Sciences Division.



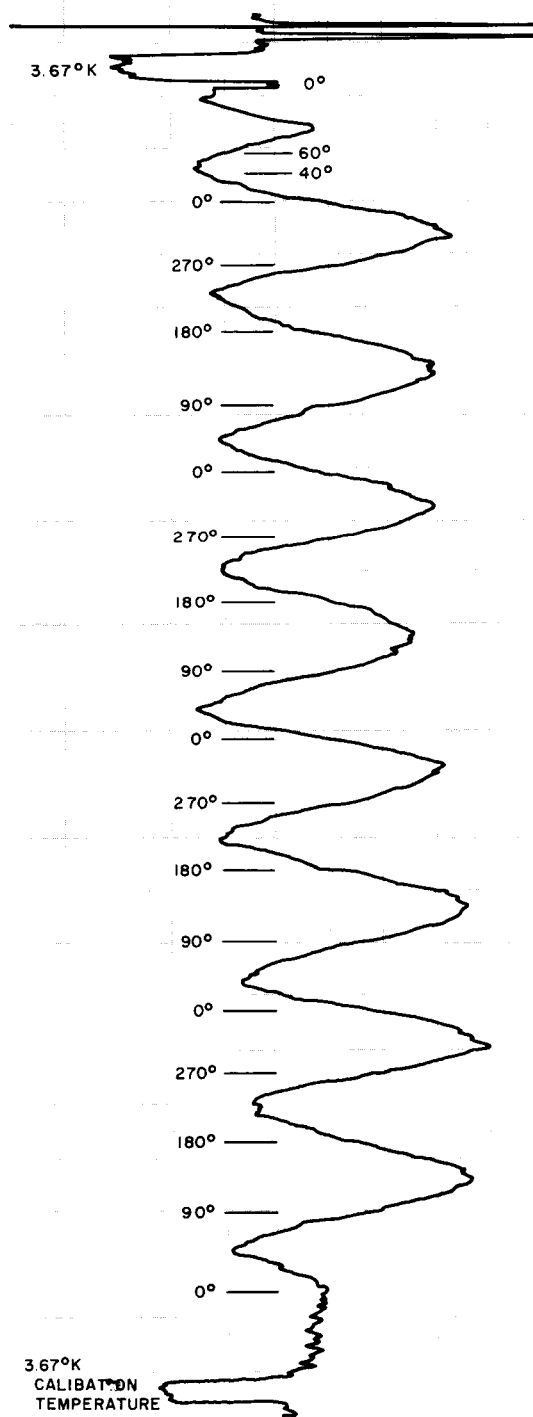
W. H. Pickering, Director
Jet Propulsion Laboratory

Space Programs Summary No. 37-22, Volume III

Copyright © 1963, Jet Propulsion Laboratory, California Institute of Technology
Prepared under Contract No. NAS 7-100, National Aeronautics & Space Administration

Contents

I. Résumé	1
II. Engineering Development	4
A. S-Band Cassegrain Diplexer and Associated Filters	4
B. Mark I Ranging Subsystem	5
C. Modified Scientific-Atlanta Pattern Recorder	6
D. Remote Control Digital Positioning System	7
E. S-Band Communication Component	7
III. Research and Development	10
A. Experimental Low-Noise System	10
B. Ground Antennas	11
C. Planetary Radar	17
D. Ranging System Development	31
E. Data Signals Discrimination	43
References	48
IV. Advanced Antenna System	49
A. Synopsis	49
B. Supporting Studies	49
References	57



— 00 56 30 UT

— STOP, BACK TO 0°

POLARIZATION ANGLE = 132°
MEASURED CLOCKWISE
FROM ANTENNA VERTICAL

PEAK-TO-PEAK TEMPERATURE $\approx 6.2^\circ$

— 00 53 00 UT

— ANTENNA POSITION
277.54° AZIMUTH
29.20° ELEVATION

CRAB NEBULA

ANTENNA TEMPERATURE VS POLARIZATION MEASURED
ON JUNE 8, 1963 WITH 85-ft ANTENNA
AT THE GOLDSTONE VENUS SITE

— START POLARIZATION
ROTATION

3.67°K
CALIBRATION
TEMPERATURE

I. Résumé

The DSIF is a precision tracking and data acquisition network which is designed to track, command, and receive data from deep space probes. It utilizes large antennas, low-noise phase-lock receiving systems, and high-power transmitters at stations positioned approximately 120° around the Earth. Its policy is to continuously conduct research and development of new components and systems and to engineer them into the DSIF so as to continually maintain a state-of-the-art capability.

Engineering developments. Two prototypes of the S-band Cassegrain diplexer and associated filters have been tested. From tests of these units it is expected that production diplexers will have a loss of 0.07 db, a VSWR of 1.05 or less, and better than 85-db rejection of 2113 Mc. The transmitter filter is a five-section band reject filter tuned to 2295 Mc. It has over 100-db rejection, and an insertion loss of 0.016 db and a VSWR of 1.04 at 2113 Mc. The receiver filter has two sections, each providing over 60-db rejection at 2113 Mc.

The Mark I ranging subsystem includes, besides units which have been described previously, a range tally, a readout register, and an output buffer. The range tally stores the current range number in a 31-bit circulating register consisting of a delay line and three binary adders-subtractors. The latter three units add algebraically the range numbers corresponding to changes made in the Chinese-number adder, doppler-number adder, and the modulo-number adder. Periodically, on demand from the data handling system, the contents of the tally are fed into the readout register, which in turn sets the relays of the output buffer.

A Scientific-Atlanta pen recorder has been modified to accept signals directly from a standard DSIF receiver so that a transponder can be used as the RF source when making antenna pattern measurements.

A digital remote control system has been installed at the Goldstone Echo Station to vary attenuation and polarization of the transponder on the collimation tower.

Signal transmission may be done by wire or radio with positioning accuracies of $\pm 0.1^\circ$ on the attenuator and $\pm 1.0^\circ$ in polarization.

Low-noise systems. The development of a traveling wave maser for the DSIF is essentially complete with all specifications being met except that of noise temperature. However, the approach to be taken in a future program to reduce the noise temperature is understood. Pertinent performance specifications are noise temperature $16 \pm 2^\circ\text{K}$, gain 30 ± 1 db, and 1-db bandwidth 11 Mc. The closed cycle refrigerator was found to be satisfactory for field operation.

Ground antennas. The servo system on the 30-foot antenna at the Goldstone Venus site is still under test. As installed, the minimum tracking rate is $0.10^\circ/\text{sec}$. This is too high for pattern measurement work and a temporary modification, including servo valves, has been installed which reduces this rate to less than $0.004^\circ/\text{sec}$.

The Mount Tiefert S-band antenna range was successfully used to make antenna pattern measurements of the 85-ft Az-El antenna at the Goldstone Venus site. A standard horn antenna whose gain had been carefully measured by two independent methods was used on Mount Tiefert. The gain of the 85-ft antenna was found to be 54.01 ± 0.15 db at 2388 Mc. The measurements indicate that the Mount Tiefert range is essentially free of multipath problems and that the 85-ft antenna is mechanically unsymmetrical between elevation and azimuth when pointing toward the horizon.

The transportable instrumentation system which is being built to measure the structural and mechanical properties of large ground antennas will be capable of automatically scanning and recording the outputs of 12 extensometers, 12 wire span resistances, 12 strain gages, and 50 thermocouples. It is nearly completed.

Planetary radar. Following reinstallation of the 100-kw amplifier after rework a high back power of 1.05% was encountered. This was reduced to its former value of 0.32% by tuning the waveguide adjacent to the klystron. False crowbar actions are being triggered by noise pulses. An effort will be made to cure this by shielding. The high-voltage rectifier tubes have developed an increasing number of internal arcs. The manufacturer is attempting to cure this, but meanwhile tubes from another source are being tested. The noise power from the klystron with no drive and varying beam voltages was measured.

Tests on the Mod IV radar receiver continue. A thermal test was made to determine the liquid coolant requirements. Closed-loop frequency response tests of the 31.44-Mc, 30.455-Mc, and the 500-kc loops were made which in general agree with the calculated figures. Two anomalies will require further investigation. Harmonic and spurious output levels and reference oscillator stability measurements were made which indicate satisfactory operation.

A linear voltage controlled oscillator using solid-state components and frequency feedback has been developed which is significantly better than the old vacuum tube VCO's. The stability is about 4 times better and the linearity and phase noise are about $\frac{1}{3}$ that of a compensated vacuum tube VCO.

In order to partially automate the technique of using astronomical radio sources for boresight and gain calibrations of 85-ft antennas, a sequencer has been developed, which can record pertinent data in a format which is compatible with the Model 1620 digital computer. The station data handling equipment is used to generate the punched paper tape and printer output with the normal locations of the doppler data being used for the digital reading of the output of the Dicke radiometer. The computer program for reducing the data is nearly complete.

In order to use astronomical radio sources for antenna calibrations, it is necessary to know the noise temperature and polarization characteristics of these sources. Careful measurements of source intensities and polarizations have been made on 14 sources including the Moon and the Sun. The first results of this data show that the Crab Nebula should be very useful since it has relatively high intensity, is small in diameter, and is only slightly polarized. The Moon, Sagittarius, and NGC 5128 are not so useful because of their large diameters.

The new design of a water rotary joint appears to be satisfactory. Dynamic and life testing at JPL will be conducted as soon as the vendor completes one unit.

Ranging system development. The stored program controller in the Mod II ranging equipment now has all the capabilities necessary for completely automatic control of ranging operations. It has many of the characteristics of a small general purpose computer. Capabilities which have been added recently include the arithmetic operations of shift, multiply and divide, the control function of program interrupt and a printer and paper tape punch as peripheral equipment. A total of 18 test program routines have been written which will determine

the operational capability of the stored program controller. Additional programs will be written which will make it possible to test all parts of the machine.

Acquisition of a telemetry modulated RF carrier by a phase lock receiver is generally susceptible to spurious sideband locking effects. A subsystem capable of discriminating against virtually any type of modulation which is suitable for modulation of a tracked carrier has been developed and subjected to preliminary tests. Primary limitations of the discriminator are: (1) signal strength must be somewhat above predetection threshold and (2) the fundamental frequency of any subcarrier must exceed the loop-bandwidth but not exceed the predetection bandwidth.

Data signal discriminator. In order to test the performance of a detection system where a data signal is mixed with white gaussian noise a mixing system has been designed, constructed, and tested. It is linear over a wide range of signal and noise levels and has a frequency response of ± 0.1 db from 10 cps to 100 kc.

Advanced Antenna System. A contract for the final design, fabrication, and erection of a 210-ft parabolic antenna at Goldstone has been executed with the Rohr Corporation of Chula Vista, California.

Three sample tests for evaluating the STAIR computer program, for computing the position of a best fit paraboloid, have been made. The program was used to calculate an idealized structure for an 85-ft polar mount antenna. RF ray tracing shows that deflection of the feed horn is required to minimize the RF boresight error in elevation.

Fair correlation was found between a digital and an analog analysis of a hydrostatic bearing system with constant oil film height and varying grid spacing and truncation constants. It appears necessary to increase the computer iterations from 300 to 1000 to improve this correlation. It is also planned to modify the program to include the effect of velocity on the pressure pattern.

II. Engineering Development

A. S-Band Cassegrain Diplexer and Associated Filters

A prototype S-band Cassegrain diplexer (SCD) and its associated filters have been developed by Rantec Corporation to JPL specifications and have been delivered for initial high-power diplexing tests. Background information on the S-band diplexer and filter development program was given in *SPS 37-17*, Vol. III.

The SCD is shown in Fig. 1. It is not of radical construction, but the detail design work has been conducted with great care to achieve the lowest possible insertion losses. The SCD consists of two 3-db sidewall couplers connected by 2200-Mc cutoff waveguide sections, with transitions from dual waveguide to WR-430 flanges on each end. The couplers are especially designed to provide good balance and very low VSWR, and the cutoff sections incorporate tuning elements to reduce internal mismatch.

The first prototype delivered was not perfectly matched, and consequently had a rather high loss of 0.13 db at

2295 ± 5 Mc. However, the second prototype has a loss of only 0.09 db, and production units using extruded waveguide sections may better the design goal of 0.07 db (equivalent to 5°K excess noise temperature). The 2295 ± 5 Mc VSWR is 1.05 or less over the full band.

The SCD rejection at 2113 ± 5 Mc exceeds 85 db. The transmitter-to-antenna insertion loss is 0.010 db, and the VSWR does not exceed 1.04 over the bandwidth. In operational use, the SCD will carry 10 kw of transmitter power.

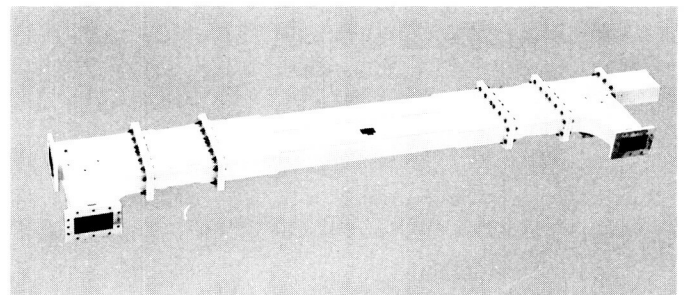


Fig. 1. A prototype S-band Cassegrain diplexer

a. S-band transmitter filter. Shown in Fig. 2 is the S-band transmitter filter (STF) which, used in conjunction with the SCD, eliminates klystron beam noise. (See *SPS 37-20*, Vol. III, for a discussion of diplexing noise problems at L-band.) The STF is a five-section, band-reject filter tuned to 2295 Mc. It provides in excess of 100-db rejection over the receiver band, with an insertion loss of 0.016 db and VSWR of 1.04 at 2113 Mc.

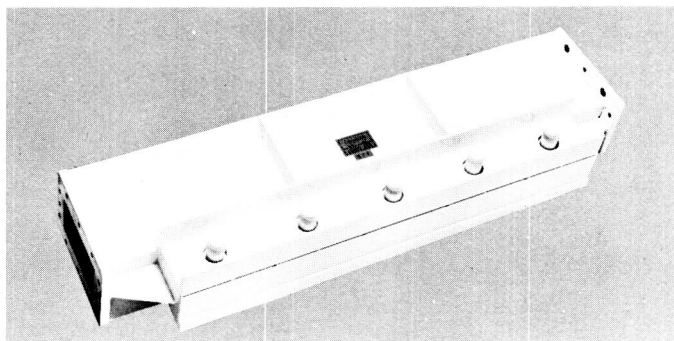


Fig. 2. S-band transmitter filter

b. S-band receiver filter. Filtering of the transmitter signal in each of the error channels of the microwave system is provided by an S-band receiver filter (SRF), one of which is shown in Fig. 3. It is comprised of two sections of 2200-Mc cutoff waveguide, each providing over 60-db rejection at 2113 ± 5 Mc.

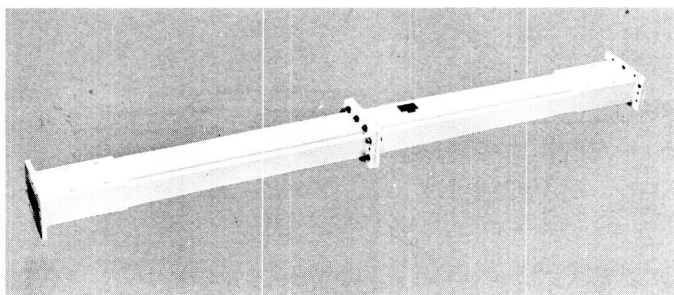


Fig. 3. S-band receiver filter

B. Mark I Ranging Subsystem

The Mark I ranging subsystem is being designed and built to equip the DSIF with the capability of ranging

on passive satellites and spacecraft "turnaround" transponders to distances of 800,000 km. A summary of the basic theory of operation and a brief over-all description were given in *SPS 37-20*, Vol. III, pp. 12-15. In *SPS 37-21*, Vol. III, pp. 16-18, a detailed account was given of the design and operation of four of its functional units: transmitter coder, receiver coder, Chinese number generator, and timer. In this summary the design and operation of three more of the subsystem functional units are described.

1. Range Tally

From the user's viewpoint the range tally may be considered the heart of the ranging subsystem, since it is in this unit that the output information is synthesized. The range tally stores the current range number in series-binary form in a $31\text{-}\mu\text{sec}$, 31-bit circulating register, consisting of a magnetostrictive delay line and three binary adders-subtractors which, for brevity, will simply be called adders. The three sequential adders add algebraically the range numbers corresponding to the indicated changes in range or corrections as follows.

a. Chinese-number adder. This adds the equivalent of the appropriate Chinese number each time a 1-bit shift is made of a receiver-code component with respect to its transmitter-code component counterpart. (See also "Chinese-number generator," *SPS 37-21*, Vol. III, pp. 17-18.) This adder is used only during ranging code acquisition.

b. Doppler-number adder. This adds the equivalent of the appropriate doppler cycle incremental count as it occurs, viz., $\frac{1}{4}$ -cycle increments of "clock" doppler or $\frac{1}{2}$ -cycle increments of "rf" doppler, depending on the system's mode of operation.

c. Modulo-number adder. The greatest range number required of the ranging subsystem is that corresponding to the maximum unambiguous range which, in turn, is given by the product of the four code component lengths in bits. This "modulo" number is permanently available as an output of the Chinese-number generator. Whenever the accumulated range number exceeds the "modulo" number, the latter is subtracted from the accumulated range number total. Likewise, whenever the range number goes negative, a "modulo" number is added. These functions are performed in the modulo-number adder. The range tally is cleared, i.e., reset to zero, when the transmitter and receiver coders are synchronized, under program control.

2. Readout Register

The readout register is a static shift register consisting of 31 flip-flops. Once per second a readout command pulse is received from the data handling system. This is translated into a 31- μ sec gate which, in turn, causes the range number currently circulating in the range tally storage to feed into and fill the readout register. The contents of the register remain static until the next readout command.

3. Output Buffer

The output buffer consists of relays which are controlled by the ranging subsystem and which are sensed by other subsystems, specifically the RF receiver and the data handling subsystems. The former group of relays (not shown in Fig. 4) perform various operational and interlock functions. The latter group are the data output relays, which are driven, one-for-one, by the flip-flops of the readout register. Their configuration can then be

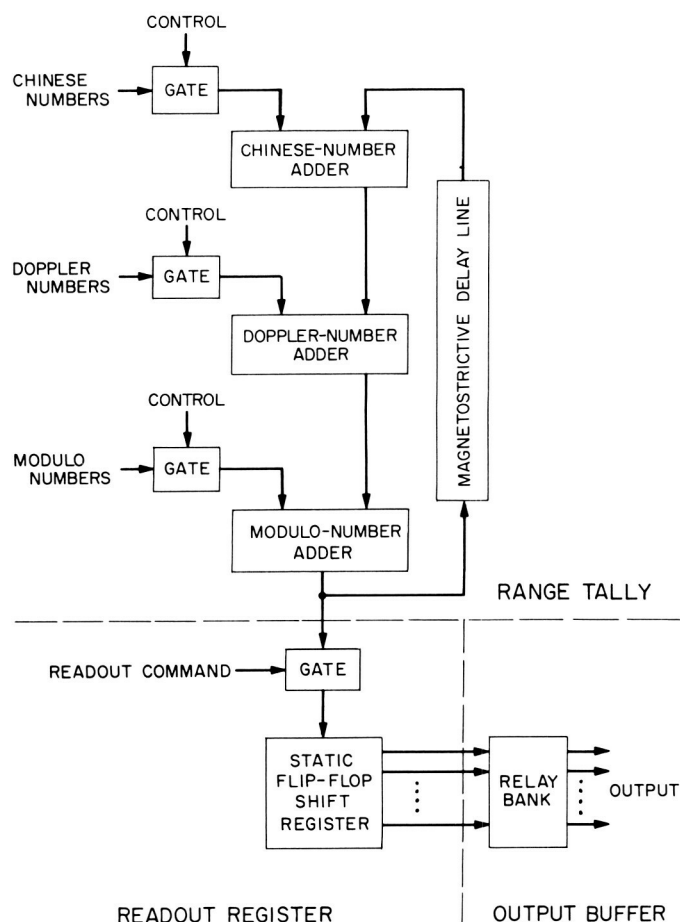


Fig. 4. Portion of DSIF Mark I ranging subsystem block diagram

sampled by the data handling system at intervals of one or more integral seconds. The output is thus in range units in binary (or octal) form, from which it may be converted into decimal measures of time or distance.

C. Modified Scientific-Atlanta Pattern Recorder

A modified standard recorder (Fig. 5), purchased from the Scientific-Atlanta Corp., Atlanta, Georgia, was performance tested at the Goldstone Echo site and was found quite satisfactory. The recorder makes strip chart recordings of antenna signal strength variations to show the electromagnetic radiation pattern characteristics of the antenna.

The modification consists of a series of transistors substituted for the bolometer amplifier and pen function amplifier of the standard recorder. Designed as a plug-in module, the transistor package readily converts the standard recorder to the special recorder. The transistor chain is aligned so that the transistors fire one at a time at various voltage levels to linearize the AGC voltage output

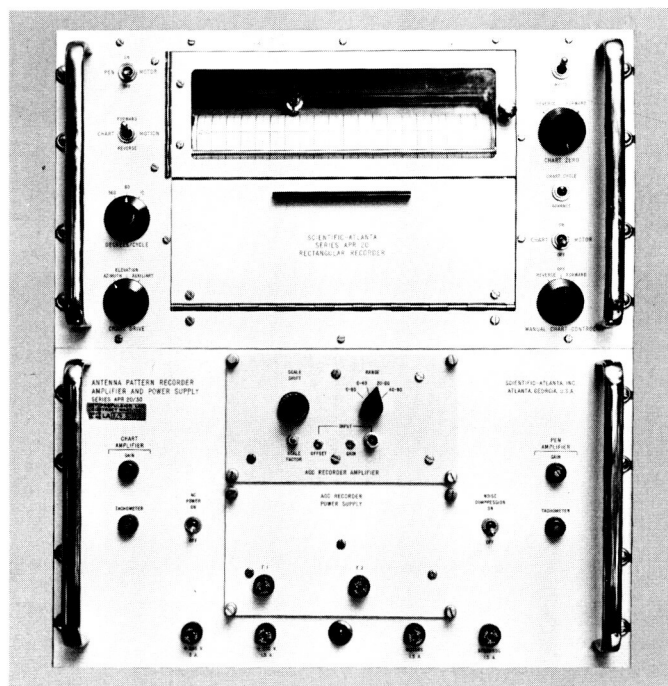


Fig. 5. Modified Scientific-Atlanta recorder

of a DSIF receiver. The linearized voltage is then fed to a standard log periodic pattern recorder.

The modified recorder offers these advantages:

- (1) The transponder is used as the RF signal source in lieu of the 5- to 10-w signal source previously required.
- (2) The full dynamic range of the receiver is made available for pattern recordings.
- (3) The receiver circuitry is not disturbed to take a pattern.
- (4) Set-up time to take a pattern is reduced from 2 days to less than 4 hr.

Purchase orders for six additional recorders have been written for distribution as a GSDS item throughout the DSIF.

D. Remote Control Digital Positioning System

A digital system for remote control positioning of the transponder attenuator and polarization of the collimation tower antenna, from the receiver station (Fig. 6) of the control room, has been designed, purchased, and installed at the Goldstone Echo collimation tower and control room. This system is capable of setting the transponder attenuator to an accuracy of $\pm 0.1^\circ$ and polarization of the antenna to an accuracy of $\pm 1.0^\circ$.

No sacrifice in the adjustment range of transponder attenuation or antenna polarization has resulted by the introduction of this remote control system. Seven on-off toggle switches are provided for future remote control applications. Since the system is designed for pulse encoded operation, the transmission path between transmitter and receiver may be either a single pair of wires or a microwave link.

Several advantages offered by the system are:

- (1) Improved calibration accuracy.
- (2) Elimination of the need for good roads to the collimation tower.
- (3) Elimination of collimation tower operators.

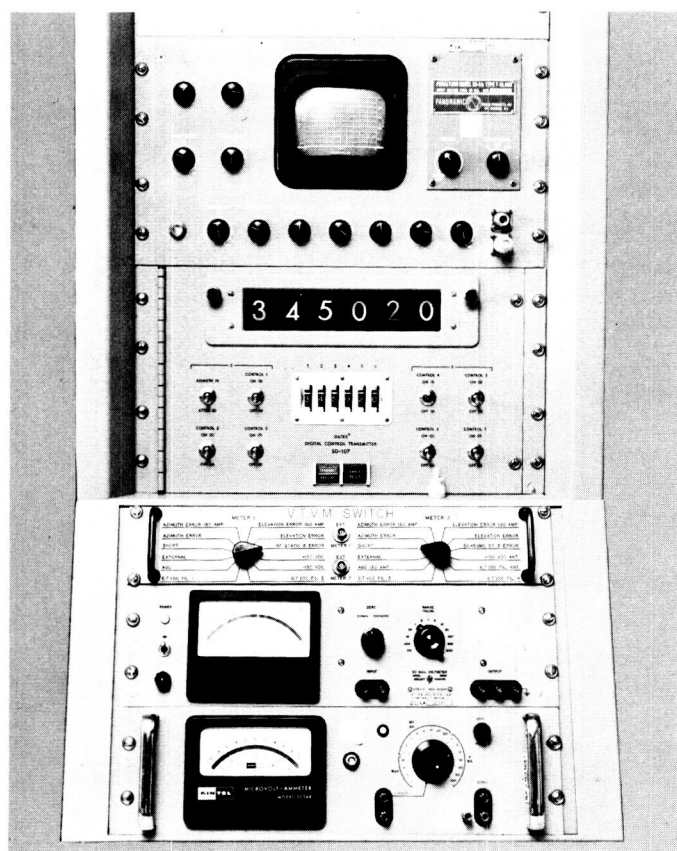


Fig. 6. Remote control positioning system transmitter

E. S-Band Communication Component

1. 5/221 Parametric Frequency Divider

The phase coherent 498-kc signal for synchronizing the range code generator, in the S-band ground system, is derived by multiplying the 22-Mc signal from the transmitter by the ratio of 5/221. In previous systems, a phase-locked-loop frequency shifter was used satisfactorily to perform this multiplication function. The limitation of a phase-locked loop is primarily its inherent narrow frequency tracking range of approximately $\pm 0.005\%$. This narrow range is due to the quartz crystal characteristics used within the automatic phase control (APC) loop. To extend the tracking range of the phase-locked-loop frequency shifter, it is necessary to change crystals and circuit elements within the VCO circuit. The assignment of several S-band frequencies, over a 10-Mc band, requires that the shifter track frequency changes of approximately $\pm 0.25\%$.

To eliminate the limitations and complexities of a phase-locked loop for deriving the range code synchronizing (clock) frequency, a circuit was developed which utilizes the nonlinear capacitance characteristics of varactors to perform the desired frequency division. The capability of capacitive (parametric) diodes to generate coherent subharmonics of the drive frequency is used extensively within the frequency divider, eliminating the necessity of using VCO circuits and APC loops.

Basically, the $5/221$ unit consists of two parametric frequency dividing circuits in tandem. The first provides an output which is $1/17$ of the 22-Mc input frequency. The second, a divide-by-13, provides an output which is $1/221$ of the 22-Mc input frequency. This signal is then multiplied by five to provide a coherent $5/221$ output. The output of each divider is also utilized in the coherent doppler chain. The block diagram shown in Fig. 7 indicates the relative position of the $5/221$ frequency divider within the RF system.

The schematic diagram of the frequency divider is shown in Fig. 8. The 22-Mc input from the transmitter VCO is applied to an amplitude limiting amplifier (Q1) whose output power is essentially constant for power input variations from +5 to +15 dbm. The output of the limiter drives a second amplifier (Q2) in a common base configuration to facilitate matching into the parametric divider circuit. The input to the divider is parallel tuned to 22 Mc; the output is tuned to the 17th subharmonic. An MA-450A varactor (D1) is used as the parametric diode in the first divider because of its comparatively low capacitance and high Q at 22 Mc. The output of the divide-by-17 is coupled to two 1.294-Mc amplifiers. One amplifier (Q3) provides a $13/221$ output which is used as one of the signals in the S-band doppler system. The other 1.294-Mc amplifier (Q4) drives a parametric divide-by-13 circuit. Because of the low input and output frequencies of the divide-by-13 circuit, a relatively high-value capacitive diode (PC 137) is used. To ensure lock range over temperature, it is necessary to parallel this diode with a

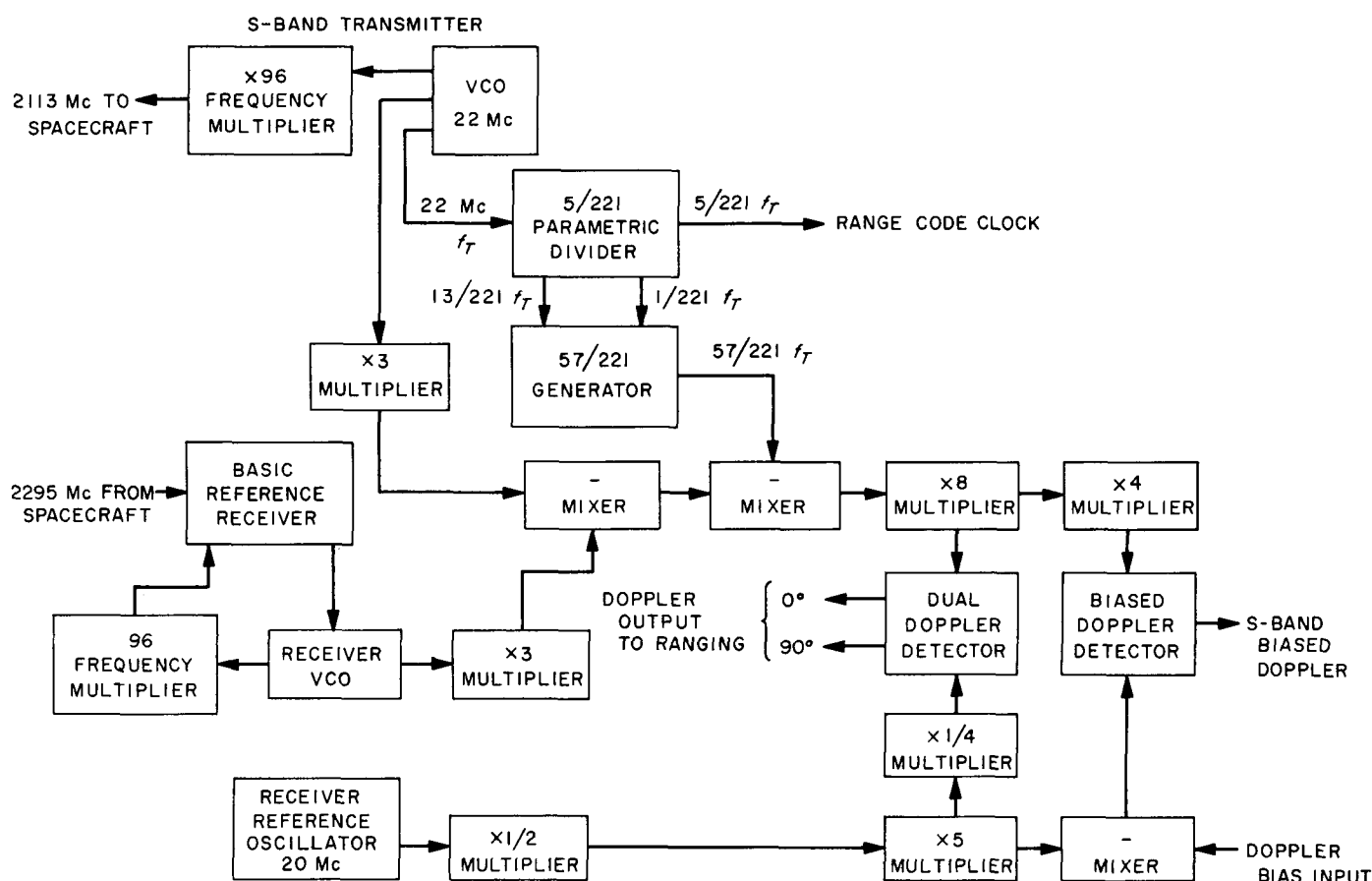


Fig. 7. Coherent range clock and RF doppler system

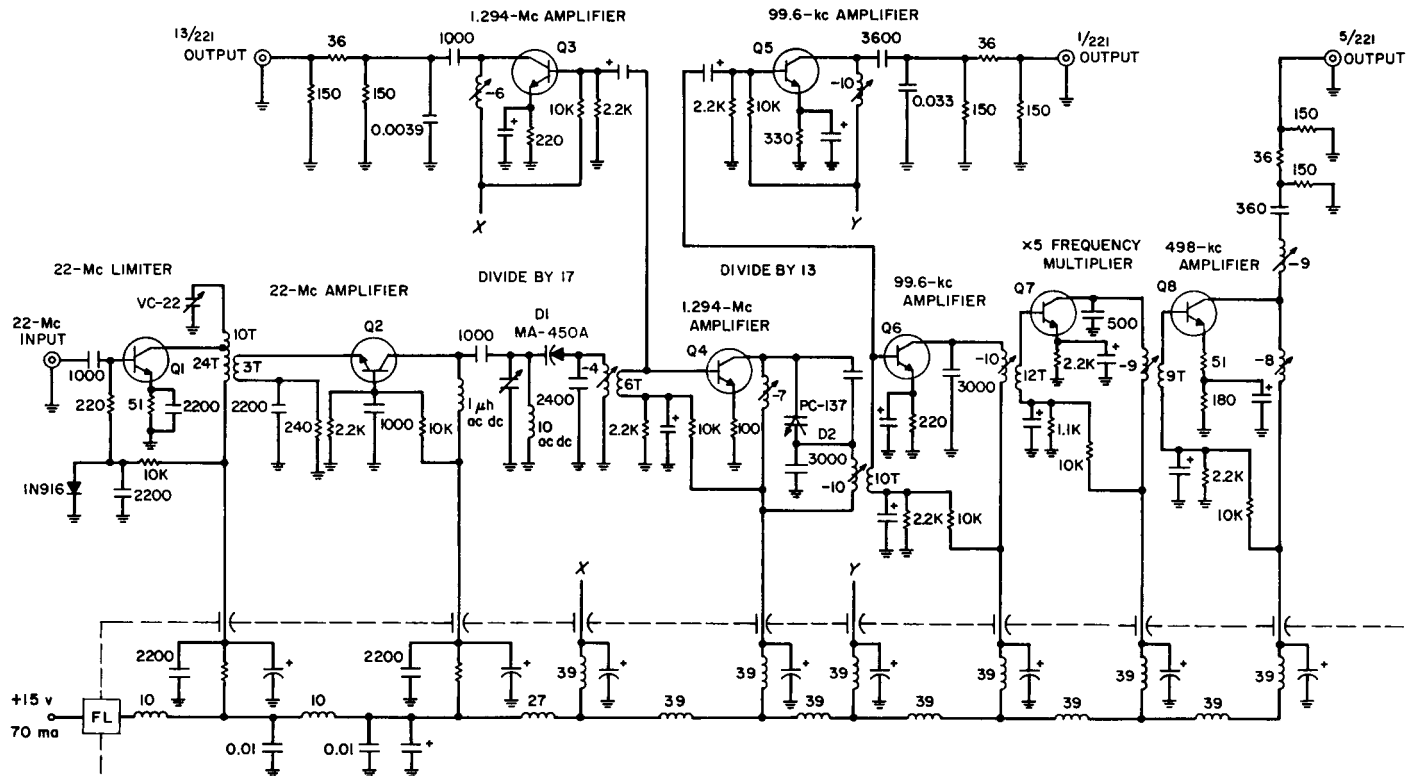


Fig. 8. 5/221 parametric frequency divider

negative temperature compensating capacitor. The 99.6-kc output from the second divider also couples to two amplifiers. One amplifier (Q5) provides a 1/221 output which also forms part of the S-band doppler chain. The second amplifier (Q6) amplifies the 99.6 kc sufficiently to drive a $\times 5$ frequency multiplier (Q7). The 498 kc at the output of the frequency multiplier is amplified by Q8. The amplifier output is 5/221 times the 22-Mc input frequency and serves as the coherent clock signal.

Unlike the phase-locked loop, the parametric frequency divider can provide coherent lock ranges in excess of $\pm 1\%$,

thereby eliminating the necessity for making circuit or system alterations when a frequency change is executed.

Measurements indicate the phase stability of the parametric frequency divider to be similar to that of a phase-locked loop. Fig. 9 shows the resultant phase noise produced at the output of a 498-kc phase detector when two parametric divider outputs are compared. Fig. 10 shows the resultant phase noise when a parametric divider is compared with a phase-locked loop. In each case the peak-to-peak phase jitter is approximately 0.085 deg.

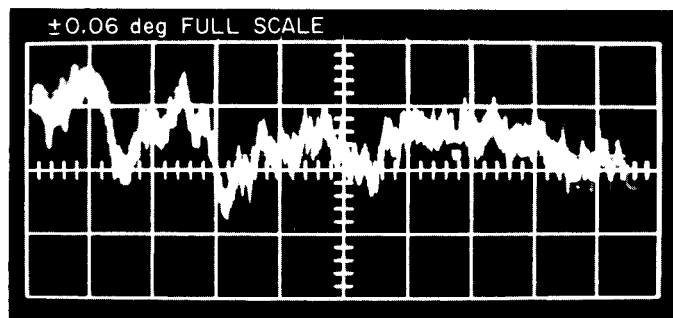


Fig. 9. Phase jitter at phase detector output: two parametric dividers compared

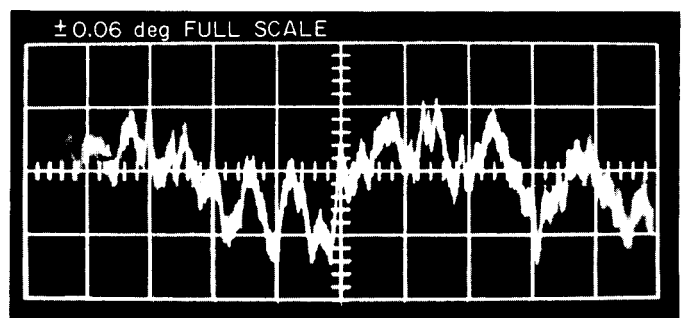


Fig. 10. Phase jitter at phase detector output: parametric divider compared with a phase-locked loop

III. Research and Development

A. Experimental Low-Noise System

1. TWM for DSIF

The development of a prototype S-band traveling wave maser (TWM) for the DSIF has been essentially completed. This report summarizes the performance specifications for the system.

Nearly all of the technical requirements of JPL Specifications 8007A for a prototype 2295/2388-Mc TWM have

been met. Although the noise temperature of the TWM has been found to be somewhat higher than desired (13°K instead of 8°K), a plausible explanation has been given (SPS 37-21, Vol. III). The approach to be taken in a future program to reduce the noise temperature is understood.

Table 1 summarizes the specifications for a 2295-Mc TWM system. All values have been ascertained as realizable.

Table 1. TWM performance table

Item	Description	Specification	Item	Description	Specification
1	TWM system noise temperature (CCR at 4.3°K) at 2295 Mc at input W/G	$16 \pm 2^\circ\text{K}$	6	VSWR, maser output at 2295 Mc	< 1.5
2	Gain (CCR at 4.3°K) at 2295 Mc	$30.0 \pm 1.0 \text{ db}$	7	Maser forward loss	27 db
3	Maser bandwidth 1 db at 2295 Mc 3 db at 2295 Mc	11 Mc 15 Mc	8	Maser reverse loss	$> 80 \text{ db}$
4	System gain stability (with open-loop klystron pump) For 12 hr For 10 min For 10 sec	$\pm 0.3 \text{ db}$ $\pm 0.05 \text{ db}$ $< \pm 0.02 \text{ db}$	9	Pump power required	75 mw
5	VSWR, maser input at 2295 Mc	< 1.5	10	Magnet trim current	300 ma (max)
			11	Monitor receiver gain stability 10 sec 10 min 12 hr	$< \pm 0.05 \text{ db}$ $< \pm 0.2 \text{ db}$ $< \pm 1.0 \text{ db}$
			12	Monitor receiver Predetection 3-db bandwidth	4.5 Mc
			13	Receiver noise figure	8.0 db
			14	Time required for system off and warm to in-spec operation (with precooling)	6½ hr

The closed cycle refrigerator has been found to be satisfactory for field operation. After 2,000 hr of operation, the crosshead assembly was overhauled; the compressor appears to be completely satisfactory.

It may be concluded that fieldworthy S-band TWM's for the DSIF antennas are feasible.

B. Ground Antennas

1. 30-Ft Diameter Azimuth-Elevation Antenna

a. Servo test.

Introduction. In SPS 37-21, Vol. III, the data reduction of the dynamic testing was discussed. The reduction of the open-loop resonant data is continuing; the transfer function data has been abandoned.

b. Discussion. In order to determine which type of data is valid, additional tests were conducted. Comparing the two types of data, reduced to the same common form phase-amplitude versus frequency, it was apparent that if the resonant frequency test were indeed conducted open-loop, the transfer function tests were invalid. A check was made comparing phase-amplitude versus frequency of the input (from a Model 202A variable frequency generator) and the output of the servo valve driver. Runs were made from 0.8 to 40 cps and the data reduced. There was no perceptible change in either phase or amplitude; therefore, it was concluded that the resonant frequency test was conducted open-loop. For this reason, transfer function data is considered invalid and will have to be redone.

When the antenna servo system was first conceived, the prime consideration was for accurate position pointing and tracking. This was to be accomplished through a RF tracking feed or a taped computer program using the high-accuracy encoder-type readout. However, in conducting radiation pattern tests, a smooth manual rate is necessary. From SPS 37-20, Vol. III, p. 30 it may be noted that during acceptance testing the minimum smooth tracking rate in azimuth was 0.10 deg/sec. The elevation rate was somewhat lower, but this improvement is mainly due to the increased gear ratio. The pattern

measurement work, however, required a rate approaching sidereal or below (approx 0.004 deg/sec).

The rate loop system was optimized at the time of the antenna acceptance. The gain of the rate loop greatly depends on the amount of pressure feedback that can be obtained. Pressure gain is based on the hydraulic resonance and the corner frequency of the servo valve. The system as installed had a resonance and corner of approximately 15 cps. The most feasible method of raising this value was to obtain a servo valve that had a higher corner frequency. Because the high velocity is not a requirement for pattern measurement, a small servo valve was installed. The new valve yielded a maximum rate of approximately 2.5 deg/sec but gave a corner frequency of greater than 40 cps. With the new valve installed, the pressure feedback gain was raised approximately 20 times. The resulting increase in rate gain lowered the minimum smooth tracking rate to less than 0.004 deg/sec.

During the testing, it became apparent that additional rate gain could be obtained if the noise level and the quadrature voltage could be reduced. At the present time, the rate system is operating on a threshold of 2 mv with a noise level of approximately 28 mv. Investigations are currently underway to determine methods of obtaining an improvement.

These changes are not considered permanent. The system can be reconverted to its original condition for RF and computer tracking. Conversion kits have been made to allow for this changeover to be accomplished in a few hours.

2. S-Band Antenna Gain and Pattern Calibrations

Introduction. A 2388-Mc gain standard horn antenna has been calibrated to within a probable gain error of 0.1 db. This horn has been used, in conjunction with the Mt. Tiefert remote range, to calibrate the 85-ft Venus site antenna gain at 2388 Mc, resulting in a gain figure of 54.0 ± 0.15 -db probability of error (p.e.) at low elevation angles. Radiation patterns were taken of the antenna, indicating low-angle structural deformation of the antenna in the elevation plane.

a. Standard gain horn calibration. In preparation for 2388-Mc gain tests at Goldstone, a pair of horn antennas was accurately gain calibrated. The two antennas are dual mode conical horns, one of which is identical to that utilized in the 85-ft antenna feed system at the Venus site (SPS 37-17, Vol. III, pp. 16-18); the other antenna is an

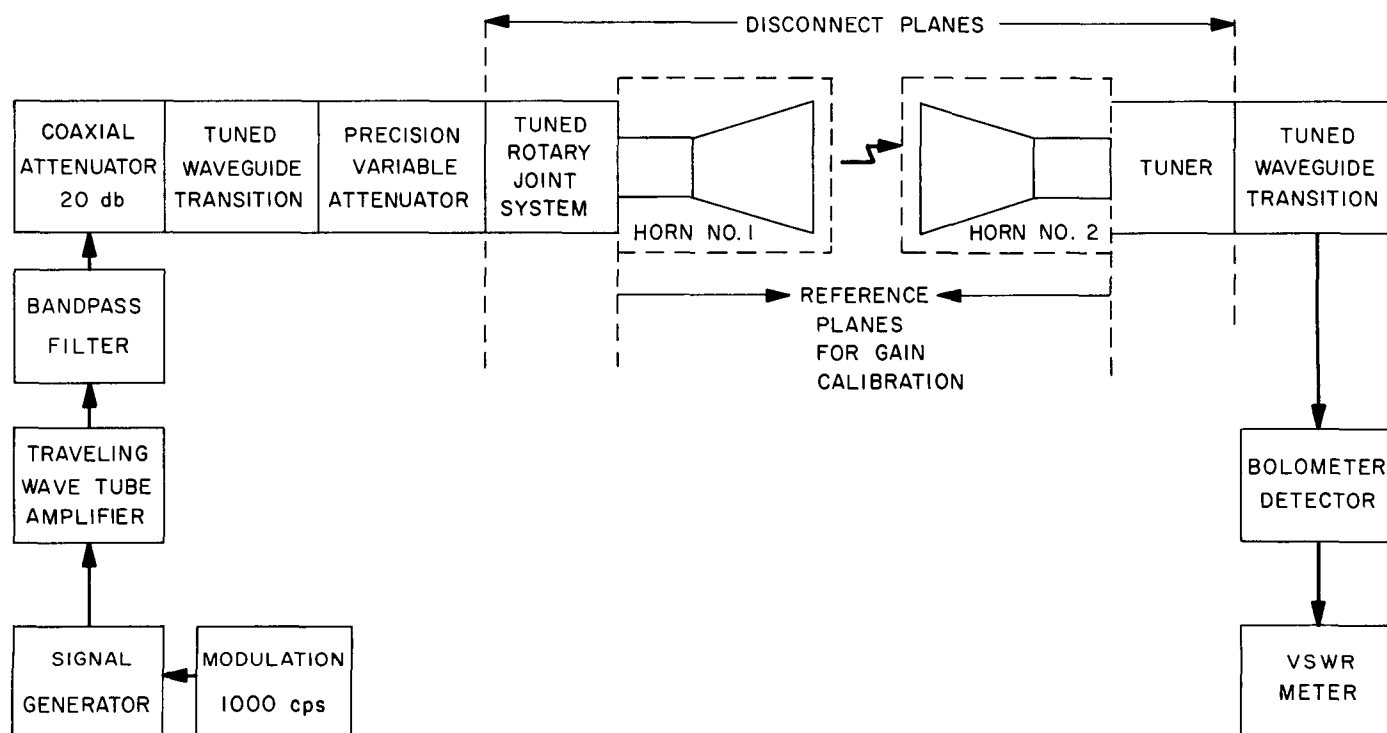


Fig. 1. Block diagram for horn gain calibration

electrically identical sheet metal version of the feed system horn. This type of horn (Ref. 1) is ideal for gain standard applications since it has the desirable properties of (1) very low sidelobes, (2) negligible cross-polarized radiation, (3) a well-defined phase center, close to the aperture, (4) equal beamwidths in all planes, and (5) usability without recalibration for any type of polarization.

Two independent methods were utilized in the gain calibration. In the first method, the conventional two-antenna space loss technique was used; the block diagram for these tests is shown in Fig. 1. Linear polarization was used throughout all tests. Tests were performed as a function of polarization (to check the multipath environ-

ment) and also as a function of horn spacing; the spacing was varied between $3D^2/\lambda$ (three Rayleigh distances) and $6D^2/\lambda$. Braun's correction technique (Ref. 2) was utilized, suitably modified to account for the dual mode horn aperture distribution, in order to predict the true far-field gain. Table 2 shows the measured results as a function of spacing.

Table 2. Horn gain versus spacing

Phase center spacing, ft	Uncorrected gain, db	Correction, db	Corrected gain, db
30	21.88	0.28	22.16
40	21.96	0.20	22.16
50	22.00	0.14	22.14
60	22.11	0.10	22.21
Average: $G_1 = 22.17$ db			

Table 3. Horn gain calibration errors

Space loss method		Pattern integration method	
Error	Estimated magnitude, db	Error	Estimated magnitude, db
Attenuator calibration	0.10	Pattern reading uncertainty	0.10
Spacing correction	0.10	Phase front curvature	0.04
Multipath	0.05	Pattern calibration	Negligible
Antenna interaction	0.05	Center of rotation	Negligible
Equipment instability	0.03	Angular uncertainty	Negligible
Reading uncertainty	0.03	Integration	Negligible
Range measurement	Negligible	Frequency	Negligible
Waveguide insertion loss uncertainty	Negligible	rms total: p.e.2 = 0.11 db	
Mismatch	Negligible		
Frequency	Negligible		
rms total: p.e.1 = 0.16 db			

In the second method of gain calibration, radiation patterns of both horns were made as a function of spacing and these were integrated to determine the horn gain, yielding a value of $G_2 = 21.95$ db for the gain, a discrepancy of 0.22 db between the two methods. An analysis of the possible errors is given in Table 3. The two gain results presented in Table 3 may be regarded as statistically independent measurements of the gain, in the presence of additive noise. Under this assumption, the final result for expected gain must be obtained by weighting according to the individual rms errors. It can be shown that, statistically:

$$G_H = \frac{(p.e._2)^2 G_1 + (p.e._1)^2 G_2}{(p.e._1)^2 + (p.e._2)^2} \pm \left\{ \frac{(p.e._1)(p.e._2)}{[(p.e._1)^2 + (p.e._2)^2]^{1/2}} \right\} p.e. \quad (1)$$

or

$$\text{Horn Gain: } G_H = 22.02 \text{ db} \pm 0.09 \text{ db } p.e. \quad (2)$$

b. Venus site antenna gain tests. The block diagram of the system utilized for the Goldstone gain tests is shown in Fig. 2. Table 4 shows the measurement parameters.

The atmospheric loss was calculated from data published by Van Vleck (Ref. 3), assuming Hogg's (Ref. 4) suggested value of 750 Mc for the oxygen spectrum broadening factor $\Delta\nu$. This result corresponds to assuming an "equivalent" atmosphere height at 2388 Mc of 5.8 km. The weather at the time of measurement was clear and dry, under which conditions the attenuation due to water vapor is negligible (Ref. 4). The estimated errors in the Venus gain measurement are shown in Table 5.

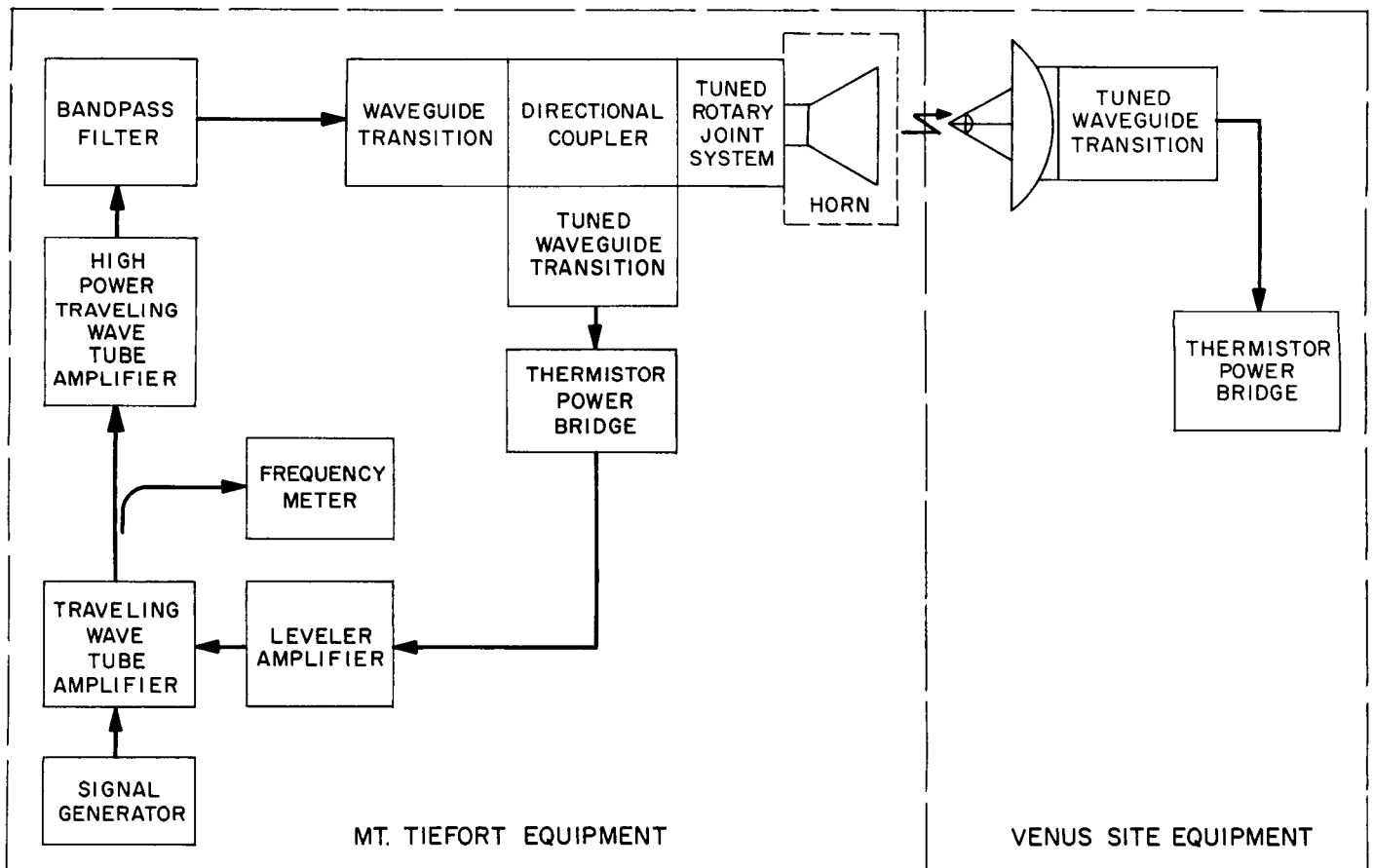


Fig. 2. Block diagram for 85-ft antenna gain tests

Table 4. Venus site gain measurement parameters

Parameter	Calculated or measured value
Coupler output power	+ 10.00 dbm
Coupler calibration	- 25.40 db
Insertion loss (Tiefort)	- 0.04 db
Insertion loss (Cassegrain cone)	- 0.12 db
Horn gain	+ 22.02 db
Range	6.7321×10^4 ft
Atmospheric loss	- 0.15 db (calculated)
Received signal	- 15.10 dbm (vertical polarization)
	- 15.13 dbm (45° polarization)
	- 15.15 dbm (horizontal polarization)
	Average - 15.13 dbm

Table 5. Venus site antenna gain calibration errors

Error	Estimated magnitude
Horn gain	0.09
Power transmitted to power received	0.05
Multipath	0.05
Coupler calibration	0.05
Atmospheric loss	0.05
Mismatch	0.05
Insertion loss	0.03
Boresight (Venus site)	0.02
Range	0.01
Boresight (Tiefort)	Negligible
Frequency	Negligible
Phase front	Negligible
Polarization alignment	Negligible
rms error: 0.15 db	

The 2388-Mc gain of the Venus site antenna, *at the horn output*, may be determined from Tables 4 and 5. The result is:

$$\text{Elevation angle} = 0.8^\circ$$

$$\text{Venus site antenna gain} = 54.01 \text{ db} \pm 0.15 \text{ db p.e.}$$

$$\text{Venus site antenna aperture efficiency} = 0.598 \pm 0.020 \text{ p.e.} \quad (3)$$

The establishment of an absolute accuracy for this result is somewhat subjective; a value of two or three times the probable error is presumably reasonable. The agreement between the above result and that previously published (see SPS 37-18, Vol. III, p. 25; Gain = 54.3 db ± 1.0 -db absolute accuracy) is reasonable. Conceivably, the result stated in this report could be averaged with

the previous result; however, it is felt that insufficient data are available on the probable error of the previous calibration to warrant its use.

An important point should be made relative to the above gain calibration. As will be described below, the radiation pattern tests show an elevation plane beamwidth (independent of polarization) of 0.328° and an azimuth plane beamwidth of 0.038° , indicating structural deformation of the antenna in the elevation plane. If this effect is real, it is not unreasonable to expect that the gain at a 45° elevation angle (the angle at which the surface was originally set) is approximately $0.328/0.308$ (or 0.3 db) higher than the value given above. Presumably this point will be resolved at a later time by structural calculations and/or radio source tests. If this effect really did exist, the gain at 45° elevation angle would be in exact agreement with the value previously published (SPS 37-18, Vol. III, p. 25).

c. Venus site antenna pattern tests. Measured azimuth patterns for vertical and horizontal polarization are shown in Fig. 3; the elevation patterns are shown in Fig. 4. The patterns were taken by hand at position increments of 0.040° , requiring approximately 30-min test time for each of the patterns. In the elevation patterns, the angular displacement between the vertical and horizontal polarizations is apparently caused by mechanical backlash in the flexible coupling between the elevation axis and the Datex

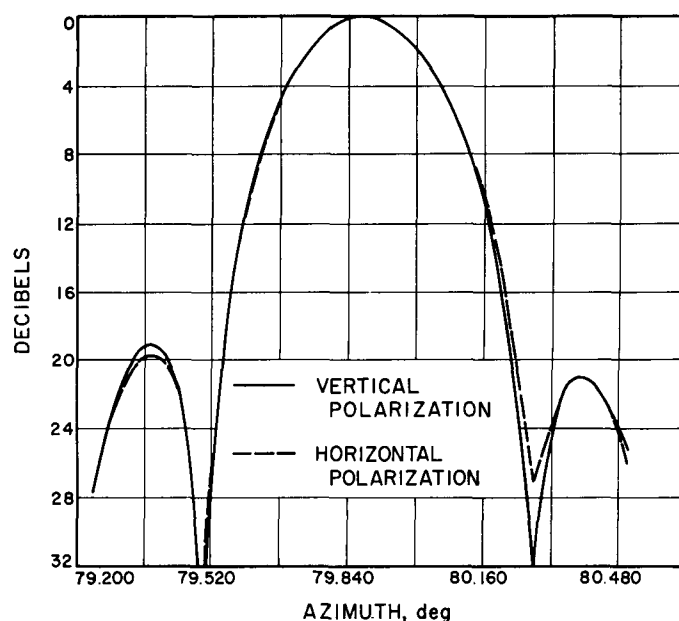


Fig. 3. Azimuth patterns of 85-ft Az-El antenna

angle encoder. The two elevation antenna patterns were made with the antenna movement in opposite directions; up for horizontal polarization and down for vertical polarization. Fig. 4 indicates a backlash of approximately $\pm 0.006^\circ$ from the true elevation, as a function of antenna movement direction.

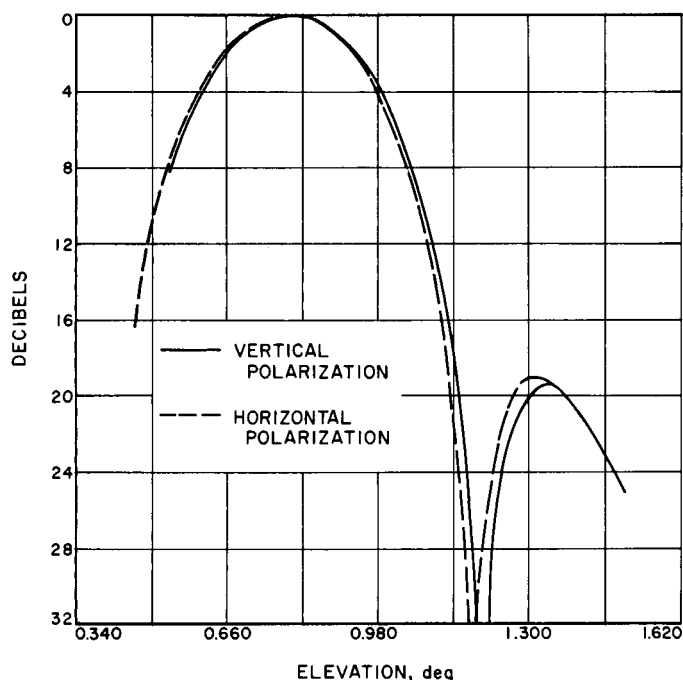


Fig. 4. Elevation patterns of 85-ft Az-El antenna

The true RF boresight position of Mt. Tiefert is, from Figs. 3 and 4:

$$\begin{aligned} \text{Azimuth: } 79.878^\circ \\ \text{Elevation: } 0.794^\circ \end{aligned} \quad (4)$$

The antenna full half-power beamwidths at 0.8° elevation angle are given in Table 6.

Table 6 and Figs. 3 and 4 strongly imply two things:

- (1) The feed system has symmetrical radiation properties.
- (2) The antenna is mechanically unsymmetrical between elevation and azimuth in the horizon position.

The antenna structure is presently being studied analytically to determine the nature of the apparent astigmatism observed.

Table 6. 2388-Mc Venus site antenna beamwidths

Pattern plane	Vertical polarization	Horizontal polarization
Azimuth	0.308°	0.308°
Elevation	0.328°	0.328°

The lack of polarization dependence displayed in Table 4 and the high quality of the patterns in Figs. 3 and 4 indicate that the Venus site-Mt. Tiefert S-band antenna range is essentially free of multipath problems, and will prove to be a valuable facility for evaluation of the RF effect of future mechanical and feed system modifications to the antenna.

3. Antenna Instrumentation

Introduction. A transportable instrumentation system is being built for use in research and development testing of the structural and mechanical properties of large ground antennas. It will be used on the 30- and 85-ft antennas this year and, later, on the 210-ft diameter Advanced Antenna System. The system will be first used for the structural and thermal testing to be conducted as part of the 85-ft Az-El antenna resurfacing work late this Summer. There is a detailed description of the instrumentation system in SPS 37-20, Vol. III and a short progress report in SPS 37-21, Vol. III.

a. Preparations for 85-ft Az-El tests. For the initial tests on the 85-ft Az-El antenna, a low-speed data-logging system will be employed. Automatic scanning and recording will be provided with maximum capability as follows:

- (1) 12 extensometers, Group A.
- (2) 12 wire span resistances, Group B.
- (3) 12 strain gages, Group A.
- (4) 50 thermocouples, Group C.

A pre-patch system provides flexible programming and permits recording on a common data system. Also, up to seven channels of real-time recording of simultaneous phenomena can be accommodated with a spectral bandwidth of dc to 10 kc using multi-channel, magnetic tape recording.

Fig. 5 (a), (b), (c) shows the extensometer locations for the initial deadload deflection testing to be conducted on the 85-ft Az-El antenna.

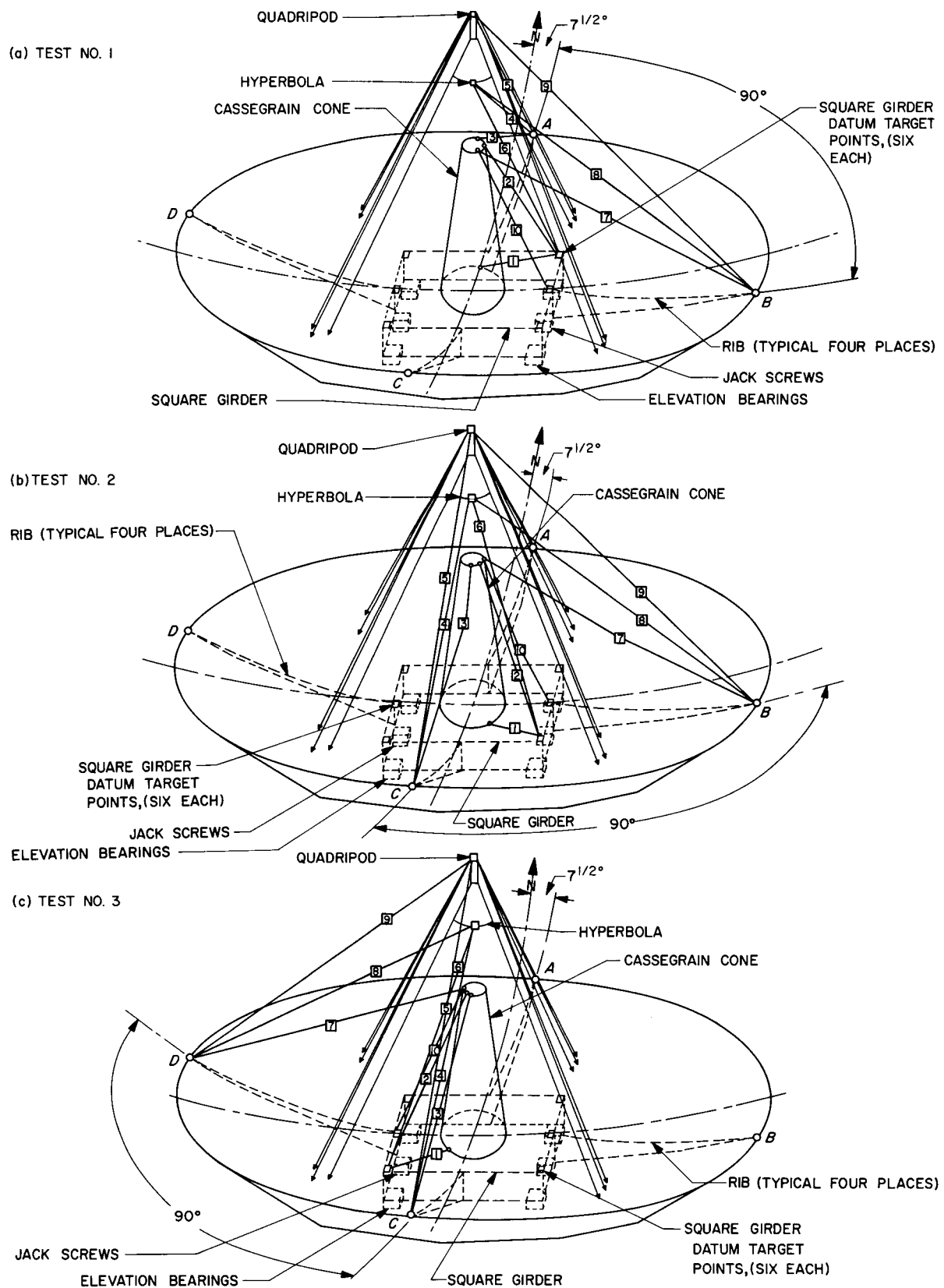


Fig. 5. Extensometer locations for 85-ft Az-El antenna tests

C. Planetary Radar

1. Mod III Transmitting System, 2388 Mc, 100 kw

Since the last status report in SPS 37-21, Vol. III, pp. 47-49, the transmitter has been operating on the Mercury radar experiment. The operating time during this experiment has been used to accumulate information on those areas in the transmitter requiring correction in order to improve the reliability of the system.

a. 100-kw S-band klystron amplifier. When the amplifier was reinstalled after the rework at the contractor's plant (SPS 37-21, Vol. III, pp. 47-49) the back power was 1.05% of the forward power. Prior to removal of the amplifier for rework, the back power was 0.32% of the forward power. This high back power of 1.05% limited the forward power at the start of the Mercury experiment to approximately 85 kw in order not to exceed the allowable back power into the klystron. The waveguide associated with the klystron amplifier was removed and the flanges lapped but this did not improve the VSWR. The waveguide adjacent to the klystron was then tuned with clamps and the resulting back power was reduced to again approximately 0.32%. This reduction in back power allowed completion of the Mercury experiment with approximately 100 kw of transmitted power.

The instrumentation in the klystron amplifier used to measure the klystron body current provides two outputs: a reading of the normal body current on the control meters and a sharp pulse to trigger the crowbar in case of a klystron body arc. Measurements made during this last operational period indicate that a number of false crowbar actions are being triggered by large noise pulses in this portion of the crowbar logic circuit. This pick-up will be reduced to an acceptable level during the shut-down after the Mercury experiment.

b. Beam power supply. As reported in SPS 37-21, the rectifier tubes in the beam power supply appeared to be capable of meeting the requirements of the power supply. However, as the Mercury experiment has progressed, the rectifier tubes have been experiencing internal arcs at an increasing rate. This has been discussed with the tube manufacturer, and the tube is now being redesigned to meet the service requirements for this power supply. A set of rectifier tubes, which will be tested during the shut-down after the Mercury experiment, has been procured from a second source.

c. Klystron noise power. In order to design future systems using the 100-kw klystron amplifier, the noise power

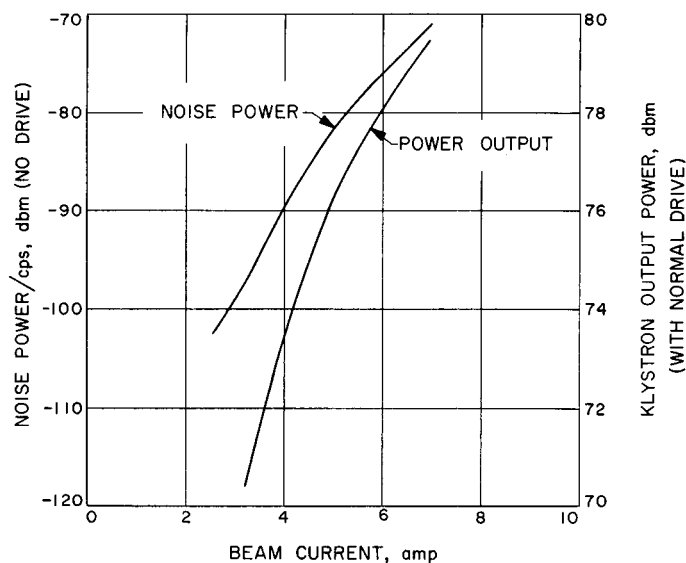


Fig. 6. Output power and noise power versus klystron beam current

from the klystron (with no drive and various beam voltages), was required. The output from the forward-power coupler was connected to the input of the TRAC(E) Mod III receiver. The output of the 455-kc IF was measured with an rms voltmeter for various values of beam current. These readings were then duplicated using a calibrated signal generator to obtain a numerical value for the noise power. Since the limiting bandwidth of the receiver during these tests was 32 kc, the noise power was calculated on a cycle-per-second basis and plotted in Fig. 6. Fig. 7 is a plot of noise power with no drive against output power with normal drive.

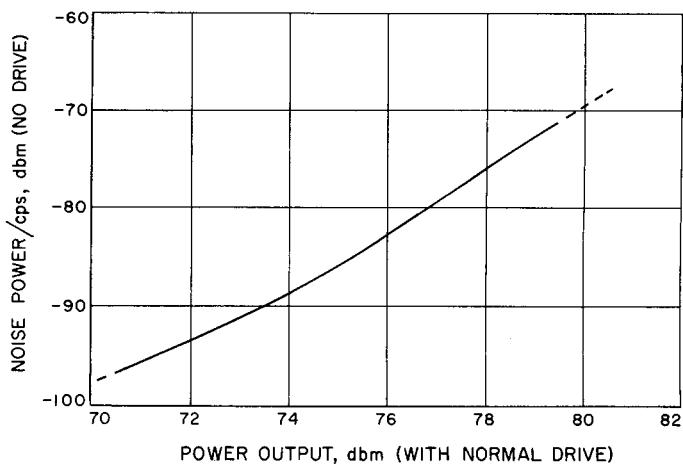


Fig. 7. Klystron noise power versus output power

2. Mod IV Planetary Radar Receiver

The Mod IV planetary radar receiver has been installed in the Control Building (G51) at the Venus site, Goldstone Tracking Station. Installation of the "front-end" components in the antenna will be made following completion of the current Mercury-Venus planetary radar experiment. Measurements of receiver parameters additional to those reported in SPS 37-21, Vol. III, have been made.

a. Liquid cooling. Requirements for a coolant chiller to be used to stabilize the operating temperature of the receiver were determined at the laboratory by running tap water through the system. The test was instrumented with a multi-channel recorder; inlet and exhaust water temperature, flow rate, pressure, and equipment temperatures at critical points were measured. Table 7 gives a summary of the results of one heat run. The equipment was operated for 1.5 hr with no water flow, and all doors closed. Then water was turned on and the equipment operated 14.5 hr. Only the first and last data points for each condition are presented.

b. Bandwidths, coherent reference synthesizer loops. Closed-loop frequency response of the two reference clean-up loops (30.455 and 31.44 Mc) and of the code clock switch loop (500 kc) were measured. A block diagram of the coherent reference synthesizer is shown in SPS 37-21, Vol. III, Fig. 48. The reference input to each loop was phase modulated and the loop response monitored at the phase detector output. In mechanizing the tests, the phase modulator was driven by a Hewlett Packard Model 202 low-frequency function generator. A tunable bandpass filter was used with an oscilloscope to observe the output of the phase detector.

Theoretically, the response is:

$$1 - H(j\omega) = \frac{1 - \frac{\tau_1}{G\alpha} \omega^2}{1 - \frac{\tau_1 \omega^2}{G\alpha} + j\tau_2 \omega}$$

(SPS 37-21, Vol. III, p. 57) where

G = open-loop gain

$$= K_v K_d \times 360 \times \alpha \times M$$

α = limiter suppression factor = 1

M = multiplication ratio = 1

K_v = VCO constant

K_d = phase detector constant

τ_1, τ_2 = time constants of the compensation lag network

The constants for each loop are:

Loop	K_v , cps/v	K_d , v/1°	τ_1 , sec	τ_2 , sec	$2\beta_L$ loop bandwidth, cps
30.455 Mc	100	0.667	1500	0.3	5
31.44 Mc	100	0.208	938	0.25	3
Switch loop	17	0.45	21	0.135	12

Figs. 8, 9, and 10 present the theoretical and observed closed-loop frequency response for the 31.44-Mc loop,

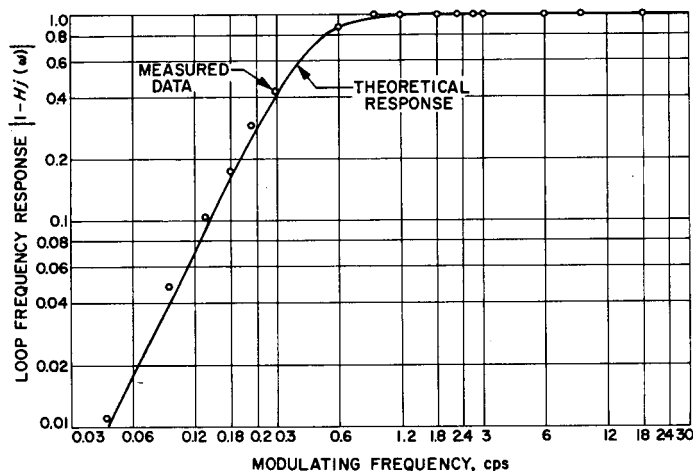


Fig. 8. Closed-loop frequency response
31.44-Mc loop $2\beta_L = 3$ cps

Table 7. Thermal measurements on Mod IV planetary receiver with and without cooling water

Water				Room air temperature, °F	Typical cabinet temperature, °F		Instrument cabinet temperature, °F		Elapsed time	Remarks
Inlet temperature, °F	Exhaust temperature, °F	Pressure, psig	Flow rate, gpm		Top	Bottom	30-Mc counter	Power supply		
—	—	—	—	73.2	72.5	72.5	82	83	0	Start test Water off
—	—	—	—	74.4	79.4	79.6	107	92.1	2 hr, 30 min	Water on End test
63.2	71.9	6.02	1.3	74.8	81.4	77.5	94.3	72.5	2 hr, 55 min	
62.3	74.0	5.92	1.3	72.0	70.0	65.8	87.0	65.1	17 hr	

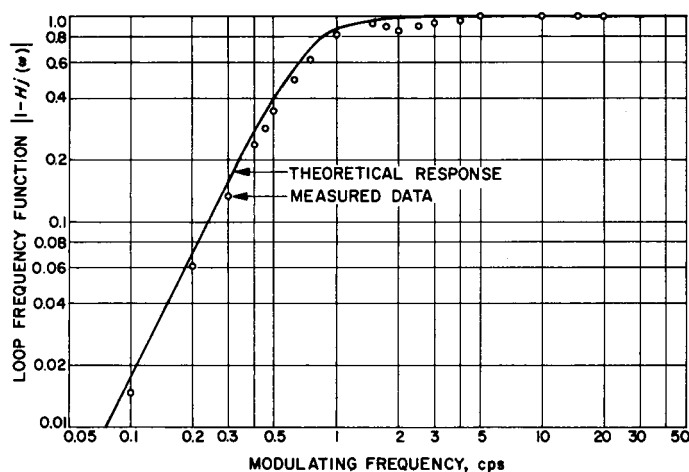


Fig. 9. Closed-loop frequency response
30.455-Mc loop $2\beta_L = 5$ cps

the 30.455-Mc loop, and the 500-kc switch loop, respectively. The anomaly occurring at 2 cps in Fig. 8 was thought to be due to overdamping; however, experimental changes in the damping factor produced effects centered at 0.75 cps [3-db point of $(1 - H_{j\omega})$]. The 30-Mc phase modulator employed in the test was flat to ± 0.4 db over the frequency range 0.1 to 100 cps. In Fig. 10, the curve drops away from the theoretical for frequencies above 4.8 cps. The measured data has been corrected for nonlinearities in the phase modulator and detectors. Further investigation is required.

c. Spurious signals on coherent references. Harmonics and other spurious outputs on the coherent references measured to be less than -60 db below the fundamental were:

Coherent reference fundamental frequency	Spurious signal	
	Frequency, Mc	Level, db
500 kc	None	
1 Mc	2	-51
1 Mc	3	-52
30 Mc	10	-55
30 Mc	15	-45
30 Mc	60	-37
30.455 Mc	60.9	-43
30.455 Mc	91.3	-49
31.44 Mc	62.8	-41
31.44 Mc	94.3	-47

d. Reference oscillator stability. Included in the receiver are six crystal-controlled but non-phase-coherent reference oscillators: 455.0 kc, 448.079 kc, 454.768 kc,

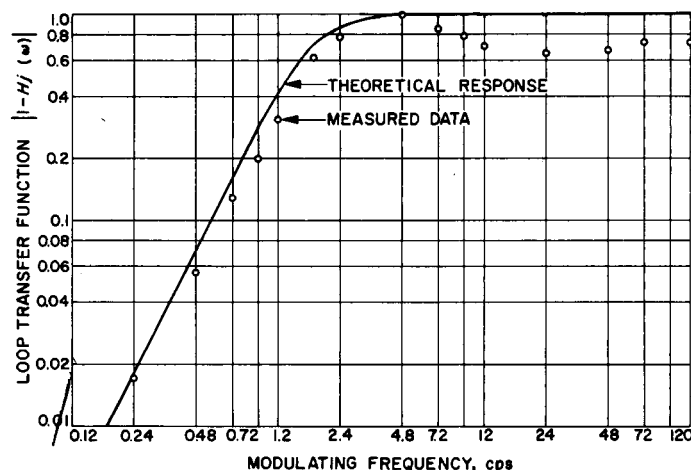


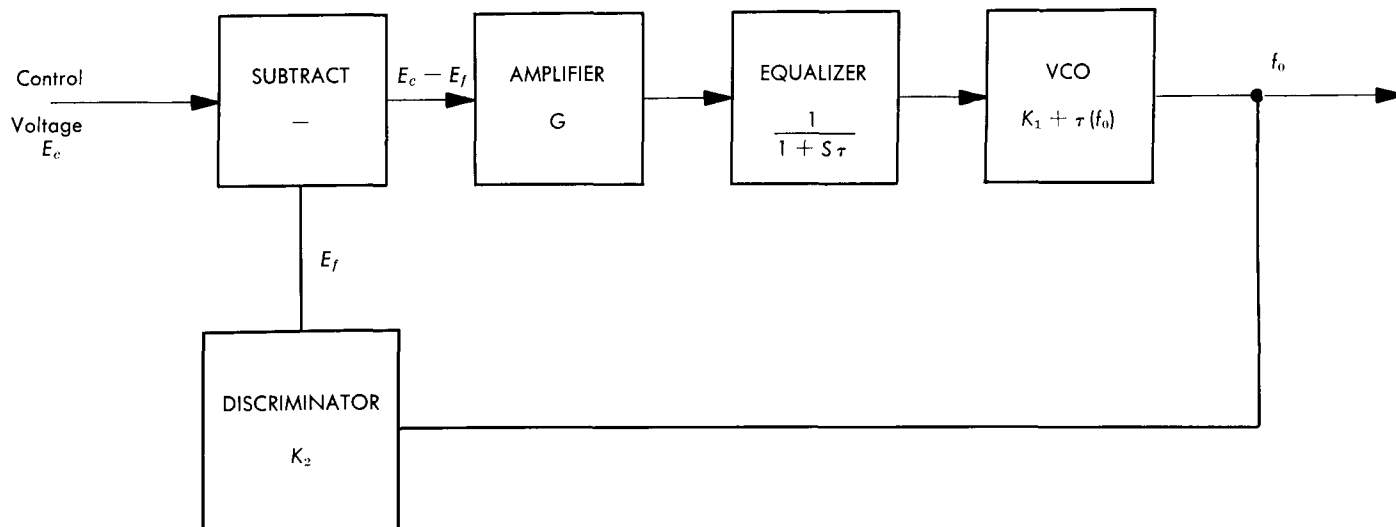
Fig. 10. Closed-loop frequency response
code-clock loop $2\beta_L = 12$ cps

456.05 kc, 459.0 kc, and 471.667 kc. The frequency stability of these oscillators was checked with a printing frequency counter whose resolution was ± 0.1 cps using a time base derived from a rubidium vapor maser. Each oscillator was checked for a 2-hr period twice daily for 3 consecutive days. There was no variation in frequency recorded within the resolution of the counter.

e. Additional tests. Testing of the receiver is continuing and the results will be reported in future *Space Programs Summaries*. These include system tests and measurement of coherent leakage in the main loop using the AM spectrum analysis computer.

3. A Linear Voltage Controlled Oscillator Using Frequency Feedback

The requirements on a voltage controlled oscillator (VCO), which is to be used as a digitally controlled VCO in a programmed local oscillator, are in many ways more stringent than are the requirements on a VCO used in a normal (synchronous) manner. For both modes of operation the VCO must have (1) low phase noise and (2) a definite range of useful frequency shift. The oscillator in the digitally programmed equipment must also exhibit (3) stability, from one 10-sec period to the next of less than $\frac{1}{4}$ cps when multiplied by 75, i.e., 7×10^{-9} for a 475-kc VCO. Moreover, the linearity in cps/v should be nearly constant in order to adjust the digital control loop gain for optimum response without ringing. A requirement of (4) constant sensitivity within $\pm 10\%$ is reasonable in order to achieve this response.



$$\text{LOOP TRANSFER FUNCTION, } F(s) = \frac{f_0}{E_c} = \frac{G [K_1 + \sigma(f_0)]}{1 + s\tau + K_2 G [K_1 + \sigma(f_0)]}$$

where G = AMPLIFIER GAIN $\approx 10^4$ v/v

K_1 = VCO SENSITIVITY = 10 cps/v

$\sigma(f_0)$ = VCO NONLINEARITY = ± 2 cps/v maximum

τ = EQUALIZER TIME CONSTANT = 20×10^3 sec $\left\{ \begin{array}{l} \text{determined by} \\ \text{digital loop} \\ \text{requirements} \end{array} \right.$

K_2 = DISCRIMINATOR SENSITIVITY (ASSUMED CONSTANT) = $1/6$ v/cps

$$F(s) = \frac{10^4 (10 \pm 2)}{1 + s 20 \times 10^3 + \frac{10^4}{6} [10 \pm 2]} \cong \frac{6}{1 + s \frac{20 \times 10^3}{10^4 (10 \pm 2)}}$$

$$\cong \frac{6}{1 + \frac{s}{5 \pm 1}}$$

STEADY-STATE, $F(0) = 6$ cps/v

EFFECTIVE LOOP TIME CONSTANT = $1/4$ to $1/6$ sec

Fig. 11. VCO with frequency feedback

The vacuum-tube VCO's used in the present Venus experiment have an adequately low phase noise (Req. 1) of 0.045° peak-to-peak in $2B_L = 5$ cps. The frequency range (Req. 2) is also sufficient, ± 100 cps. The 10-sec stability figure is somewhat marginal, reaching at times a value of 20×10^{-9} . The linearity figure is very poor also,

with careful adjustment $\pm 50\%$ change in slope over the frequency range may be achieved. This has been improved by using a nonlinear potentiometer to compensate for the VCO nonlinearity. The sensitivity of the over-all system of VCO and potentiometer is now constant within $\pm 15.1\%$.

A new solid-state VCO has been developed similar to the 30-Mc VCO described in SPS 37-15, Vol. III, pp. 34-36. The phase noise of the new VCO is somewhat lower than that of the old VCO, 0.028° peak-to-peak in $2B_L = 5$ cps. The 10-sec stability figure for the new VCO is typically 5×10^{-9} , a four-fold improvement over the vacuum-tube units. The frequency range is comparable to that of the old VCO, and is typically ± 100 cps. While the linearity is actually slightly better than the old VCO, $\pm 20\%$, the curve is not of a type which is easily compensated by potentiometer loading as was done for the old VCO. A feedback system for linearizing the VCO by means of a linear discriminator has been developed. A block diagram of the system and a table of system equations and constants are given in Fig. 11. With this system the linearity is constant within $\pm 10\%$.

Curves of performance characteristics of (a) the vacuum-tube VCO, (b) the solid-state VCO, and (c) the solid-state VCO with feedback, are given in Fig. 12. A condensation of the data is given below:

	Stability, 10 sec	Linearity	Phase noise at 475 kc $2B_L = 5$ cps
Vacuum-tube VCO, uncompensated	20×10^{-9}	$\pm 33\%$	0.045° peak-to-peak
Vacuum-tube VCO, compensated	20×10^{-9}	$\pm 15.1\%$	0.045° peak-to-peak
Solid-state VCO	5×10^{-9}	$\pm 20\%$	0.009° peak-to-peak
Solid-state VCO with feedback	5×10^{-9}	$\pm 10\%$	0.028° peak-to-peak

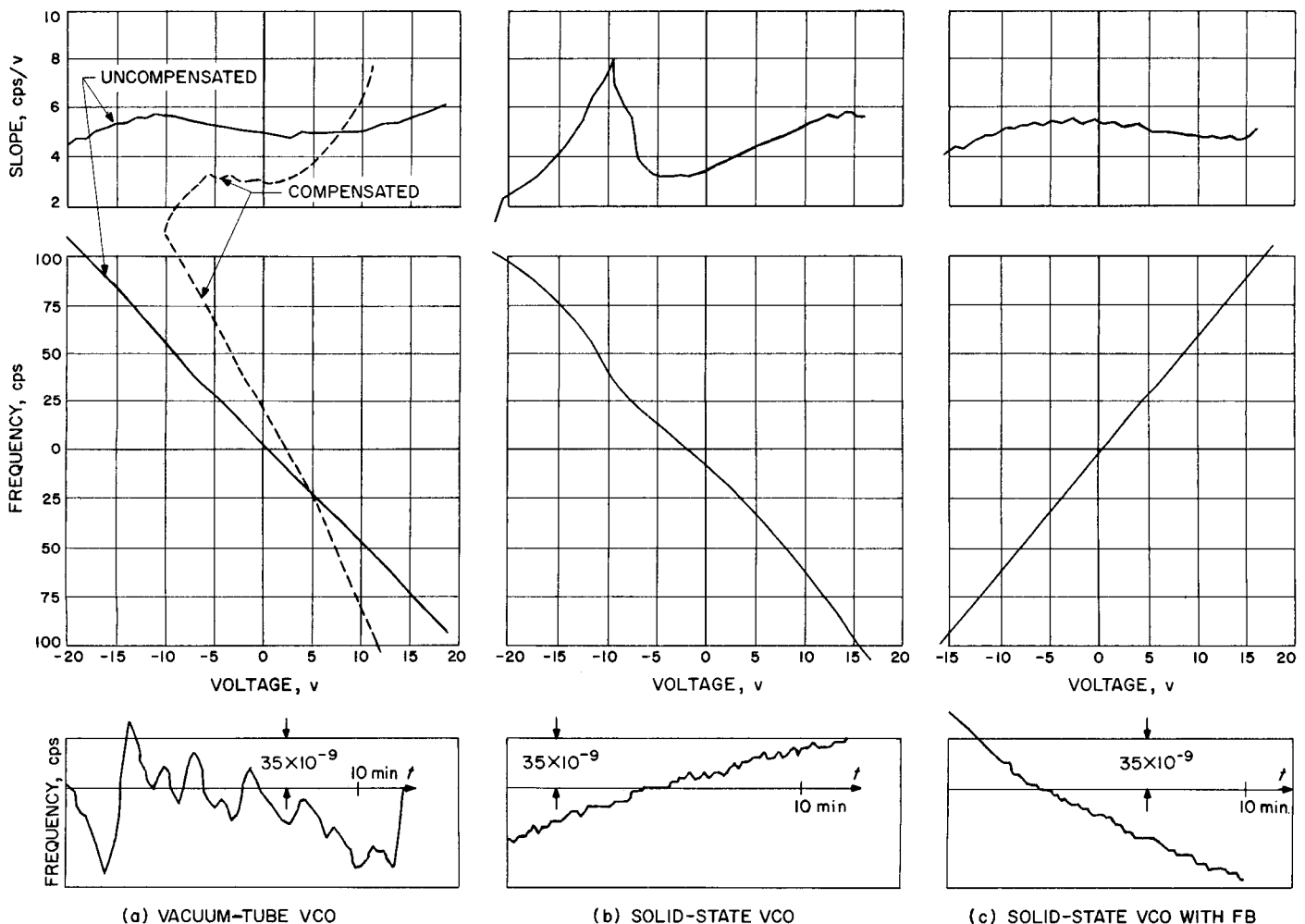


Fig. 12. VCO performance characteristics

4. Radio Astronomical Techniques for Ground Antenna Calibration

a. Boresight and gain calibrations of DSIF antennas.

Abstract. An automatic data system is under development to facilitate the calibration of the DSIF antennas by radio astronomical techniques. Previous radio astronomy antenna calibration programs at JPL have required excessive hand data reduction (SPS 37-14, Vol. I, pp. 99-105). In recent tests, a timing sequencer was used to standardize the radiometer data format, allowing automatic data reduction by a digital computer.

Discussion. During the 960-Mc Cassegrain experiment (above-mentioned SPS) drift curve data were recorded digitally using a voltage-to-frequency converter and a cycle counter. The digital information was later used with hand computations to obtain star transit times and source antenna temperature. At the time, digitization was employed because of its stability and resolution, its format

was not designed for automatic data reduction. The reduced transit times and associated antenna coordinates were then fed into a digital computer program to obtain refraction corrections, corrected hour angle and declination, and plots of declination error and hour angle error as a function of hour angle. Figs. 13 and 14 show the hour angle and declination errors obtained by observing the Crab Nebula. Gain loss was also obtained as a function of antenna elevation angle.

The data reduction time for the 960-Mc Cassegrain experiment was such that the techniques could not be employed for general operational calibrations. To mechanize these techniques for a complete digital computer reduction so that they may be used for operational DSIF boresight and gain calibrations, a sequencer has been developed to enable the pertinent data to be recorded in a format which is compatible with the 1620 digital computer.

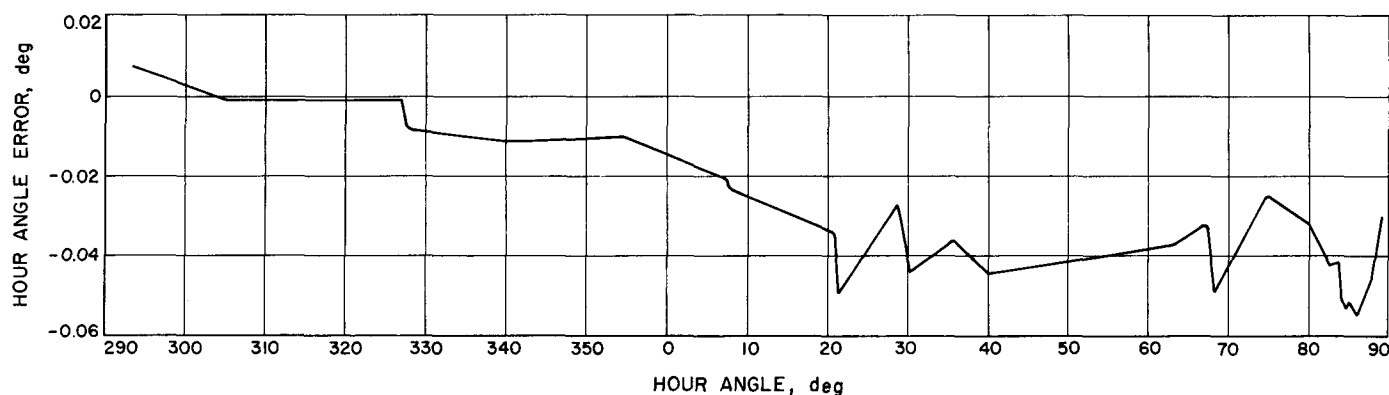


Fig. 13. Hour angle error versus hour angle for Crab Nebula

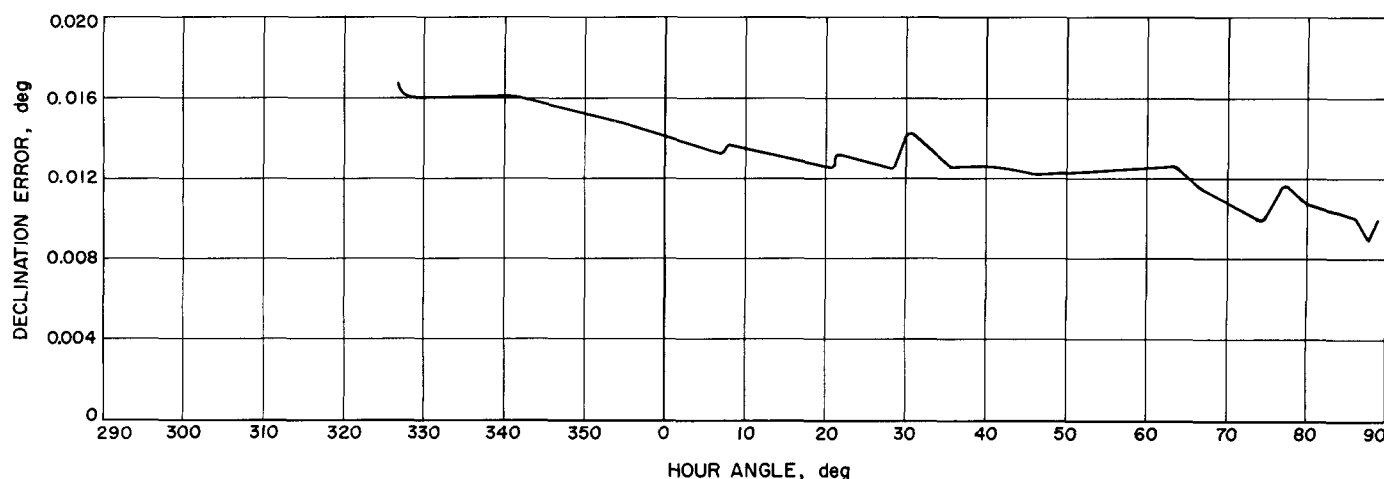


Fig. 14. Declination error versus hour angle for Crab Nebula

STATION NUMBER	DATA TYPE	TIME	HOUR ANGLE	DECLINATION	FREQUENCY (TEMPERATURE)	DAY NUMBER
3	2	084902	330488	040734	0000594	156
3	2	084912	330476	040734	0000588	156
3	2	084922	330500	040734	0000596	156
3	2	084932	330526	040732	0000584	156
3	2	084942	330514	040732	0000598	156
3	2	084952	330514	040732	0000594	156
3	2	085002	330512	040734	0000597	156
3	2	085012	330512	040734	0000594	156
3	2	085022	330512	040734	0000596	156
3	2	085032	330508	040734	0000589	156
3	4	085112	330508	040734	0000717	156
3	4	085122	330508	040732	0000749	156
3	4	085132	330508	040732	0000748	156
3	4	085142	330508	040732	0000754	156
3	4	085152	330508	040732	0000749	156
3	4	085202	330508	040732	0000745	156
3	1	085323	330508	040732	0000608	156
3	1	085324	330508	040732	0000603	156
3	1	085325	330508	040732	0000609	156
3	1	085326	330508	040732	0000611	156
3	1	085327	330508	040732	0000607	156
3	1	085328	330508	040732	0000610	156
3	1	085329	330508	040732	0000611	156
3	1	085330	330508	040732	0000611	156
3	1	085331	330508	040732	0000615	156
3	1	085332	330508	040732	0000614	156

Fig. 15. Radiometer data format

The present system test involves the use of a Dicke radiometer (SPS 37-18, Vol. III, pp. 65-68) and the Echo site 85-ft polar-mount antenna to measure drift curves of some intense radio stars at 2295 Mc. The radiometer output information is recorded on a strip chart recorder and the dc voltage output is also fed into a Dymec DY 2210 voltage-to-frequency converter. This ac signal is then sent to the station data system and is recorded on the equipment normally used for counting and recording doppler frequency. The output of the data system is transcribed onto punched paper tape.

The format of the equivalent paper tape output is shown in Fig. 15. The data type column may have digits 1, 2, 4, or 8. The digit 1 indicates that the source is drifting through the main beam, 2 indicates that a baseline calibration is occurring, 4 indicates a noise tube calibration, and 8 indicates either switching transients or bad data and this data is automatically sorted out and discarded.

A synchronous drive motor and cam arrangement (Figs. 16 and 17) has been constructed to automatically switch the data type number and fire the noise tube. Fig. 18 illustrates the timing sequence employed. Every 15 min, the antenna is moved during a 1-min interval to a new orientation.

The punched paper tape is converted into IBM cards and all No. 8 data type cards are sorted out on the card sorter. The remaining cards are then processed in the IBM 1620 digital computer.

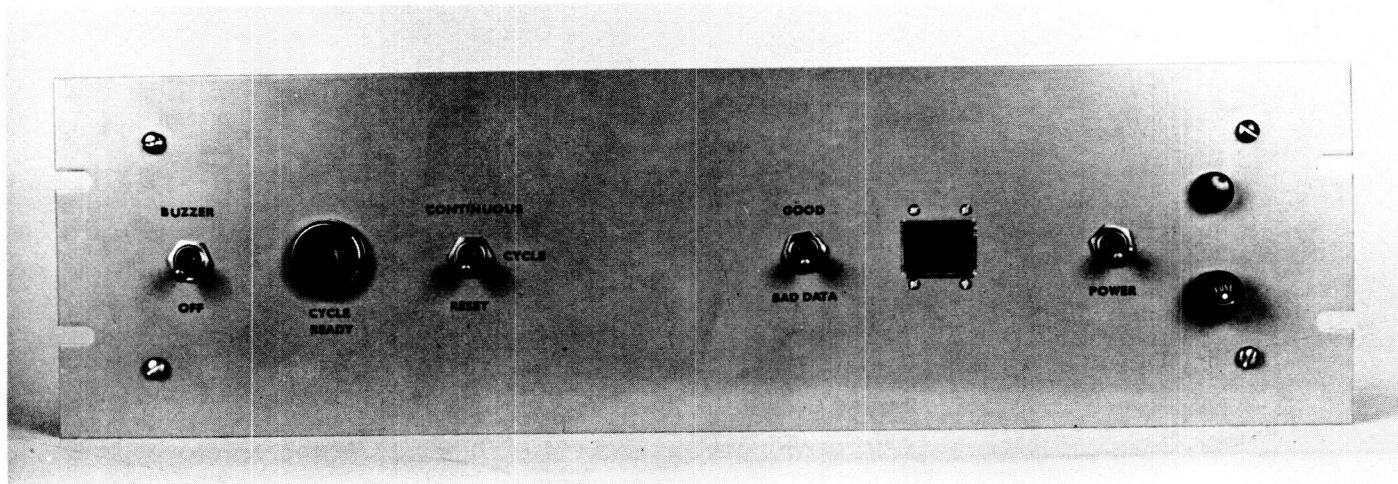


Fig. 16. Radiometer data timing sequencer



Fig. 17. Radiometer data timing sequencer

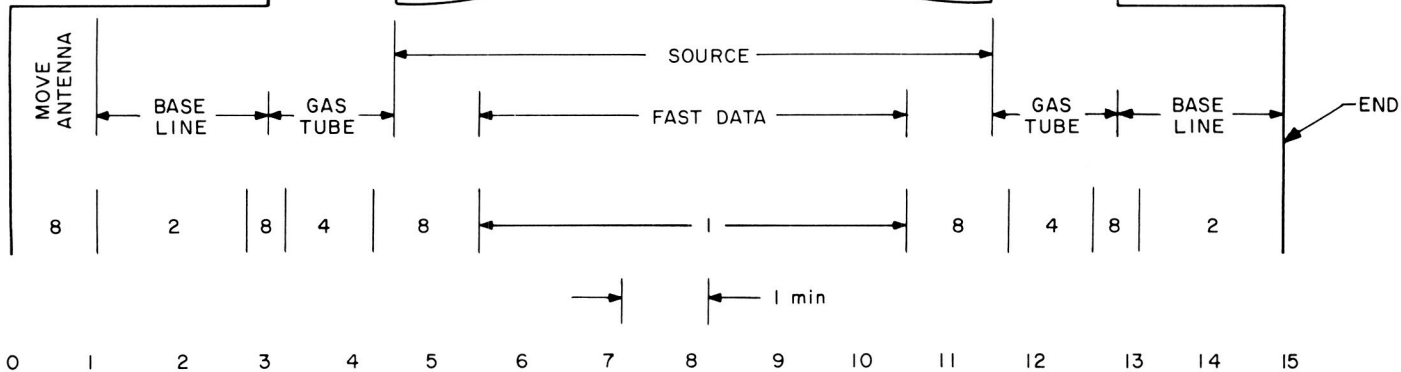


Fig. 18. Drift curve timing sequence

The digital computer processing program is almost complete. The program has several functions. The first is to perform a linear correction for all points to correct for baseline drift. Then the known source position and the antenna coordinates (obtained through the courtesy of the California Institute of Technology Radio Observa-

tory) are used to compute the time of the expected drift curve crossing. Then a least squares fit to the drift curve is performed (either second or fourth power polynomial may be used at the option of the operator) and the observed crossing time is obtained. This is used to derive the hour angle boresight error. The maximum of the

smoothed drift curve is compared with the gas tube pulse to determine the effective antenna temperature at the given declination angle. The apparent 3-db width of the smoothed drift curve is also measured.

A raster scan will be employed in which declination, as well as hour angle, is stepped every 15 min. By curve fitting the peak temperatures as a function of declination, it will be possible to determine the hour angle and declination boresight error. Thus, after tracking several radio sources throughout their visibility periods, it will be possible to determine the radio frequency boresight angle errors as a function of antenna orientation.

The determination of absolute antenna gain can be made from the antenna temperature produced by the intense sources. The accuracy of the absolute gain, however, will be largely a function of the uncertainties in known absolute source flux densities at the frequency measured. The relative gain measurement of antennas throughout the DSIF should be possible to within 5% by using carefully tested temperature standards and careful microwave measurement techniques.

b. 85-ft Az-El antenna radiometric tests. A program of radio-astronomy temperature and polarization measurements has been conducted using the Goldstone 85-ft Az-El antenna. The measurements have been made at 2388 Mc; the purpose of the program is to further evaluate a high-performance, low-noise antenna system (SPS 37-18, Vol. III, pp. 24-30). More data on source intensities and source polarizations at this frequency are provided for reference purposes for future gain calibrations of DSIF antennas. Fourteen sources (plus the Sun and the Moon) have been measured. This is of special value due to the recent precise gain measurement of the antenna (p. 11 of this *Summary*). This program was conducted at night following the daily radar experiment on Mercury or Venus.

Radio astronomy programs have been conducted at JPL for several years for the purpose of testing large ground antennas (p. 22 of this *Summary*; SPS 37-18, Vol. III, pp. 24-30; RS 36-6, Vol. I, pp. 51-59; RS 36-9, Vol. I, pp. 40-43; SPS 37-10, Vol. I, pp. 71-75; SPS 37-14, Vol. I, pp. 99-105; and Refs. 5-11). Radio astronomy techniques are used to:

- (1) Focus the antenna and obtain relative and absolute gain measurements.

- (2) Test the minimum zenith antenna temperature (for a quiet sky background) and antenna temperature as a function of elevation angle.
- (3) Measure antenna beamwidths and, sometimes, side-lobe levels.
- (4) Measure antenna boresight errors (relative to the antenna axes digital angle encoders).
- (5) Measure antenna polarization effects.

Brief polarization tests of some strong radio sources have been conducted on two previous occasions at JPL (Table 8). The intent on these two occasions was to determine inherent antenna system polarization rather than to calibrate sources, and the tests were too cursory to be of general interest. The present program will provide rather precise data which will be of use for future performance evaluations of DSIF antennas.

The radiometer system is part of the normal planetary radar system. A block diagram is presented in Fig. 19. An outline of component location in the Cassegrain feed support cone is presented in Fig. 20. The parametric amplifier and radar receiver are disconnected for the polarization tests and the monitor receiver is connected directly to the maser. This is necessary to obtain a lower noise figure for the monitor receiver system. The parametric amplifier is bypassed to obtain the best possible amplitude stability because the system is operating as a total power radiometer. The radiometer system temperature is typically 37 to 38°K at the zenith position. Short-term (minutes) amplitude stability is about 0.1°K with the antenna stopped. Peak-to-peak noise jitter is of about the same magnitude, for a 1-sec time constant and 1-Mc bandwidth. Thus, a sensitivity of about 0.1°K is available for some measurements.

The limiting sensitivity for the present experiment, therefore, will be caused partly by the inherent system

Table 8. Previous source polarization tests at Goldstone

Source	Apparent polarization, % (uncorrected for antenna effects)	
	960 Mc	2388 Mc
Cassiopeia A	2.2	0.8
Cygnus A	1.6	—
Crab Nebula	3.3	3.0
Omega Nebula	—	0.6
Orion Nebula	—	<0.4
Collimation tower test	2.4	<1.0

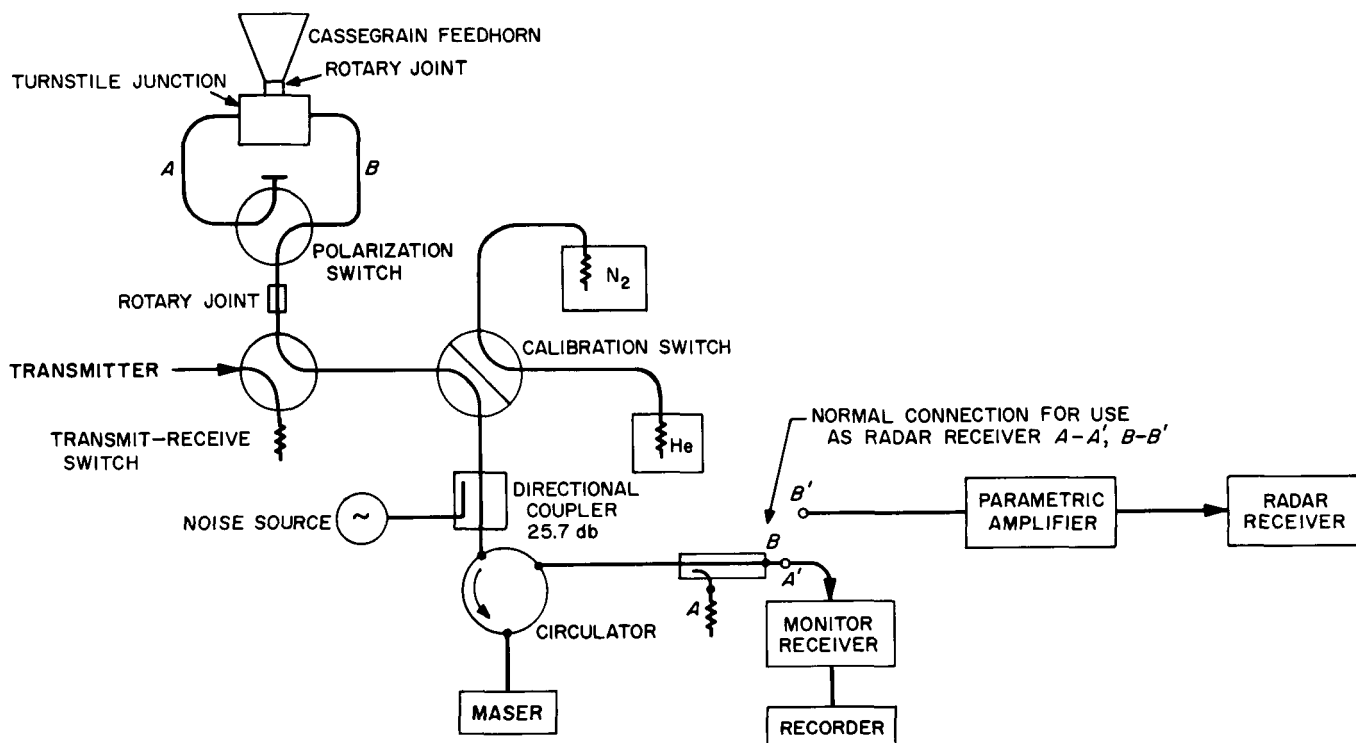


Fig. 19. Radiometer system block diagram

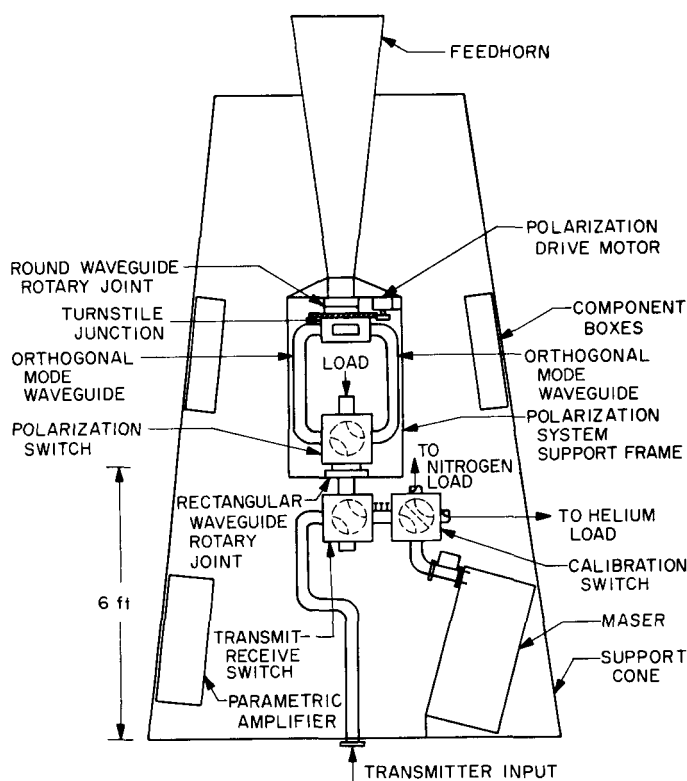


Fig. 20. Cassegrain cone installation

polarization. There is a minimum residual variation of system temperature of 0.34°K peak-to-peak due to rotation of the antenna polarization, at an elevation angle of 85° . This was obtained with a system temperature of 38°K . With the system temperature increased to 94°K by turning on the noise tube, the polarization induced variation of temperature was only 0.01°K higher. This indicates that the maser (or receiver) gain is not being affected by polarization rotation. Fig. 21 is a test record of a measurement showing the residual temperature variation with polarization rotation at a low (22°) elevation angle. Fig. 22 shows that the temperature variation with polarization rotation increases as a function of elevation angle to about 1.4°K at a 12° elevation angle. It appears that the residual minimum 0.34°K peak-to-peak temperature variation is due to the antenna system. The rotary joints in the waveguide feed system are a possible source of the residual variations. The rotary joints have been measured several times with a VSWR "wow" of less than 1.01. This was tested at the calibration switch "looking" toward the antenna through both rotary joints. Thus, there does not appear to be any way for VSWR "wow" to be causing the residual variations. These residual variations are probably due to variation in the ground temperature contribution to the antenna temperature caused by a quadripod reflection effect or perhaps by mesh sur-

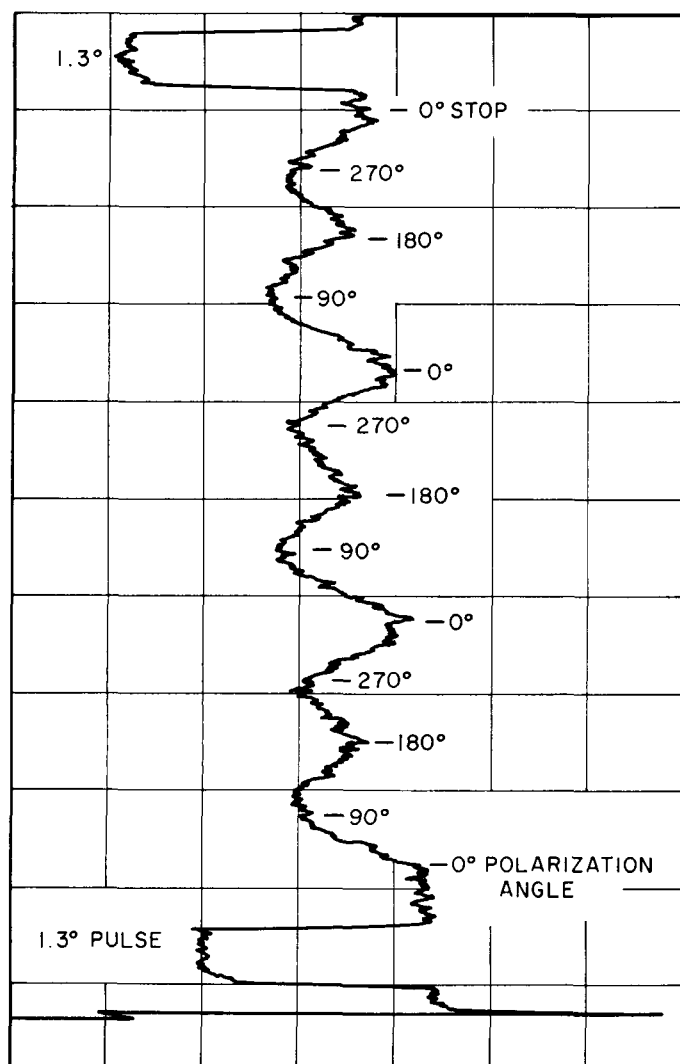


Fig. 21. Antenna temperature versus polarization angle

face leakage. It is known that the intensity of thermal emission from the ground is a strong function of receiver polarization. Thus, as the antenna elevation angle decreases, the ground temperature contribution through the sidelobes increases, and therefore the variation in temperature due to polarization increases.

Data reduction for the present measurement program is almost complete; preliminary data on source antenna temperatures and polarization are presented in Table 9. Not all of the sources listed in the table are useful to focus the antenna or for gain comparison. The extended angular size is a source of error in the case of the Moon and NGC 5128. In addition, the polarization of NGC 5128 can be troublesome. The Crab Nebula is quite useful; it is intense and of reasonably small diameter. It is polarized to a

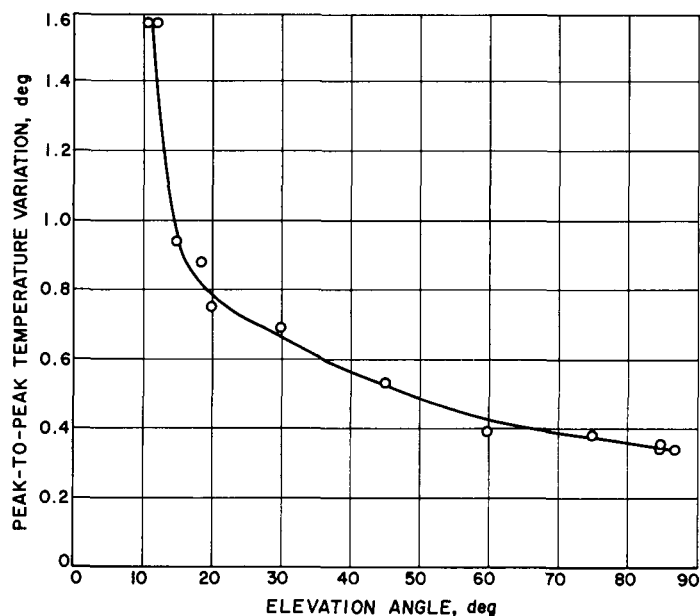


Fig. 22. System polarization versus elevation angle

small extent; however, this is not a serious handicap. Fig. 23 shows the polarization test part of a data run on the Crab. (This run was taken about a week from the date of occultation by the solar corona.)

Table 9. 2388-Mc source temperature data

Source	Relative antenna temperature, °K	Polarization, %
Cassiopeia A	160	<0.3
Cygnus A	89	<0.3
Omega Nebula	(≈ 55)	<0.3
Sagittarius A	(≈ 52)	<0.3
Hercules A	(≈ 3)	Polarized (but data reduction not complete)
NGC 5128	17.5	Polarized (but data reduction not complete)
M87	13.2	<0.8
Hydra A	(≈ 2.5)	—
Orion Nebula	41	<0.5
Crab Nebula	82	(≈ 2.5)
3C-123	(≈ 1)	Polarized (but data reduction not complete)
3C-286	(≈ 1.4)	Polarized (but data reduction not complete)
3C-353	(≈ 4)	Polarized (but data reduction not complete)
3C-273	3.8	—
Moon	120	—

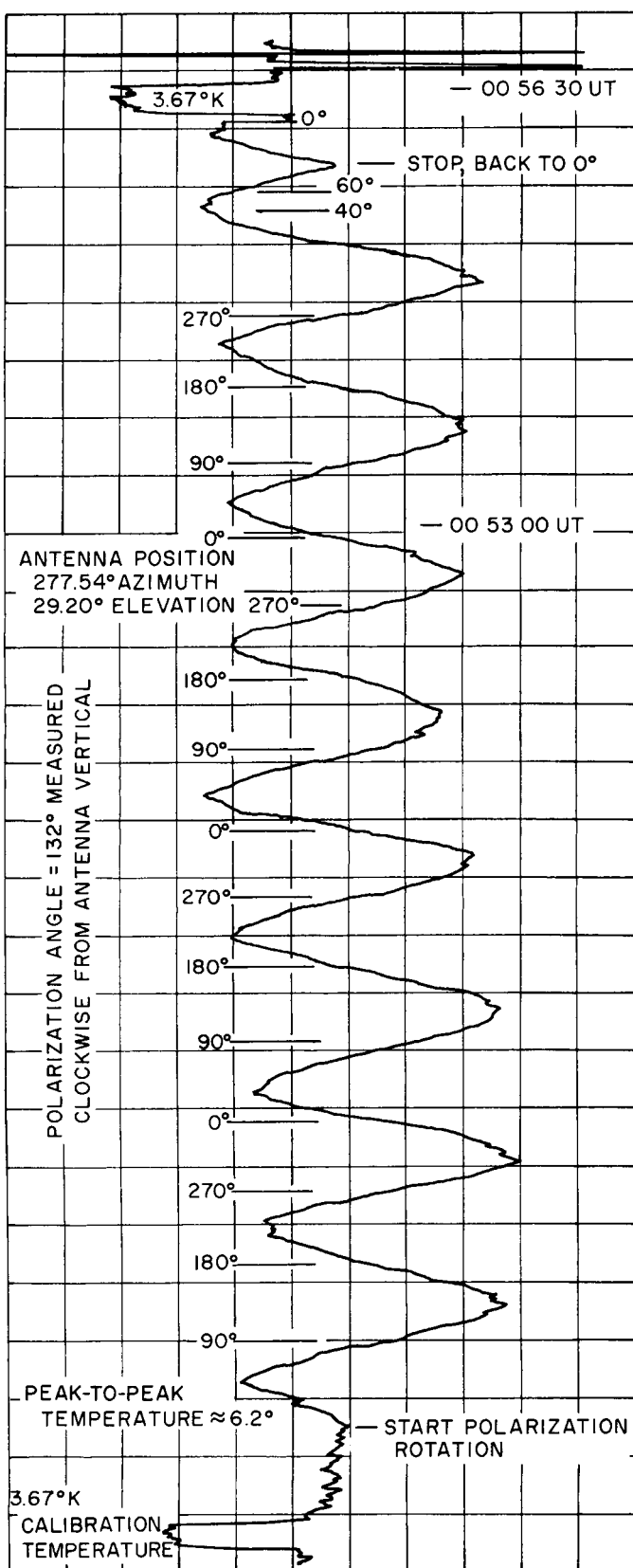


Fig. 23. Polarization test of the Crab Nebula

A complete data run consisted of the following measurements: boresighting in azimuth and elevation, temperature measurements while tracking the source, temperature measurements off the source in both directions of azimuth (to quiet sky regions), temperature measurement of the source again, a polarization measurement while tracking the source as in Fig. 23, a temperature measurement again; then the antenna was moved back to the coordinates corresponding to the center of the polarization test. The system temperature was then remeasured, a "background" polarization test made, and the run was complete. Several complete runs are needed if accurate source polarization data is desired. Then, the apparent rotation of the antennas azimuth-elevation coordinate system with respect to the galactic plane may be used to help remove the residual system polarization from the data.

Taking data by this means has provided a significant amount of RF boresight information, some of which has been reduced and is plotted in Fig. 24. Fig. 24 shows azimuth boresight error versus elevation angle; the azimuth error increases with elevation angle by approximately the secant of the elevation angle. This results principally from lack of orthogonality of the antenna beam and the antenna elevation axis. (The error in "antenna beam coordinates" resulting from the non-orthogonality is independent of the elevation angle.)

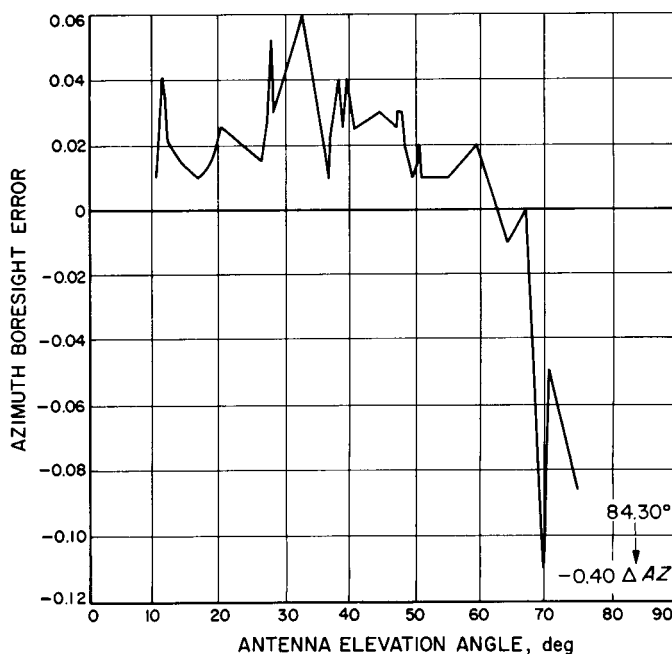


Fig. 24. Azimuth boresight error versus elevation angle

Fig. 25 shows elevation boresight error versus elevation angle reduced from the same data.

Any nonautomatic technique of RF boresight test and correction requires a significant amount of time. This spreads out the reference angles and can confuse the error plots. Figs. 24 and 25 are preliminary; the reference angles will be rechecked. Research in techniques for automatic radio source tracking equipment as a means to alleviate this problem was started in 1962; some work in this area is discussed in the preceding article.

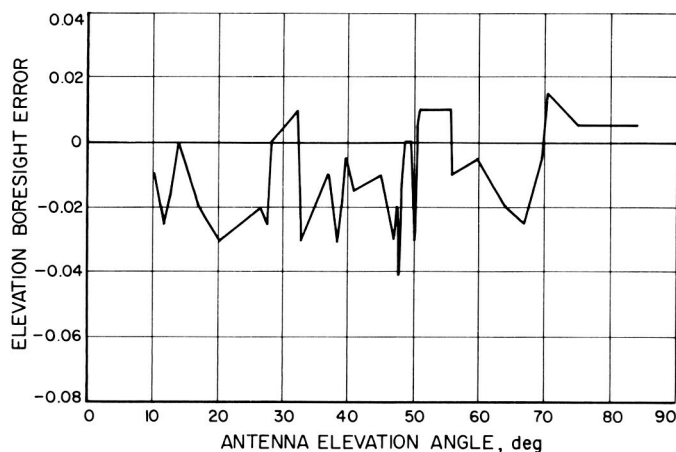


Fig. 25. Elevation boresight error versus elevation angle

5. Water Rotary Joint for Az-El Antenna

Introduction. Following is a progress report on fabrication and assembly phase of the program to build a high-capacity water rotary joint for the 85-ft Az-El antenna. In SPS 37-21, Vol. III, p. 41, the award of a contract for the water rotary joint was discussed. At present, fabrication and assembly are in process.

The environment of the assembly dictated the use of nonferrous materials. All items were fabricated from either forged "donut-type" billets or thin sections of rolled flat stock. This yielded a sound and relatively inexpensive method of obtaining the basic raw stock. Care was taken in fabrication processing to make sure each component was stress-relieved prior to final machining. This assures proper dimensional stability.

The design of the face seal configuration was based on salvaging as much as possible of the assembly of the unworkable design. Fig. 26 shows the inner rotating shell of the old assembly. The entire assembly was utilized in

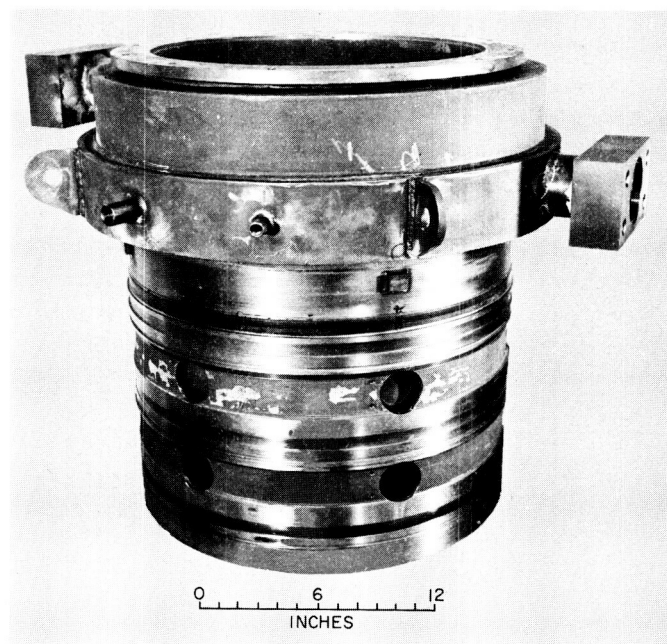


Fig. 26. Inner rotating shell assembly

the new design. Rework was required to adapt this assembly, but as shown in Fig. 37 on p. 42 of SPS 37-21, Vol. III, the over-all design concept was not compromised. The salvage enabled a large savings in cost as well as delivery time. Instrumentation ports were added as a permanent part of the assembly, allowing for monitoring of both temperature and pressure in supply and return lines as the unit is installed on the antenna.

Fig. 27 is the outer stationary shell assembly. This figure shows the relative size of assembly as well as the

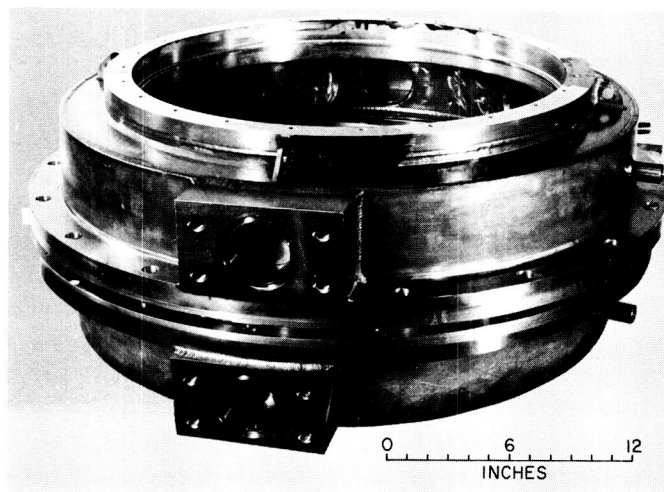


Fig. 27. Outer stationary shell assembly

massive flanges required to meet the proof pressure of 250 psig. JPL's stress calculation indicates an adequate safety factor over the maximum operational pressure of 150 psig. Permanent pressure and temperature instrumentation ports are also included in each of these halves.

Fig. 28, the rotating face, and Fig. 29, the stationary carbon face represent the actual seal surfaces. From experience it has been found that the two surfaces may be lapped independently and still afford a very adequate seal. Each piece is lapped flat within 2 helium light wavelengths over any peripheral distance of five inches. Prior to the application of water pressure, these surfaces are preloaded to 20 psi. This pressure is sufficient to prevent leakage when the water pressure inside is at or near atmospheric. At elevated pressure, because of the self-

sealing design, the pressure of the fluid provides the additional force necessary to obtain a tight seal. Manufacturing tolerances have been held to the absolute minimum but even with this stringent requirement, there will still be a pressure gradient across the face of the seal. The pressure between the seal surfaces is a maximum in the water chamber and reduces to approximately atmospheric about 50% of the way through the seal surfaces. The pressure gradient does, however, perform a useful purpose in providing some lubrication across the sealing surfaces.

The bearing retainer and wiper (Fig. 30) provide a method for both bearing retention and preload. In an assembly of this size, it was felt that shimming to obtain preload would be a difficult if not an impossible task. To

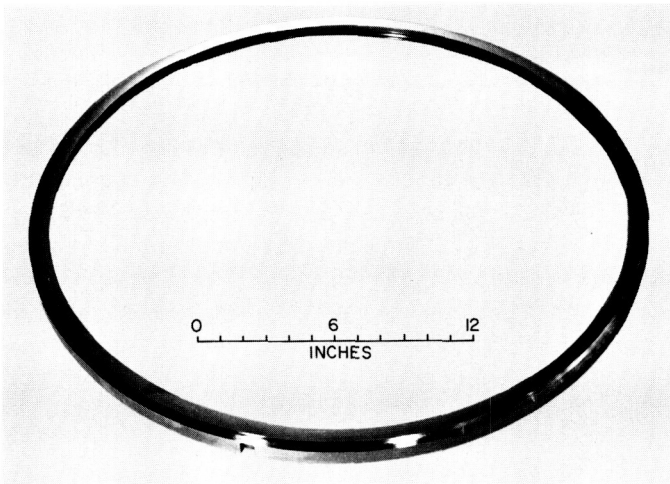


Fig. 28. Rotating face

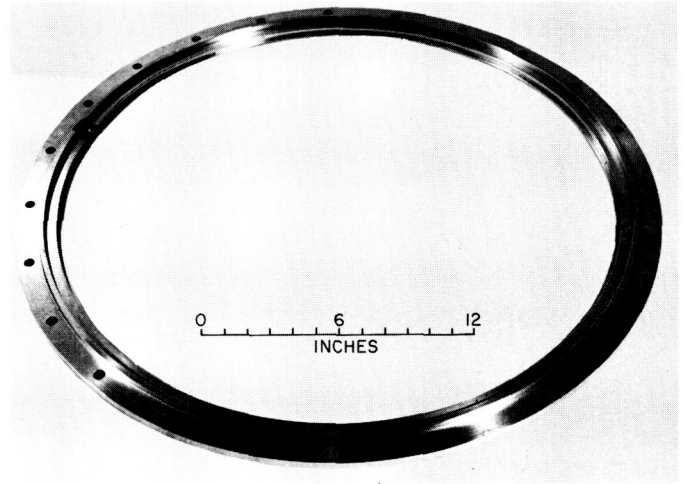


Fig. 30. Bearing retainer and wiper

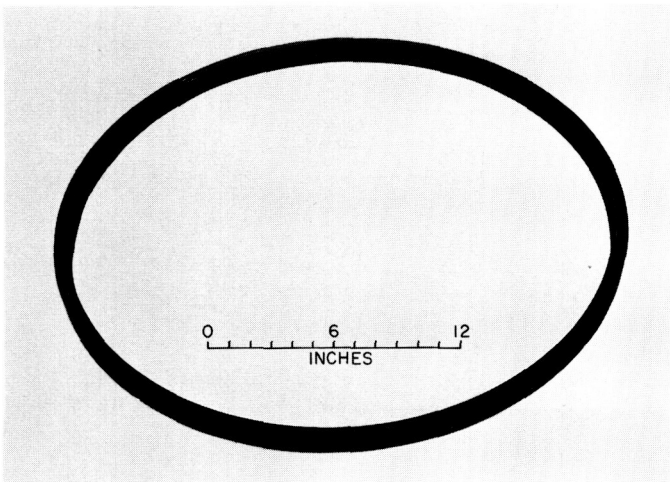


Fig. 29. Stationary carbon face

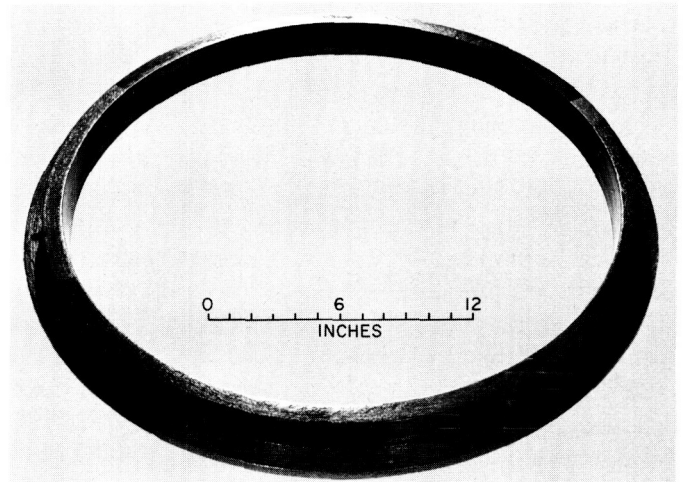


Fig. 31. Mock bearing

make preload practical (and the value is to be held to 0.001 to 0.003 in.), the components will be preassembled and the end interferences measured. From these values the retainer will then be ground to yield the precise preload. Preload is required to maintain a controlled concentricity between the inner and outer shell assembly.

During final assembly of all the components, various assembly aids are required. The mock bearing (Fig. 31) is one of these aids. This item replaces the bearing retainer, ball bearing and the bearing seal in the early stages of assembly. The carbon face is extremely brittle and will nick easily. The mock bearing provides sufficient lead-in to assure safe assembly.

After assembly, the vendor will perform proof pressure and leakage testing. The dynamic and life testing will be conducted at JPL.

D. Ranging System Development

1. Transponder Ranging System

a. Stored program controller. The stored program controller (SPC) used in the Mod II ranging equipment now has all the capabilities necessary for completely automatic control of ranging operations and other types of deep space tracking missions. The SPC has been developed to the point where it has many of the characteristics of a small, general-purpose computer, so that it can be used for theoretical studies and data reduction as well as control operations. Capabilities which have been added recently include the arithmetic operations of shift, multiply, and divide, peripheral equipment such as the printer and the paper tape punch, and the control function of program interrupt.

b. Arithmetic operations.

Shift. Eight shift operations have been provided in the SPC, all characterized by a '1' in the tens digit of the op-code. Shifting consists of moving the digits of a word to the right or to the left, by shortening or lengthening the circulation path so that a given digit appears earlier or later, relative to its former phase. Since the words circulate least significant bit first, if a digit appears one pulse period earlier than it formerly did, its weight has been divided by two, while if it appears one pulse period later, its weight has been doubled.

Shift operations can also be categorized as Arithmetic or Logical. In a logical shift, the digits that are shifted out of one end of a register are shifted into the other end, so that no digits are lost, but their positions are changed. This type of operation is used in logical manipulations, such as picking out successive 4-bit groups of a word in the process of converting from decimal to binary. An arithmetic shift, on the other hand, discards the digits that are shifted past the end of the register, and writes zeros into the other end. Thus, an arithmetic shift right is a division by a power of two, discarding quantities less than the value of the least significant bit, 2^{-24} in single precision work. A shift left corresponds to a multiplication by a power of two, until the most significant nonzero digit of the word passes into the sign position, at which time the process becomes a doubling modulo 2. Since this is an abnormal result, on arithmetic shifts the overflow indicator will be turned on if the sign digit changes on the left shift.

Another specification to be made is the register or registers involved in the shift. The accumulator (AC) can be shifted by itself in arithmetic shifts; the multiplier-quotient register (MQ) can be shifted by itself in logical shifts; and the AC and MQ can be coupled together as a double-length register for either arithmetic or logical shifts. In the case of AC-MQ arithmetic shifts the AC is considered to contain the most significant digits and the MQ the least.

The final specification to be made is the number of places to be shifted. This is accomplished by using the address portion of the order as an exponent or shift control number. The Arithmetic Unit has a five-stage counter which receives the exponent at the beginning of the operation, and then counts backward by subtracting '1' for each shift until the counter contents reaches zero. A zero-detector stops the shifting process and signals completion of the shift.

Following is a listing of the eight shift op-codes, their mnemonic symbols, and a brief description of each:

- 10 (ALS) AC left shift; arithmetic shift, overflow possible
- 11 (ARS) AC right shift; arithmetic shift, no overflow possible
- 12 (LLS) Long left shift; AC and MQ left, overflow possible
- 13 (LRS) Long right shift; AC and MQ right, no overflow possible

- 14 (LGL) Logical left shift; AC and MQ left logical, no overflow
- 15 (LGR) Logical right shift; AC and MQ right logical, no overflow
- 16 (RQL) Rotate MQ left; MQ logical left, no overflow
- 17 (RQR) Rotate MQ right; MQ logical right, no overflow

Double precision shifting operations are possible. If the pertinent registers have been properly loaded with double precision operands, the shift orders will all function properly, treating each register as a 50-bit entity. This brings up a point about the size of the exponent in a shift order. Since 5 bits are provided, the number of shifts is necessarily limited to 31. In a single-precision operation, anything more than 24 shifts will shift the number completely out of the register, so that in the case of ALS and ARS all significance would be lost. In double precision operations, 31 shifts is not sufficient to shift an entire register-length, so if this is desired, two shift orders must be used in succession.

The shift operations are mechanized by changing the length of the register(s), lengthening by inserting an extra delay unit, and shortening by bypassing a delay that is normally used. In the case of a lengthening operation no information is lost; the long path is enabled for one word-time and at the end of that time a pulse copies an end-around digit into the proper location. If the register is shortened, there is not enough space to contain all the digits, so at the start of the enabling step the end-around digit is copied into a storage flip-flop, where it waits until the end of the step, when it is written back into the register.

A shift of one position takes one word-time; since no data selection is made, the operation can proceed as soon as the op-code is recognized. Control unit timing considerations permit a shift of two places in single-precision, (or one place in double-precision) to be made and still select the next order in sequence without loss of time. If more than two shifts are required, the control unit will wait for the order to appear in the next major cycle, so that the full 31 shifts may be performed in one major cycle, single precision, or two major cycles if double precision.

Multiplication. Two basic forms of multiplication operations have been provided, Fraction and Integer. In the fractional case, the number is taken to represent a binary fraction with absolute value less than 1. Taking a 5-bit

number as an example, 01000 equals one-half, the radix ('decimal') point being just to the right of the left-most digit, which is the sign digit. If 01000 is multiplied by itself, i.e., $\frac{1}{2} \times \frac{1}{2} = \frac{1}{4}$, or $01000 \times 01000 = 00100$. More precisely, $01000 \times 01000 = 001000000$, since if two n -digit numbers are multiplied, the product contains $2n$ digits.

In the SPC, one factor is initially loaded into the MQ and the other is called in from memory by the multiply order. The product appears in the AC & MQ, the sign and most significant digits in the AC and the least significant digits in the MQ. In this case the multiplication is a sign and 24 bits times a sign and 24 bits, giving a sign and 48 bits for the product. The sign and the first 24 bits appear in the AC and the least 24 bits, followed by a zero, appear in the MQ.

If the numbers are taken to represent integers, again using 5-bit examples, 00001 has the value '1,' 00101 = 5, etc. Here the multiplication of 1×1 should produce a result of 1, or $00001 \times 00001 = 00000\ 00001$. In fractional notation, $00001 = \frac{1}{16}$, so $00001 \times 00001 = 00000\ 00010$. The result is that the only difference between fractional and integral multiplication is that, in the latter case, the product is shifted one more place to the right. This operation could, of course, be left to the programmer, but it is simple to provide in the design of the unit, and thereby permits the saving of an order.

The algorithm used for multiplication in the SPC can be stated generally as follows: Scan the multiplier (in MQ) starting from the least significant digit. Whenever a 0-1 transition is noted, subtract the multiplicand from the AC. Whenever a 1-0 transition is noted, add the multiplicand to the AC. For a 0-0 or 1-1, do neither. As each digit is inspected, the AC and MQ are shifted right as in LRS, until 24 shifts have been executed (49 in the double precision case). If the operation is an integer multiplication perform one extra shift.

To understand the operation of this algorithm, it is necessary to review the more conventional type of binary multiplication and its analogy to pencil-and-paper arithmetic. Usually, the rule that is followed, especially for positive operands, is to inspect the bits of the multiplier in MQ one at a time, adding the multiplicand each time there is a 1, not adding for a 0, and shifting one place for each step. If there is a group of, say, four 1's surrounded by 0's somewhere in the multiplier, i.e., $\dots 011110 \dots$, the multiplicand would be added four times, once as each '1' was sensed. Now, note that 011110 can be thought of as 100000 minus 000010, so that sub-

tracting the multiplicand as the first 1 was encountered, and then adding when the next 0 appeared produces the same arithmetic result. This modified algorithm, would be particularly attractive for use in a machine that could shift over groups of digits faster than it can add. The serial nature of the Arithmetic Unit in the SPC precludes making efficient use of this property, but it has another beneficial property which dictated its use in this case, namely, that it handles negative as well as positive operands.

In this machine, negative numbers are represented in 2's complement form. That is, the negative of a fraction, "y," is denoted by the binary representation of the number "2-y". If the classical multiplication algorithm is applied to the multiplication of two negative numbers, $(2-y) \times (2-z)$, the result is $4 + yz - 2z - 2y$. The 4 passes out of the register and is of no concern, and the yz term is the desired result. However, correction of $2y$ and $2z$ must be applied before the final result is obtained. One of these corrections is taken care of if the shifting of negative numbers is performed properly, but the other correction generally is handled by noting the sign of the appropriate operand and subtracting the other operand at the right time and place in the register.

In the subtract-add algorithm used in the SPC, this last correction is taken care of automatically by virtue of the fact that the initial operation is a subtraction, and that a right shift of a negative number is not just a division by two, but a division by two and an addition of 1.

Consider the number $-(1/4)$. This will be represented by $2 - 1/4$, or 10.0000 - 00.0100 or 1.1100, which is $7/4$. If this number is shifted right one place, it becomes 1.1110, which is $15/8$. $15/8 = (7/4)(1/2) + (1)$. The number is the correct representation for $-(1/8)$; but the addition of the extra 1 in the shifting operation effects the correction so that this algorithm will produce the correct result for any combination of signs.

The implementation of the algorithm is as follows: the multiplicand is read into the Storage Register (SR) and complemented. The least bit of the multiplier is sensed and if it is a 1, SR is added to AC, thereby subtracting the multiplicand. When the SR is added to AC, SR is complemented again, so that the next time SR is added it will be an addition of the multiplicand. AC and MQ are now shifted right one place, and the least digit of the MQ is compared with the digit that was just shifted out, which was formerly the least digit. If the two bits are different, SR is added to AC and complemented. If they are alike, no action is taken except for another shift.

Thus, each time there is a 1-0 or 0-1 transition, SR will be added to AC and then complemented, so that as these transitions occur the multiplicand is alternately subtracted and added.

A five-stage serial binary counter is provided to count the steps of the operation. A word detector recognizes the 24th count and terminates the main part of the operation. On a fractional multiplication the termination forces a zero in the least significant place of the MQ, while in integer multiplication the termination allows one more shift, thereby positioning the integer result correctly. For double precision operations, an additional binary counting stage is added ahead of the serial counter, so that the serial counter can only advance on odd-numbered steps. The serial unit reaches 24 on the 49th step, stopping the operation at the correct time.

At the start of a multiplication the AC is automatically cleared. If it were not cleared, and the operation proceeded as usual, the result would be the desired product with the old AC contents added to the low-order part of the product. This type of operation has limited utility in polynomial evaluation and number base conversion, so two additional operations have been provided which permit fractional or integral multiplication to be performed without clearing AC. It should be noted that while multiplication cannot normally produce an overflow, these multiply-and-add operations can produce overflow conditions, and the programmer should be cautious when using them.

Summarizing, the four multiplication operations are:

- 60 (MUF) Multiply, fraction
- 61 (MAF) Multiply and add, fraction
- 64 (MUI) Multiply, integer
- 65 (MAI) Multiply and add, integer

Multiplication proceeds at the rate of one word-time per bit in the multiplier, or 24 word-times plus access time for a single precision operation, resulting in 925 or 1725 μsec total time, depending on access time. Double precision uses 49 double word-times, resulting in 2525 or 3325 μsec total time, depending on access time.

Division. As in multiplication, two basic forms of division operations have been provided: fractional and integral. In each case, the dividend or numerator is loaded into the AC by earlier operations and the divide order addresses the divisor or denominator. In all cases

the quotient is produced in the MQ and the remainder in the AC. All combinations of signs can be handled, the remainder receiving the sign of the dividend and the quotient receiving a positive sign if the original operands had like signs and a negative sign if the operand signs were unlike. The reason for the remainder sign convention is that the remainder may be divided again by the divisor to produce additional quotient digits if more significance is required.

Many other computers show little interest in the remainder, generally preferring to round the quotient according to some rule which produces the smallest possible bias and to ignore the remainder completely. A critical operation in planetary ranging transponder missions involves dividing the expected range by each code component length in turn, and shifting that component according to the remainder. Thus, it can be seen that if we had to make a choice, we would have to choose the remainder and ignore the quotient. Fortunately we can retain both, but it is essential that the remainder be correct.

The algorithm used consists of comparing the dividend and the divisor, subtracting the divisor if it is equal to or less than the dividend. If the divisor is subtracted, a '1' is written into the least bit of the MQ. Then the AC and MQ are shifted left one place and the process repeated. Steps are counted in the counter used in multiplication, terminating after 24 bits of quotient have been determined.

The treatment of negative numbers by this basic algorithm would be rather complicated, so some preliminary operations are performed to convert the operands to positive form, and position them properly for the division. Afterward, terminating operations are performed to recompute the results as indicated by the sign conventions. There are other algorithms which can be used to process the various sign combinations, but they generally require additional steps to retrieve the remainder, or their strategy would not be applicable to the basic structure of the SPC.

Just after the preliminary steps (called rectification and positioning), a comparison is made to see if the initial dividend is equal to or greater than the divisor, so that the quotient would have a magnitude of 1 or greater. If it is, a Divide Check flip-flop is turned on and the operation is terminated immediately. The Divide Check flip-flop can be interrogated as Input Signal 21027 (DCK). It is reset at the beginning of the next division operation.

The basic divisions assume that the dividend is in the AC; integer division is accomplished by moving the dividend into the MQ, clearing AC, rectifying MQ if necessary, shifting AC and MQ left one place and then proceeding with the division. In fractional division the MQ is cleared initially. Both fractional and integral division have a double-dividend option, where it is assumed that the AC and MQ contain a double-length dividend. In this case neither register is cleared, the two are rectified if necessary, shifted left one place if integral division is called for, and then the division proceeds as before.

Summarizing, the four division operations are:

70 (DVF) Divide, fraction

71 (DDF) Divide double, fraction

74 (DVI) Divide, integer

75 (DDI) Divide double, integer

Division is a variable-time operation, requiring one word-time per bit, plus one word-time per '1' in the quotient, plus a variable amount of preliminary and final operation time, depending on the signs and the nature of the operation, as well as access to the divisor. Considering double precision operations, the variation is even larger, so that operation times can vary from 825 to 5625 microseconds. Thus it appears advisable to try to avoid the use of division operations when operation speeds are critical.

c. Peripheral equipment.

Printer. A Hewlett-Packard digital printer has been added to permit the printing of results. A register of 48 flip-flops can be loaded by the computer in various formats, permitting printing of up to 12 decimal digits. The Mod II ranging equipment has an 11-column printer, while the Mod III has a 12-column unit, but the devices are otherwise identical from the programmer's standpoint. Printing modes available include octal, decimal and blank (for extra spacing).

Octal printing is accomplished by merely storing a number in address 22201 (PRO). This loads the register, placing the octal word in the right-most eight columns, and placing blank codes in the other columns, and finally pulses the printer mechanism to initiate its mechanical operation.

Decimal printing requires two steps; first, the lower order six decimal digits are loaded into the right six columns by storing a number at 22202 (PDL), then the

high order five or six digits are loaded into the left columns by storing at 22203 (PDH), which action also initiates the printer cycle.

Blank printing is called for by pulsing signal 23006 (PRB), which loads the entire register with blank codes and then triggers the printer.

Ready signal 21026 (PRR) is false any time the printer is not available for use, as when it is in the process of completing a previous operation. This signal should be tested before attempting a print operation, or the operation may be lost.

Paper tape punch. A Friden (Commercial Controls) paper-tape punch has been added to permit punching tapes in a format which can be read by the SPC tape reader. It punches words consisting of sign and eight octal digits, followed by a space code which signifies that the end of the word is coming, and then a final character which may be a Tab Carriage Return or Stop code, the latter being used as an end-of-file signal.

The Punch subsystem uses a circulating storage register, picking out one character at a time and placing it in a one-character static register. Each time the punch completes one character a new character is transferred to the static register. One additional option is available, that of punching blank tape. This is useful in providing tapes with sufficient leader and trailer to permit easy threading into the reader and spooler.

- (1) Storing a word at 22200 (PUW) initiates the Punch Word mode. If no further action is taken the word will be finished with a Tab code.
- (2) If 23001 (PCR) signal is true any time after the word is sent to PUW, but before the last character is punched, the word will finish with a Carriage Return code, except as noted below.
- (3) If 23002 (PEF) signal is true any time after the word is sent to PUW, but before the last character is punched, the word will finish with a End-of-file (Stop) code, regardless of activity of PCR.
- (4) Any time 23003 (PBT) is true, it erases all other storage in the punch sub-system and causes the punching of blank tape. A single PSE command addressing this signal will cause a single feed-hole to be punched.
- (5) Punch ready signal 21023 (PUR) is false if the punch is not available. It should be tested before any punching operation.

d. Program interrupt.

Need for interrupt. When a stored program controller is to be used in a real-time control application, it is likely to be called upon to perform several unrelated and generally asynchronous tasks. For example, the job which occupies most of its time might be the calculation of power spectra on the basis of data from the planetary radar receiver, but another job would be to supply angle data to the antenna pointing equipment every two seconds. If one man is programming the entire operation he might program interruptions to his spectrum calculations with sufficient frequency that he would always be able to recognize when the next angles are to be needed and provide them on time. However, this is a difficult task to perform, especially when there are a multitude of sub-routines in the main program, all of variable and unpredictable lengths. The job becomes even more difficult when different programmers are involved, and virtually impossible if the main (spectrum) program needs to be replaced at some time later in the day when the mission changes, with the requirement that the angle pointing must continue without pause.

One solution to this sort of problem is to provide a separate piece of hardware for each little job and not try to interlace them into one machine. However, when one machine is capable of doing all the jobs, providing the scheduling could be done, it seems uneconomical to have a multiplicity of machines.

The solution proposed for this problem in most control computers is to provide for an automatic program-interrupt feature (sometimes known as a Sequence Break). Typically, when an interruption is required, at the first safe opportunity, such as the completion of the next operation, the program counter (which tells where the next order is to be found) is transferred to a temporary storage location, and replaced by a previously determined address which forces control of the machine to transfer to that address. Sometimes special hardware is supplied to save all the volatile information, such as the contents of AC, MQ and the index registers that might be used by the interrupting program. In other cases (and this is the approach in the SPC) the preservation of information will be performed by programming, i.e., software rather than hardware. After making sure that no information will be lost in the interruption, the interrupting signal is analyzed to see what action is called for, if a multiplicity of interruptions is possible, the control is transferred to the appropriate subroutine. On completion of this task or tasks a de-interrupt subroutine replaces the information that had been saved, and then replaces the original program counter contents and the main program

continues as if it had not been interrupted. The only way the main programmer would know he was being interrupted would be if he was keeping track of real time and noted that his computation efficiency was somewhat reduced.

Where there are many devices that may interrupt, the problem of priorities arises. If some of the interruptors required very fast servicing, it might be necessary to provide for one interrupt to interrupt another. This generally requires a hardware priority chain and a great deal of storage so that each of the possible interruptors had assigned to it sufficient storage for all the volatile information it will displace. Fortunately, in the operations foreseen for the SPC, it appears that each of the interruptions will be short enough that any other interruptor can wait until the current one is finished. Thus,

one of the SPC interrupt constraints is that only one interruption will be allowed at a time. When the volatile information has been saved, the interrupt analysis program will attempt to ascertain which device interrupted the main program. By interrogating the indicators or signals in order of priority, the highest priority which is active will automatically be serviced first. Generally, upon completion of the high priority interrupt, it will be pertinent to also service any others that are active before returning to the main program, thereby saving the time that would be wasted in replacing the volatile information, performing one operation in the main program and then interrupting and saving everything again.

Mechanization. Fig. 32 shows the logical elements involved in controlling the interrupt operations. To permit signal A to interrupt the program, the programmer sets

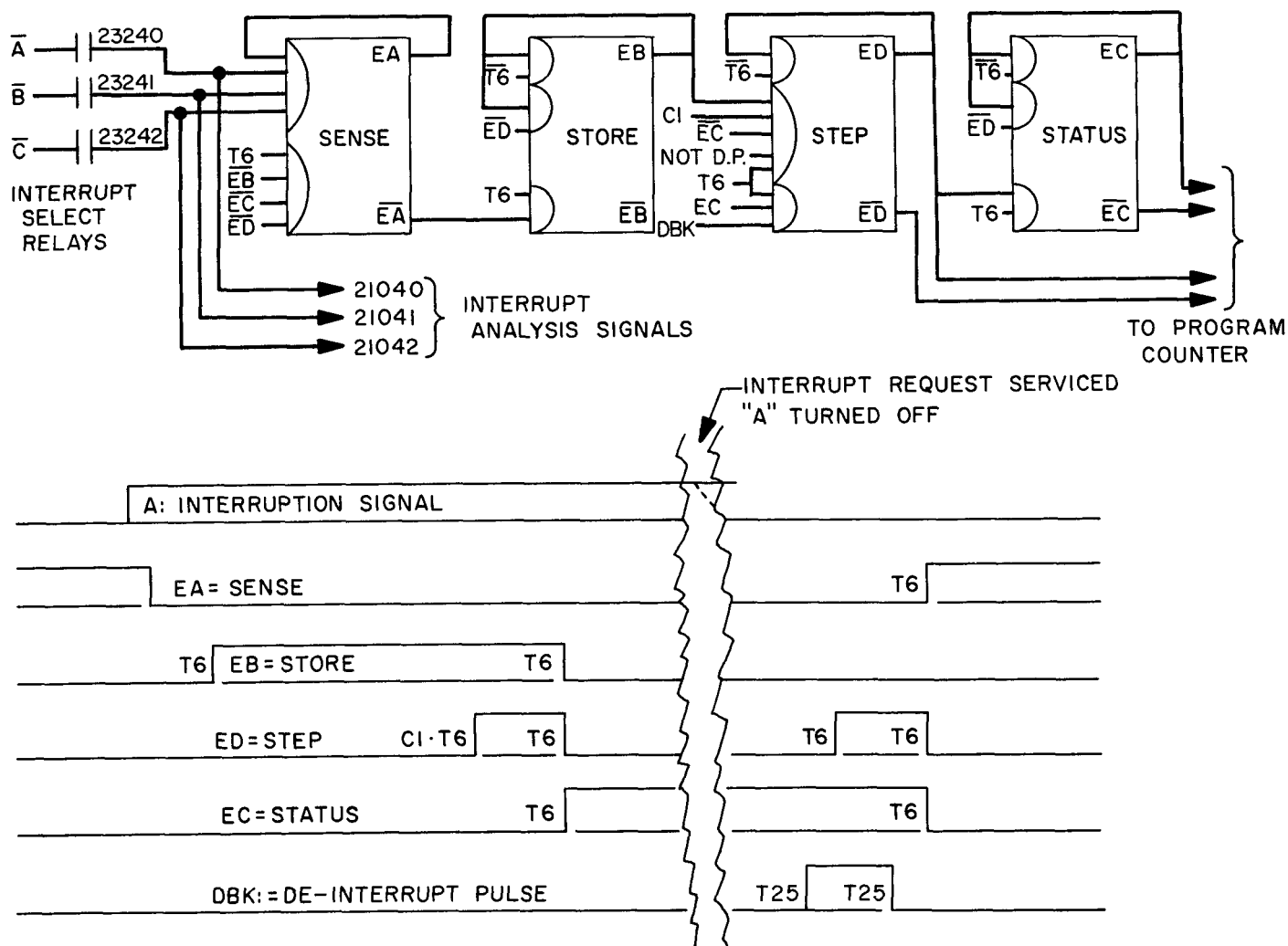


Fig. 32. Interrupt controls

External Output Signal 23040, closing a relay contact which connects the negation output of A to EA, the interrupt sense flip-flop. When A goes true, EA will be reset and input signal line 21040 will go false. The negation output of EA enables EB to set, thereby storing the fact that a request for interrupt has been received. EB then enables gate a on ED, which will eventually perform the interruption. Conditions on ED require that the machine not be in a double precision state, not in interrupt status, and that the control unit be in state CI, the last execute cycle which indicates that all arithmetic operations are complete, the program counter has been replaced if a transfer has been requested, or that the program counter has been incremented on a skip operation. When all these conditions are satisfied, ED comes on for one word-time, resetting EB, setting EC and effecting the displacement of the program counter as will be described shortly.

To terminate the interruption, after replacing all the volatile information, signal 23021 (DBK for De-Break) is pulsed, and ED is again triggered for one word time. This turns off EC, and EA sets again, when EB, EC and ED are all false.

Fig. 33 shows the connections in the control unit. The program counter subsystem consists of the adder CM and CN, interrupt gate CT, storage line CQ, and transfer gate CU. Transfers are effected by erasing the old contents at CU and replacing with new information under control of CK. Normal incrementing and skipping is performed in the serial adder consisting of CM and CN, with increments coming from CL. Interrupt gating is performed at CT.

The first time ED comes on, EC is off, so ED erases CT, copying its contents into EE and EF for storage, leaving a next-order address of 00000. The interrupt program, starting with the information-saving orders, starts at

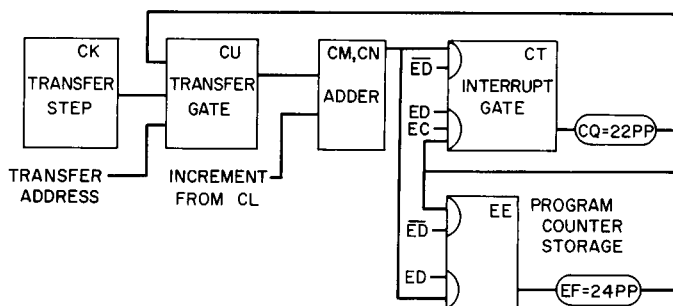


Fig. 33. Interrupt gating

00000. When ED comes on for the second time, when DBK is pulsed, ED with the help of EC exchanges the contents of the program counter storage line and the main program counter line, thereby replacing the previously displaced next-order address. At this time the program resumes its normal course.

The interrupt facility has the capability of accepting up to 10 signals. So far, four have been connected and addresses assigned, and the pertinent addresses have been reserved for the rest of the signals. The four signals now connected are the ready signals from the tape reader, the character read facility of the tape reader, the printer and the punch. This allows these devices to be used on an interrupt basis. Without interrupt, if the programmer wants to print four words, he must test the printer ready signal for each word to be printed and the machine is tied up with this operation until the last word has been transmitted. Using the interrupt, the programmer can send the first word to the printer, select its relay and continue with his computation. When the first printing operation is complete the printer ready signal interrupts the program and allows a subroutine to print the second word and then return to the computation. The process continues until the subroutine recognizes that the last word has been transmitted, at which time it resets the printer's interrupt relay. Similar operations may be performed with the other peripheral devices, so that while computing on one set of data, the machine may be reading in the next set of data, punching out the old answers and printing out intermediate results for monitoring purposes. A simulation of this procedure was tried as a test program to check out the interrupt system. The machine was told to read 100 words from tape, punch 100 words from memory and print 100 words from memory. Since the tape reader is the fastest device it would finish first; next the printer would complete its task, and finally the punch would complete. However, any one of the devices could be disabled, for instance by stopping the tape in the reader manually, and the other jobs would go on to completion. When the tape was released it would go on and finish as if it had not been interfered with.

As other interruptors are defined, addresses will be assigned, and the only wiring necessary will be to connect the negation of the signal into the proper relay contact. Likely prospects include the two-second time tick that indicates a request for antenna-pointing data, in-lock signals from receivers, keying waveforms and similar random, unrelated and/or asynchronous requests for computer operations.

2. Programming and Documentation Support Project for the Stored Program Controller

A major problem confronting the user of a complex equipment is that of determining the state of that equipment and all its component parts. On a device as complex as the Mod III stored program controller (SPC) this is a formidable task and one which would require a great deal of time to accomplish if no mechanical aids were available. Fortunately, the equipment itself can be used as an effective test instrument and diagnostic tool.

Toward this end, programs (lists of instructions) have been written using the machine's internal abilities to aid the user in determining the state of the machine. It is obvious that at some point the abilities of the machine to diagnose and/or determine its own state cannot be trusted. At this point the user must rely on external devices to check the machine's performance.

The list of programs to be described requires only one additional piece of equipment, an oscilloscope, to test the SPC.

These programs start with the assumption that the machine cannot be trusted in any of its actions. The first test, therefore, establishes that the SPC can (1) load from tape, (2) fetch and decode instructions, and (3) display the decoded instructions on the supervisory control panel. The program can further detect certain malfunctions of some operation codes. It cannot, however, completely certify those instructions if no fault occurs.

The second test establishes the operation of an instruction which can be used to test other operations or groups of operations. The TZE or Transfer on Zero Test determines the operation of the op-code completely.

The next few test routines, in like manner, determine the operation of certain basic op-codes. Once these op-codes have been checked they can be used to test more complicated operations, such as multiply and divide.

Tests already written, are listed below in the order of their use:

- (1) OP code indicator test
- (2) TZE test
- (3) Add-sub test
- (4) TPL, TMI, add-sub test
- (5) CAS test

- (6) Index tests
- (7) Sequential memory test
- (8) Logic operations test
- (9) Multiply tests
- (10) Random memory test
- (11) Single precision integer divide test
- (12) Single precision divide/mult test
- (13) Single precision $+/-$ div/mult test (single loop)
- (14) Single precision $+/-$ div/mult test (double loop)
- (15) Double precision $+/-$ div/mult test
- (16) Double precision positive divide count test
- (17) Output relay test
- (18) Input-output auxiliary tests

The programs on this list, while insufficient to test the complete machine, do provide an adequate basis for determining the operation of the machine.

It should be pointed out that, with few exceptions, the programs listed can be used for both the diagnostic or operation testing of the machine as well as for the exercising (i.e., reliability testing) of the machine.

3. Strong Signal Sideband Discriminator

Acquisition of a telemetry modulated RF carrier by a phase-lock receiver is generally susceptible to spurious sideband locking effects. A subsystem capable of discriminating within certain limitations against virtually any type of modulation suitable for carrier tracking has been developed and subjected to preliminary tests. For a more detailed introduction to this problem, the reader is referred to *SPS No. 37-21*, Vol. III, p. 80. The primary limitations of the discriminator are:

- (1) Signal strength must be somewhat above predetection threshold.
- (2) The fundamental frequency of any subcarrier must exceed the loop bandwidth but not exceed the predetection half-bandwidth.

The system as presently assembled for initial evaluation consists of an S-band test transmitter, conventional receiver carrier and AGC loops, frequency discriminator and square law detector at 455 kc, synchronous lock

detector, control and indicator logic, and an acquisition ramp generator (Fig. 34).

a. Discriminator development. The design concept to be discussed is that of a semi-automatic RF carrier acquisition system with the ability to reject possible sideband locks. The basic function involves sweeping the transmitter (or receiver) through an arbitrary frequency range representing the total uncertainty between received signal and receiver tuning frequencies. During this sweep, the receiver is rendered immune to lock (by means of a loop shorting relay) except in the immediate region of the carrier (discriminator null). Since this null must be

narrower in frequency than twice the lowest modulation component, and the over-all discriminator "S-curve" must exceed the predetection bandwidth, conventional single-stage frequency discriminators are not applicable. For instance, with a predetection bandwidth of 2000 cps and an assumed lowest sideband of 150 cps, this system requires discriminator frequency stability of better than $\pm 0.01\%$ referred to 455 kc as well as a frequency range of approximately 0.5%. Thus, the stability requirements are severe for conventional circuit elements and the frequency range too wide for a crystal discriminator at 455 kc. Therefore, third conversion to 1350 cps has been employed. The above requirements have been readily

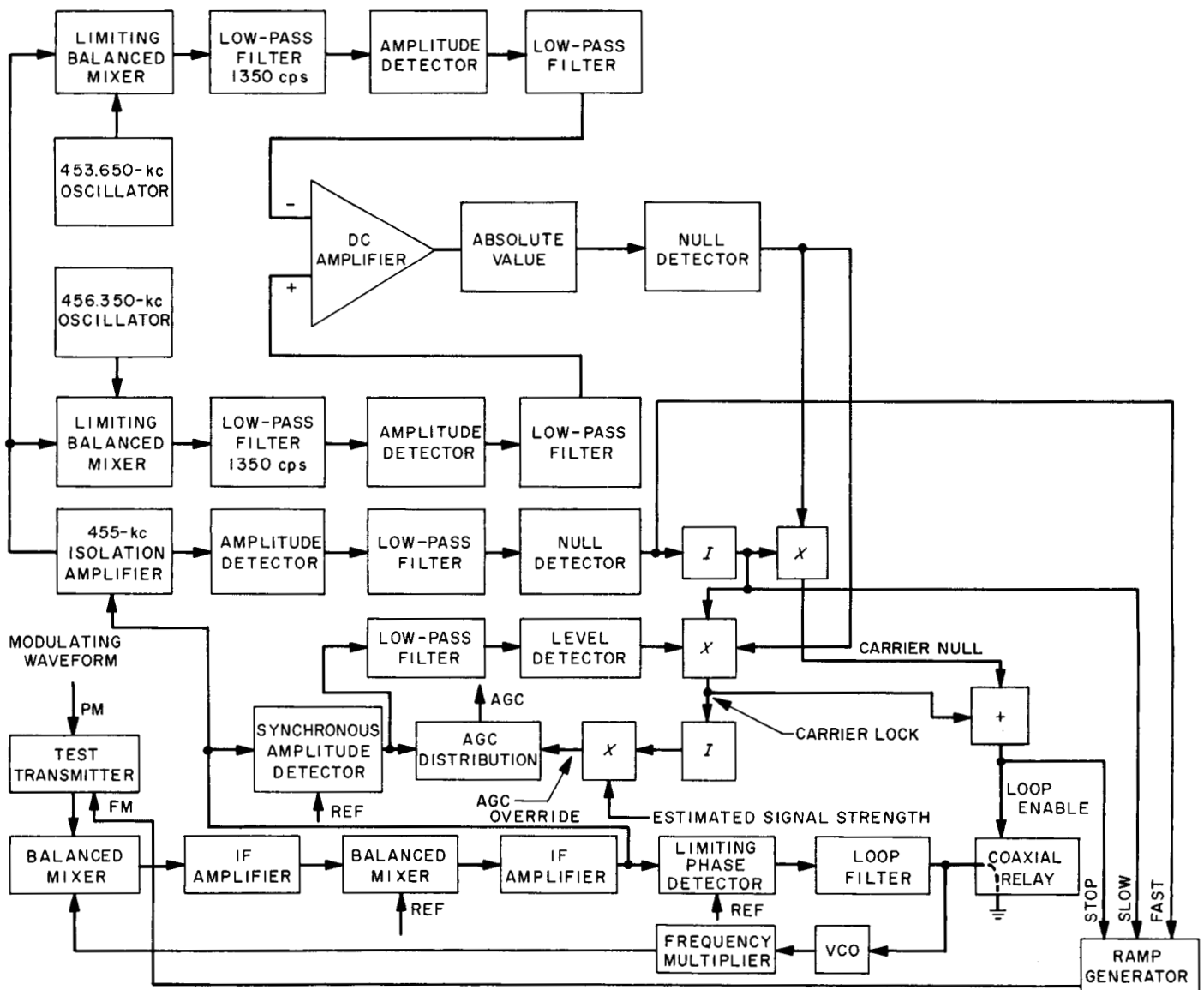


Fig. 34. Sideband discriminating acquisition system

met by means of a pair of double section RC low-pass filters, each operating as a side-tuned frequency discriminator. It was found necessary to provide strong limiting immediately ahead of the diode bridge mixers in order to reduce apparent frequency drift in the output of the discriminator due to slight changes in the self gain of conventional grid circuit limiters. In typical laboratory operation with irregular equipment warm-up times, the over-all stability including dc amplification has been better than $\pm 0.005\%$ with respect to 455 kc of which an appreciable part is attributable to the crystal oscillators.

The analog discriminator output is converted to a switching "carrier null" function by taking the absolute value of the S-curve voltage and level sensing at a value corresponding to ± 75 to 100 cps. Since the function thus generated "nulls" not only in the region of the carrier, but also for frequencies outside the IF passband, it was necessary to logically multiply the null by the output of a square law amplitude detector to provide a unique carrier null. In order that threshold noise not actuate the amplitude detector, and to maintain the discriminator above its threshold, a manual AGC override is provided for presetting receiver gain at some value corresponding to a signal level between that expected and the pre-detection threshold.

The resulting carrier null function directly controls the loop shorting relay which allows loop pull-in within a fraction of a second for strong signal lock of loops with threshold bandwidths of the order of 60 cps, recalling that the half null-width is approximately 75 cps. A conventional synchronous lock detector is employed, which, when the output is logically multiplied by the carrier null, provides a unique *carrier* lock indication independent of the fact that the loop shorting relay should inhibit any other lock. The carrier lock switch disables both the loop shorting function and the AGC override in such a manner as to allow the receiver to perform in a conventional manner to the usual loop threshold.

If the discriminator can be considered to detect the center frequency of a symmetrically modulated signal, then the degree of carrier suppression should not be a major limiting parameter for this system. Indeed, carrier suppression of up to 15 db (relative to total power) for single tone phase modulation has enabled complete functioning of the discriminator and lock indicator. However, two effects of excessive modulation index are: (1) a basic limitation related to discriminator detection of the equivalent FM (discussed in the next section) and (2) failure of the synchronous lock detector to indicate a verified carrier lock. This latter effect occurs even though the sup-

pressed carrier power exceeds that corresponding to the preset estimated signal strength. It is concluded that this is caused by total signal power limiting in the AGC channel. This would imply that the margin of linear range of the channel is somewhat less than 15 db for this particular receiver.

b. Search modes. Considering that an RF carrier frequency search cycle would in general be but one of a number of sequentially interlaced events in a program for the complete acquisition of a complex communication system, a primary requirement of the sideband discriminator and associated functions is that of minimum search and acquisition time. A number of limiting factors have been considered in both the design of the discriminator and in the development of a search program.

Initial evaluation of the discriminator was performed using a periodic linear frequency ramp whose sense was reversed upon reaching an arbitrary limit of search range. In this mode, the sweep rate is limited by the carrier loop transient error since the loop must not only lock at center tuning but continue to track the acquisition ramp. For an absolute upper bound of one radian phase error (strong signal), a practical tracking rate is considered to be that producing about one quarter radian of error.

This sweep rate is given by:

$$\frac{df}{dt} = \frac{1}{4} \frac{\alpha}{\alpha_0} \frac{1}{2\pi} \frac{32}{9} \beta_{L_0}^2 = \frac{4}{9\pi} \frac{\alpha}{\alpha_0} \beta_{L_0}^2 \text{ cps/sec}$$

For $2\beta_{L_0} = 63$ cps and $\alpha_0 = 0.16$, the strong signal ($\alpha = 1$) sweep rate results:

$$\left(\frac{df}{dt} \right)_{loop} = 830 \text{ cps/sec}$$

For a search range, ΔF , of 40 keps (equivalent to a frequency uncertainty of approximately ± 8 ppm at S-band), the search may require up to 96 sec for a full ramp period. While this time could be readily halved by using a unidirectional ramp, the time involved would still be more than an order of magnitude too great with regard to the total system acquisition discussed above. Other limitations, including telemetry response of the receiver, would probably preclude loop bandwidth widening of an amount sufficient to satisfactorily reduce this time.

The first refinement of the sweep program involved a two slope ramp in which a higher sweep rate is used until a signal appears in the IF passband. This is accomplished by using the same amplitude function developed

in connection with the carrier null discussed above. This "no signal/signal" information directly controls the time constant of the ramp generator in a "fast/slow" manner.

To a first approximation, this higher sweep rate is limited to that value which will produce a scanning overshoot of one-half the IF bandwidth in the period corresponding to the total delay time of the "signal" control function. This is approximated as follows:

$$\left(\frac{df}{dt}\right)_{max} \doteq \frac{\frac{1}{2} BW_{IF}}{\tau_{det} + \tau_{relay}} \text{ cps/sec}$$

For a 2.5-msec RF bypassing time constant in the detector, a 5-msec relay operating time, and the 2000-cps IF filter,

$$\left(\frac{df}{dt}\right)_{max} = 133 \text{ kc/sec}$$

The total search period would now be¹

$$T = 2 \frac{\Delta F - \frac{1}{2} BW_{IF}}{\left(\frac{df}{dt}\right)_{fast}} + 2 \frac{\frac{1}{2} BW_{IF}}{\left(\frac{df}{dt}\right)_{loop}} \text{ sec}$$

$$= 0.59 + 2.4 \doteq 3.0 \text{ sec,}$$

using the same parameters that resulted in 96 sec for the single-slope mode. It is evident from the above expression that, for any reasonable value of ΔF , the significant time involved is that of the second term, or the slow sweep within the passband.

This has been significantly reduced by stopping the sweep at the same time and by the same means as the loop is enabled by the sideband discriminator. As described above, this occurs on a steady state basis whenever the tuning is within one-half the carrier null width, Δf , of the center.

Still using a two slope ramp, the "slow" rate may now be increased independently of the loop transient phase error. The maximum for this rate is limited by the discriminator response time:

$$\left(\frac{df}{dt}\right)_{disc} \doteq \frac{\frac{1}{2} \Delta f}{\tau_{disc} + \tau_{relay}} \text{ cps/sec}$$

¹The 2's account for the bidirectional sweep, while the ½'s relate to the fact that the overshoot of the fast rate reduces the approach time of slow sweep to zero in the limit.

Since $\Delta f \leq 2f_m$, where f_m is the lowest expected modulation frequency (taken as 150 cps), the upper limit for a 20-msec discriminator time constant and the 5-msec relay time would be:

$$\left(\frac{df}{dt}\right)_{disc} = 6 \text{ kc/sec}$$

for overshoot to the center of the null.

The total period would now approximate:

$$T_{acq} = 2 \frac{\Delta F - \frac{1}{2} BW_{IF}}{\left(\frac{df}{dt}\right)_{fast}} + 2 \frac{\frac{1}{2} BW_{IF}}{\left(\frac{df}{dt}\right)_{disc}} \text{ sec}$$

$$= 0.59 + 0.33 = 0.92 \text{ sec}$$

This time interval is the equivalent of two unsuccessful unidirectional sweeps in the presence of a signal. A successful unidirectional sweep would require a maximum time of:

$$T = \frac{\Delta F}{\left(\frac{df}{dt}\right)_{fast}} = 0.3 \text{ sec}$$

for the limiting case of signal at band edge and the calculated maximum sweep rate.

While a reduction of time constants and elimination of mechanical devices would theoretically afford significant reduction below this value, this time interval is presently considered to be small compared to other limiting factors in a complete system acquisition program.

Of the several limiting factors in the reduction of the time constants, that associated with the discriminator is interestingly related to the parameters discussed above. Consider the effect upon the carrier null of the equivalent FM detected by the discriminator in the case of large index phase modulation. Defining:

Δf = carrier null width

f_m = fundamental modulation frequency

$\Delta \theta$ = peak phase deviation

$\Delta \theta f_m$ = equivalent peak frequency deviation

As the Δf approaches its limiting value of $2f_{m(min)}$ and the phase modulation index is increased, a new limiting relationship is established for an unfiltered discriminator output wherein the peak-to-peak frequency deviation

equals the null width, thus inhibiting the null function and, as a result, the carrier lock:

$$2\Delta\theta f_m \leq 2f_{m(min)}.$$

In the typical multichannel FM/PM system, the f_m may be as much as five times greater than $f_{m(min)}$ resulting in an unreasonably low limit on the modulation index. In practice, the peak-to-peak frequency deviation output of the discriminator output is filtered, such that:

$$\left| \Delta\theta f_m \right|_{filtered} = \left| \frac{\Delta\theta f_m}{1 + 2\pi f_m \tau_{disc}} \right|$$

The limiting expression now becomes:

$$\Delta\theta \leq \frac{f_{m(min)}}{f_m} \left| 1 + 2\pi f_m \tau_{disc} \right|$$

Fig. 35 illustrates the effect of this limitation.

c. Test results. Although a digitally programmed ramp function is contemplated for further tests, all testing to date has been accomplished using an analog ramp generator. It has been modified during the discriminator development to provide the appropriate two slope rates including the ramp stop function. The basic design of the ramp generator did not lend itself to synchronized unidirectional sweeps which have been discussed in the previous section. However, the maximum acquisition times to be expected have been approximated by placing the signal in the center of the search range and measuring the actual time from disable of lock to relock (one-half full search period). The following tabulation relates the various sweep rates to the actual sweep rates used.

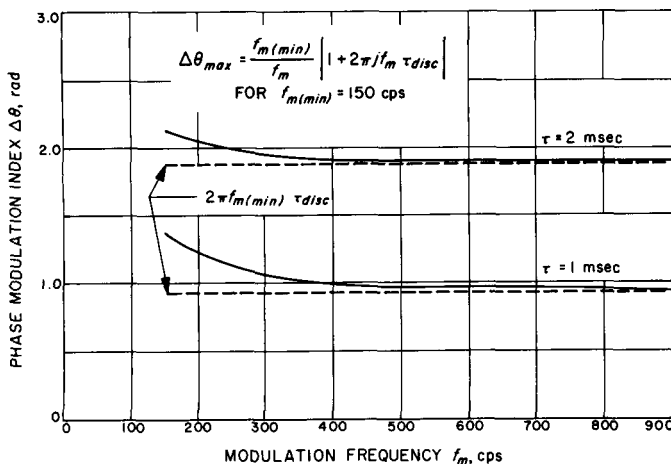


Fig. 35. Maximum allowable modulation

The test value sweep rates are derated from the maxima to allow stability margins and to approach 100% probability of acquisition.

	Calculated maximum, kc/sec	Measured maximum (100% lock), kc/sec	Test value, kc/sec
$\left(\frac{df}{dt}\right)_{fast}$	133	120	80
$\left(\frac{df}{dt}\right)_{disc}$	6	5	4

Fig. 36 presents measured acquisition times for several arbitrary search ranges. Taking into account the reduced sweep rates actually used, the measured acquisition time for a 40-kc search range may be predicted as follows:

$$T = \frac{\Delta F - \frac{93}{133} BW_{IF}}{\left(\frac{df}{dt}\right)_{fast}} + \frac{\frac{93}{133} BW_{IF}}{\left(\frac{df}{dt}\right)_{disc}}$$

$$= 0.833 \text{ sec}$$

The mean value recorded for this condition was approximately 0.95 sec (from Fig. 36).

All references to acquisition time (both predicted and measured) thus far have not included time delays of the

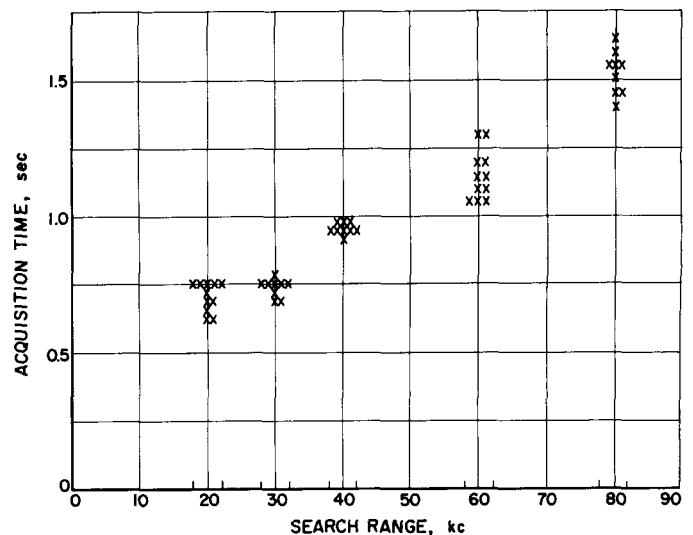


Fig. 36. Measured acquisition times for signal centered in search range

lock indicator or of AGC settling time. In these tests, time constants of 0.4 sec and 4 sec were used for the lock detector and the AGC open-loop time constants, respectively. Measured time delays with respect to time of lock were typically $\frac{1}{4}$ sec for the lock indicator and removal of AGC override plus an additional $\frac{1}{4}$ sec of AGC settling time. Thus, a successful search cycle would require $\frac{1}{2}$ sec in addition to acquisition (search and lock) time before initiation of a subsequent operation.

Although the acquisition times were measured using a single modulating tone of 300 cps with a modulation index of 1 rad, sideband discrimination capability at these sweep rates has been tested, for single and double tone phase modulation, for frequencies from 100 to 1000 cps with total carrier suppression up to 15 db.

Brief tests have been conducted using 100% square wave amplitude modulation at fundamental rates of the order of 200 to 300 cps. While acquisition times are somewhat greater, for the same sweep rates, due to earlier slowing of the sweep by higher order odd harmonics entering the passband, satisfactory immunity to sideband locking was demonstrated.

E. Data Signals Discrimination

1. Precision Signal and Noise Mixing System

Determining the performance of a detection system for a data signal in white gaussian noise requires a system which is capable of driving the detector with the sum of the data signal with power S and white gaussian noise with spectral density N_0 . This report describes such a system.

a. Design considerations. Primary design considerations for the mixing system were the requirements for (1) linear operation over a wide range of signal and noise levels, including the capability of driving loads as low as 200 ohms, (2) precision and simplicity in measuring and changing the signal power and the noise spectral density at the detector input, (3) flat frequency response over at least a 10-cps to 100-kc frequency range, and (4) use of commercially available equipment to reduce the development time and cost of the mixing system.

b. Mechanization. A functional block diagram of the mixing system is shown in Fig. 37. Fig. 38 is a photograph of the completed system.

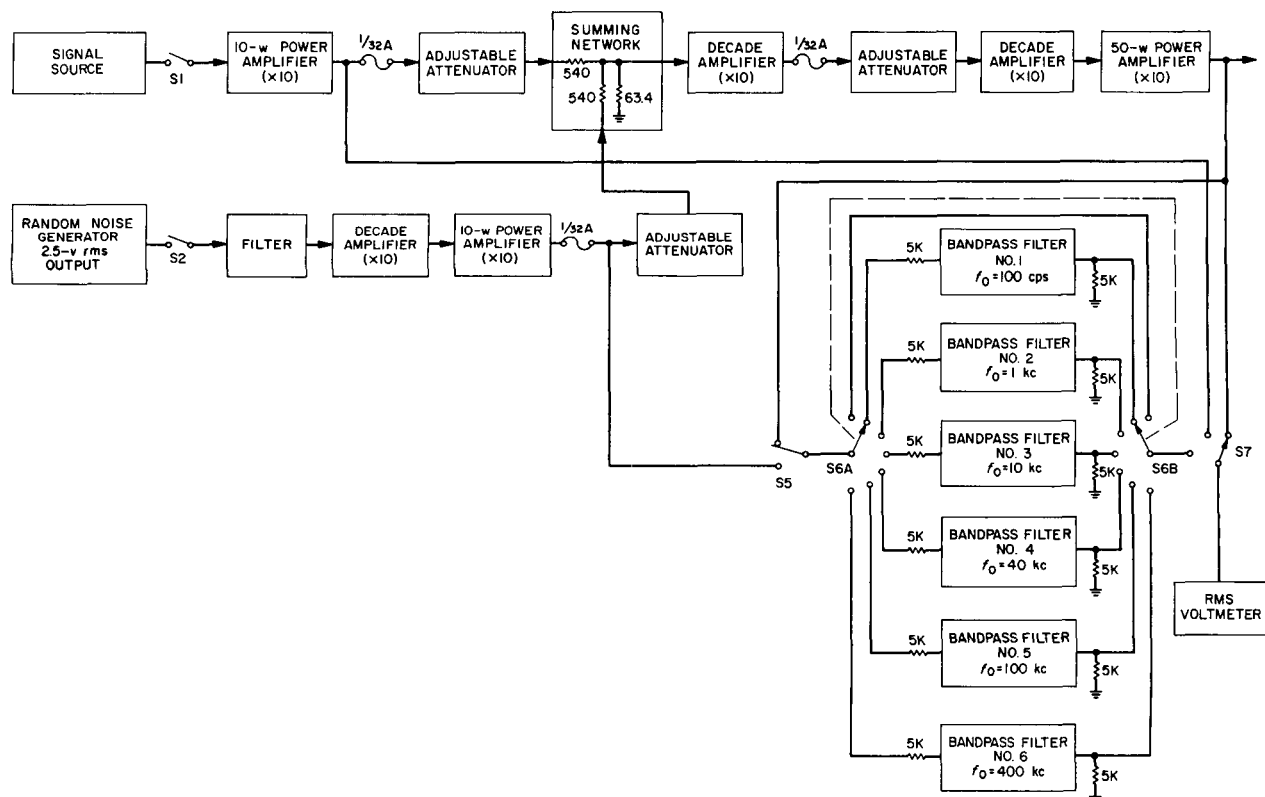


Fig. 37. Precision signal and noise mixing system functional diagram

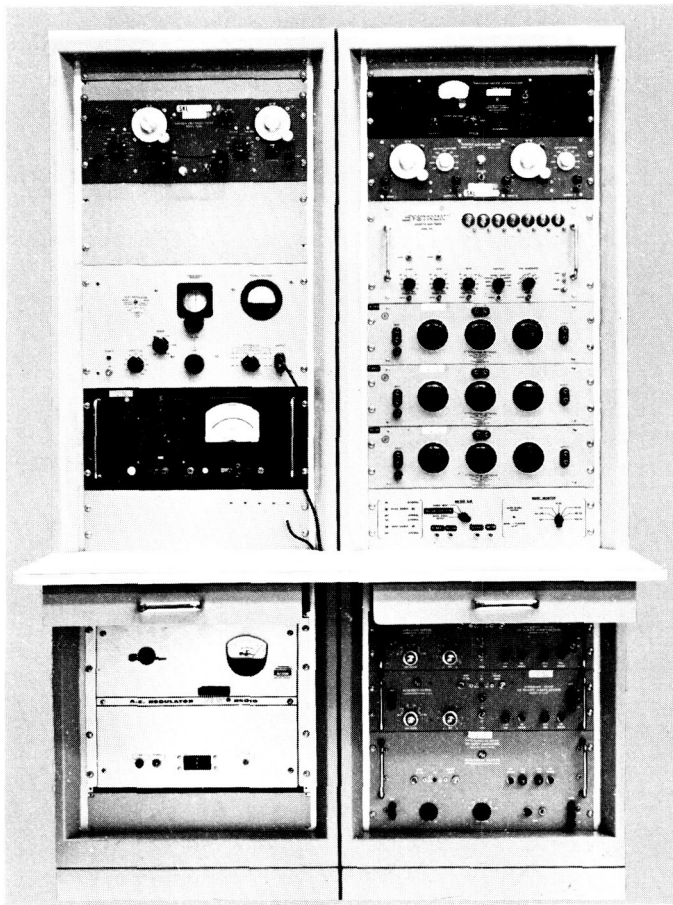


Fig. 38. Precision signal and noise mixing system

A signal source external to the mixing system drives a 10 w power amplifier to provide a 20 v rms signal into the 600-ohm load of the precision attenuator.

A generator of the gas tube type, internal to the mixing system, provides a source of white gaussian noise. A variable low-pass or bandpass filter allows the experimenter to concentrate the noise power from the system over a selectable bandwidth as in Fig. 39. The output

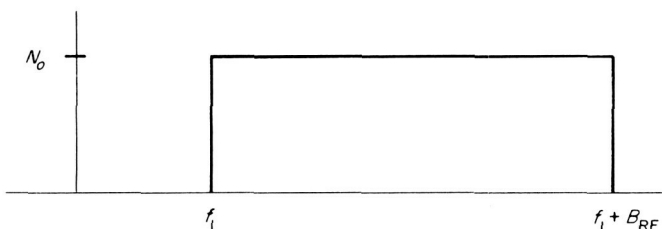


Fig. 39. Noise spectral density at the mixing system output

of the filter is amplified in two stages to provide a 20-v rms signal into the 600-ohm impedance of a second precision attenuator.

A passive summing circuit, which presents a fixed 600-ohm load to both attenuators, combines the data signal and the noise signal. A third attenuator between two stages of amplification provides a means of adjusting the level of the mixed signal without altering the signal-to-noise ratio. A 50-w power amplifier provides the required output levels.

Provision is made to monitor, via S5 and S7, the signal at the outputs of the 10-w amplifiers and at the output of the 50-w amplifier with an rms measuring voltmeter. The meter may monitor the signal directly or via a bank of six bandpass filters whose noise bandwidths are known. The filters are calibrated in such a manner that if the

Table 10. Mixing system equipment specifications

Random noise generator	
H. H. Scott, Model 811-B	
Output voltage, 0 to 2.5 v rms	
Frequency response, ± 1.5 db, 2 cps to 800 kc	
Variable filter	
Spencer-Kennedy Lab., Model 302	
Low-pass, or high-pass filter (two sections)	
Frequency range, 20 cps to 200 kc	
Insertion loss, 0.0 db ± 1.0 db, 20 cps to 20 kc	
0.0 db ± 2.0 db, 20 kc to 200 kc	
Decade amplifiers	
H. H. Scott, Model 140-BR	
Gain, $\times 1$, $\times 10$, $\times 100$	
Frequency response, ± 1.0 db, 1 cps to 1 Mc	
10-w power amplifiers	
Kron-Hite Model DCA 10R	
Output voltage, 120 v rms (no load)	
Frequency response, ± 1.0 db dc to 1 Mc	
Gain $\times 1$, $\times 10$	
50-w power amplifier	
Kron-Hite Model DCA 50	
Output voltage, 130 v rms (no load)	
Frequency response, ± 1 db dc to 500 kc	
Gain, $\times 1$, $\times 10$	
Precision attenuators	
Daven Model VT-795-6	
Attenuation, 0 to 111.0 db in 0.1-db steps	
Frequency response, ± 0.5 db dc to 1 Mc at 90-db attenuation	
Accuracy, ± 0.1 db at 1000 cps	
Monitor filters	
Airpax Electronics Model BP-577-(f_0)	
Center frequency (f_0) (100 cps, 1 kc, 10 kc, 40 kc, 100 kc, 400 kc)	
Half-power bandwidth (approximately $0.1 f_0$)	
Characteristic impedance, 5 k	
Meter	
Ballantine Model 320	
Frequency range, 5 cps to 500 kc	
Accuracy, 3%, 15 cps to 500 kc	
5%, 5 to 15 cps, 150 to 500 kc	
Crest factor, 4.5 (min)	

voltage at the filter input is white and the output voltage is V , then the noise spectral density is

$$N_o = \frac{V^2}{B_n} \frac{v^2}{\text{cps}}$$

where B_n is the noise bandwidth of the filter.

Table 10 contains a brief summary of the component specifications of the mixing system.

For testing and calibration the console shown in Fig. 38 also contains a Hewlett-Packard Model 650 test oscillator, a Model 400HR ac voltmeter, and a Systron Model 1031 counter and timer. A Sorenson voltage regulator is employed to reduce amplifier gain variation and similar changes produced by 60-cps line voltage changes.

c. Constraints and performance. A critical constraint in the use of a wideband signal and noise mixing system is the maximum rms output voltage, V_o , and the maximum peak output voltage, V_{op} , which the mixing system can deliver without appreciable distortion. Amplifiers presently available are designed with a crest factor (V_{op}/V_o) of $2^{1/2}$.

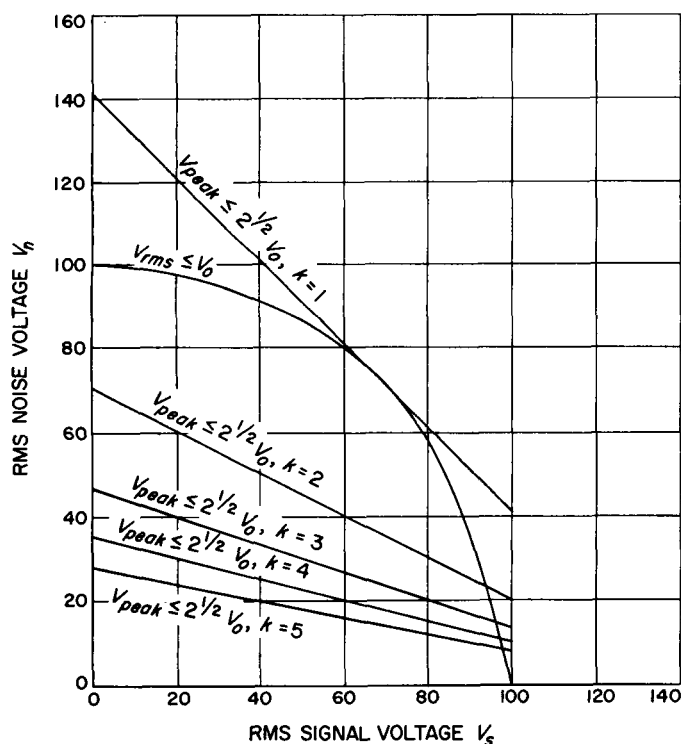


Fig. 40. Rms noise voltage versus rms signal voltage for various total output voltage constraints:
 $V_o = 100$ v rms, square wave data signal

Assuming Fig. 39 represents the noise spectrum and V_s and V_n represent the rms data signal and noise voltages at the mixing system output, and B_d is the bandwidth of the detection system,

$$\left(\frac{S}{N}\right)_{B_d} = \frac{V_s^2 B_{RF}}{V_n^2 B_d}$$

Then, if we require

$$V_{rms}^2 = V_s^2 + V_n^2 \leq V_o^2$$

for any specific data signal voltage, the maximum noise output voltage is

$$V_n(\max) = (V_o^2 - V_s^2)^{1/2}.$$

If we require that

$$V_{peak} = V_{np} + V_{sp} \leq V_{op} = 2^{1/2} V_o$$

where $V_{np} = kV_n$ and V_{sp} is the peak signal voltage, for a square wave signal, $V_{sp} = V_s$ and for any particular signal level, V_s ,

$$V_n(\max) = \frac{2^{1/2} V_o - V_s}{k}$$

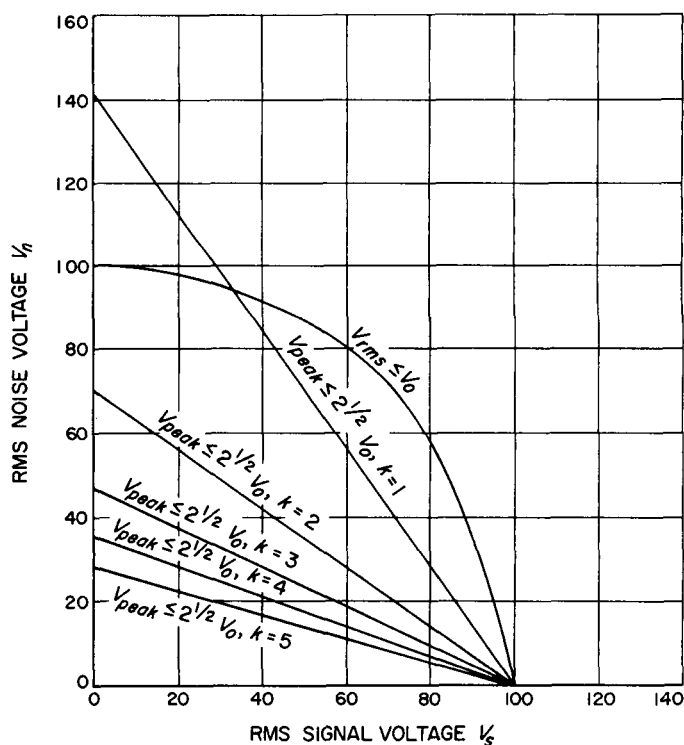


Fig. 41. Rms noise voltage versus rms signal voltage for various total output voltage constraints:
 $V_o = 100$ v rms, sine wave data signal

For a sine wave signal $V_{sp} = 2^{1/2} V_s$, and

$$V_n(max) = \frac{2^{1/2}(V_o - V_s)}{k}$$

The power amplifier which appears to be best for our application is the Kron-Hite Model DCA-50R with $V_o = 100$ v for a 200-ohm load and $V_o = 130$ v for no load. Figs. 40 and 41 present the constraints for $V_o = 100$ v rms and square wave and sine wave signals. Figs. 42 and 43 present the corresponding results for $V_o = 130$ v rms.

Defining B_{RF}/B_d as the bandwidth expansion, clearly

$$\left[\frac{\frac{B_{RF}}{B_d}}{\left(\frac{S}{N}\right)_{B_d}} \right]_{max} = \frac{V_n^2(max)}{V_s^2}$$

which by substituting one of the constraints derived above may be written in the form

$$\left[\frac{\frac{B_{RF}}{B_d}}{\left(\frac{S}{N}\right)_{B_d}} \right]_{max} = F\left(\frac{V_o}{V_s}\right)$$

$F(V_o/V_s)$ is plotted in Fig. 44 for a square wave signal and in Fig. 45 for a sine wave signal for various constraints.

The over-all frequency response of the signal channel and the noise channel has been measured and found to be flat ± 0.1 db over a 10-cps to 100-kc frequency range. Performance above 100 kc is at present unsatisfactory.

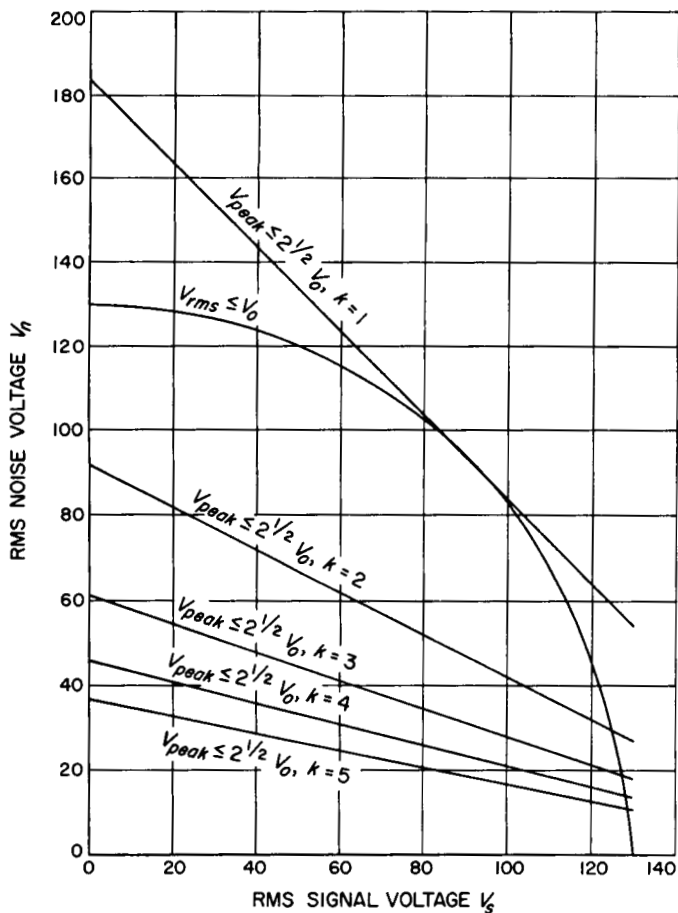


Fig. 42. Rms noise voltage versus rms signal voltage for various total output voltage constraints: $V_o = 130$ v rms, square wave data signal

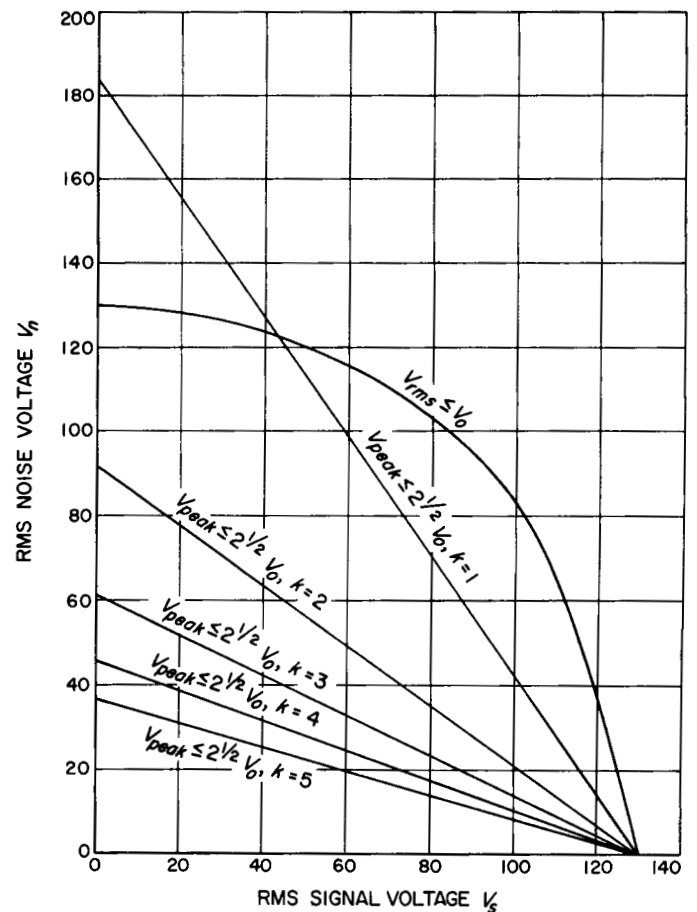


Fig. 43. Rms noise voltage versus rms signal voltage for various total output voltage constraints: $V_o = 130$ v rms, sine wave data signal

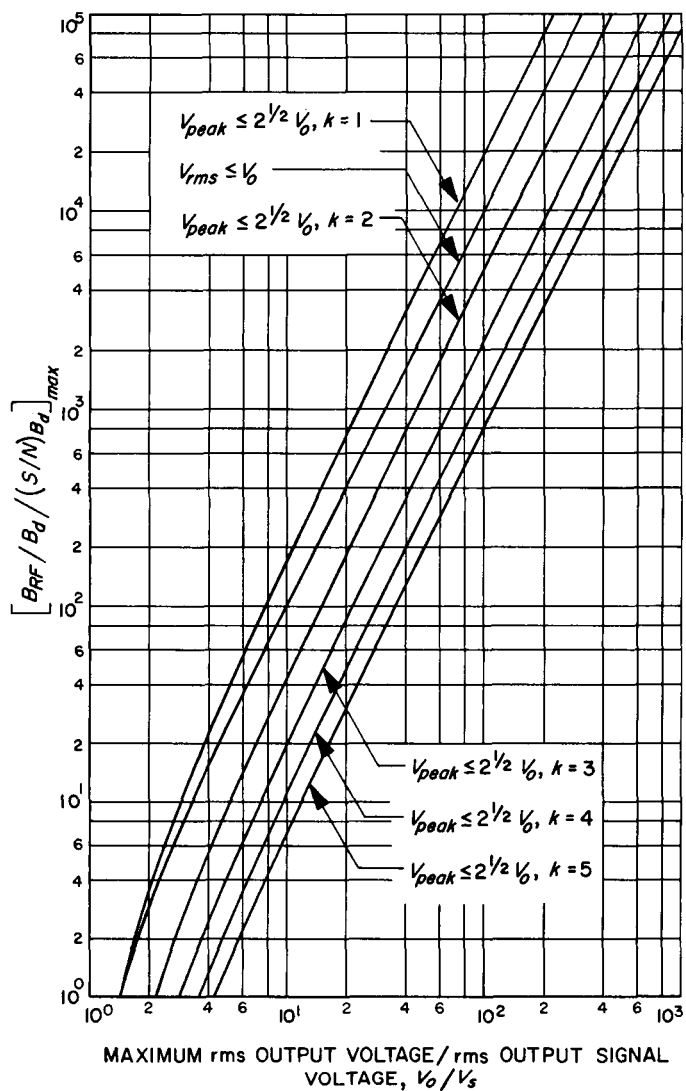


Fig. 44. $\left[\frac{B_{RF}/B_d}{(S/N)B_d} \right]_{max}$ versus V_o/V_s for various output voltage constraints: square wave data signal

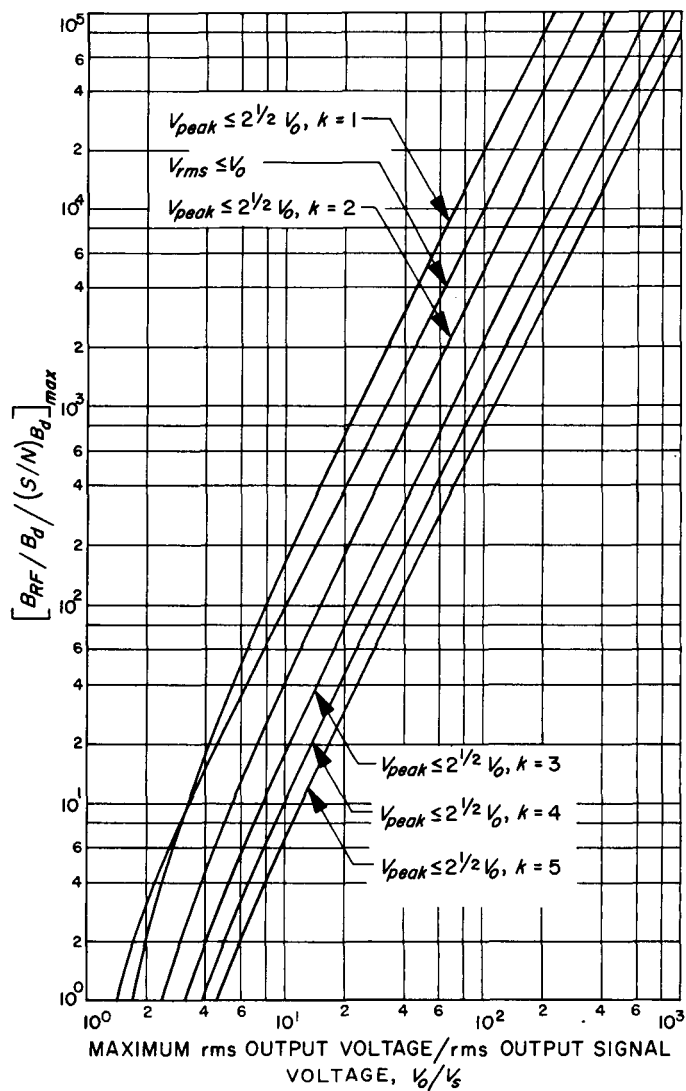


Fig. 45. $\left[\frac{B_{RF}/B_d}{(S/N)B_d} \right]_{max}$ versus V_o/V_s for various output voltage constraints: sine wave data signal

References

1. Potter, P. D., "A New Horn Antenna with Suppressed Sidelobes and Equal Beam-widths," *The Microwave Journal*, Vol. VI, No. 6, pp. 71-78, June 1963.
2. Braun, E. H., "Gain of Electromagnetic Horns," *Proceedings of the IRE*, pp. 109-115, January 1953.
3. Van Vleck, J. H., "Absorption of Microwaves by Oxygen," *Physical Review*, Vol. 71, No. 6, pp. 413-433, March 15, 1947.
4. Hogg, D. C., "Effective Antenna Temperatures due to Oxygen and Water Vapor in the Atmosphere," *Journal of Applied Physics*, Vol. 30, No. 9, pp. 1417-1419, September 1959.
5. Linnes, K. W., Merrick, W. D., and Stevens, R., "Ground Antenna for Space Communication System," *IRE Transactions on SET*, Vol. SET-6, No. 1, March 1960.
6. Stelzried, C. T., "Liquid-Helium-Cooled Coaxial Termination," *Proceedings of the IRE (Correspondence)*, Vol. 49, p. 1224, July 1961.
7. Victor, W. K., Stevens, R., and Golomb, S. W., "Radar Exploration of Venus," (includes reports on maser, radiometer, polarization tests and radiometric tests), Technical Report No. 32-132, Jet Propulsion Laboratory, Pasadena, California, August 1, 1961.
8. Stelzried, C. T., Schuster, D., and Sato, T., "An Experimental 960 Mc Maser Amplifier System Applicable to Space Communications," Technical Report No. 32-179, Jet Propulsion Laboratory, Pasadena, California, November 15, 1961.
9. Schuster, D., Stelzried, C. T., and Levy, G. S., "The Determination of Noise Temperatures of Large Antennas," *IRE Transactions on PGAP*, May 1962.
10. Levy, G. S., and Schuster, D., "Venusian and Lunar Radar Depolarization Experiments," *Astronomical Journal*, June 1962.
11. Private communication by R. Clauss.

IV. Advanced Antenna System

A. Synopsis

Negotiations have been completed on the contract with the Rohr Corporation, Chula Vista, California, for the final design, fabrication, and erection of the first Advanced Antenna System (AAS), and the contract has been executed.

Supporting studies at JPL are continuing on the hydrostatic bearing and the computer program used in the design of the reflector structure. The work initially accomplished by Franklin Institute, Philadelphia, Pennsylvania, under contract to JPL for use in the design of the hydrostatic bearing, is being extended to include the effects of bearing rotational velocity.

Test programs have been run evaluating the internal validity of the RMS computer program utilized for the reflector structure design.

One of the problems requiring consideration in the design of a precision data system, which includes the Master Equatorial, is the nonlinear friction characteristic inherent in worm gear drives. A study has been initiated to evaluate the effect on the Master Equatorial servo system of closing the servo loop around these drives. Test of four typical telescope drives will measure the torque, lash, and spring constant characteristics under operating conditions.

B. Supporting Studies

1. Computer Studies

Abstract. Three sample tests for the rms digital computer program are described. A sample calculation was made for an idealized structure of the DSIF 85-ft HA-Dec antenna. RF ray tracing shows that deflection of the feed-horn is required to minimize the RF boresight error in elevation.

a. Rms digital computer program. In SPS 37-20, Vol. III a rms digital computer program is described which computes the position of the best fit paraboloid to the displaced joints of a reflector structure. The position of the displaced joints may be computed by the STAIR (Structural Analysis Interpretive Routine) computer program (Ref. 1). The computations can be made for gravity, wind, or thermal loads. Alternately, field measurements of actual deformations can be used for inputting the RMS program. The orientation and shape of the best fit paraboloid is based on minimizing the root mean square of the RF path length differences at all the displaced joints, using the reflector areas corresponding to each displaced joint as a weighting function (Ref. 2).

Three different types of test inputs have been synthesized to test the rms program. For Test A, a computer program was coded to calculate the new positions of all

the joints of a perfect paraboloid given an increment of translation in the x -, y -, and z -directions and rotations around the x - and y -axes. Then when the new positions of the joints were input to the RMS program, the resulting best fitting operation resulted (and should result) in a perfect fit with zero normal and RF path length errors at all joints. Also, the computed new orientation of the paraboloid axes was exactly the same as the increments originally used to calculate the synthesized distortions.

For Test B, all the joints were distorted in the z -direction only (for mathematical convenience) to cause at each joint a constant path length difference of 1.0 in. from the original perfect paraboloid. It should be noted that the distortion in the z -direction for a constant path length difference is a function of the radial position of the joint. The signs of the path length differences were made alternately plus and minus throughout the antenna surface. When these distortions were input to the rms program, the result showed that the best fit paraboloid was the original one with no translation or rotation and the resulting rms of $\frac{1}{2}$ path length difference figure as weighted by areas was 0.50 in. when all areas were input as 1.0 relative areas. The printed output also showed that the individual total path length difference at each joint was 1.0 in.

For Test C, 1.0 in. in the z -direction was added to all the z -distortions of the data for Test B. This, in effect, moved the original paraboloid 1.0 in. in the z -direction with all the joints distorted from the new position the same plus or minus 1.0-in. path length difference as per Test B. The rms program gave a best fit paraboloid having the original focal length with no rotation but translated 1.0 in. in the z -direction. Again the errors at all joints were printed out as 1.0-in. path length difference to the best fit paraboloid, thus checking the input data.

As an example, the results of the deflection calculation by a structural computer program for the DSIF 85-ft HA-Dec antenna have been input to the rms program.

Fig. 1 shows the idealized structure. Of special interest in the application of the antenna is the rms error of the reflector surface and the RF boresight direction when the antenna is pointing close to the horizon. Since the reflector panels for the HA-Dec antennas are normally set to the correct paraboloid position at the zenith look, the rms error of the surface is greatest for the horizon look.

When the three-dimensional deflections of the structural joints from the computer program were input to the rms program, it computed:

- (1) The rms of the surface error.
- (2) The new vertex position of the best fitted paraboloid.
- (3) The rotation of the axis of symmetry of the best fitted paraboloid with respect to the original coordinate system.

The structural condition selected was with the declination axis horizontal. To satisfy the panel setting conditions, the resulting joint deflections were the algebraic differences of the zenith-look gravity "off-on" deflections subtracted from the horizontal-look gravity "off-on" deflections. Table 1 is a summary of the results.

Table 1. 85-ft HA-Dec antenna horizontal look gravity deflections with reflector surface set at zenith look

Joint No.	Deflection, in.			Error to best fit paraboloid, in.	
	x	y	z	Normal	Path length
1	-0	-0.163	0.125	-0.047	-0.094
2	-0.001	-0.170	0.118	-0.046	-0.093
3	-0.001	-0.170	0.100	-0.047	-0.094
4	0.006	-0.168	0.074	-0.049	-0.098
5	0.002	-0.167	0.050	-0.049	-0.097
6	0.002	-0.166	0.034	-0.047	-0.094
7	-0.002	-0.167	0.050	-0.049	-0.097
8	-0	-0.233	0.348	-0.046	-0.087
9	-0.011	-0.249	0.375	0.021	0.040
10	-0.012	-0.248	0.265	0.011	0.021
11	-0.009	-0.247	0.063	-0.054	-0.102
12	-0.006	-0.237	-0.067	-0.050	-0.094
13	-0.009	-0.219	-0.114	0.005	0.010
14	-0	-0.218	-0.128	0.026	0.049
15	-0	-0.388	0.669	-0.021	-0.036
16	-0.016	-0.437	0.712	0.107	0.184
17	-0.027	-0.436	0.486	0.090	0.155
18	-0.023	-0.417	0.101	-0.007	-0.012
19	-0.026	-0.391	-0.179	-0.003	-0.006
20	-0.036	-0.339	-0.291	0.100	0.172
21	-0	-0.334	-0.357	0.106	0.182
22	0	-0.604	0	—	—

Rms computation data

Rms of idealized structure after best fitting of original focal length paraboloid = 0.052 in.

Vertex coordinates of the best fitted paraboloid

$x = 0$ in.

$y = 1.880$ in.

$z = 0.123$ in.

Rotation of the best fitted paraboloid about the x -axis = 0.00319 rad.

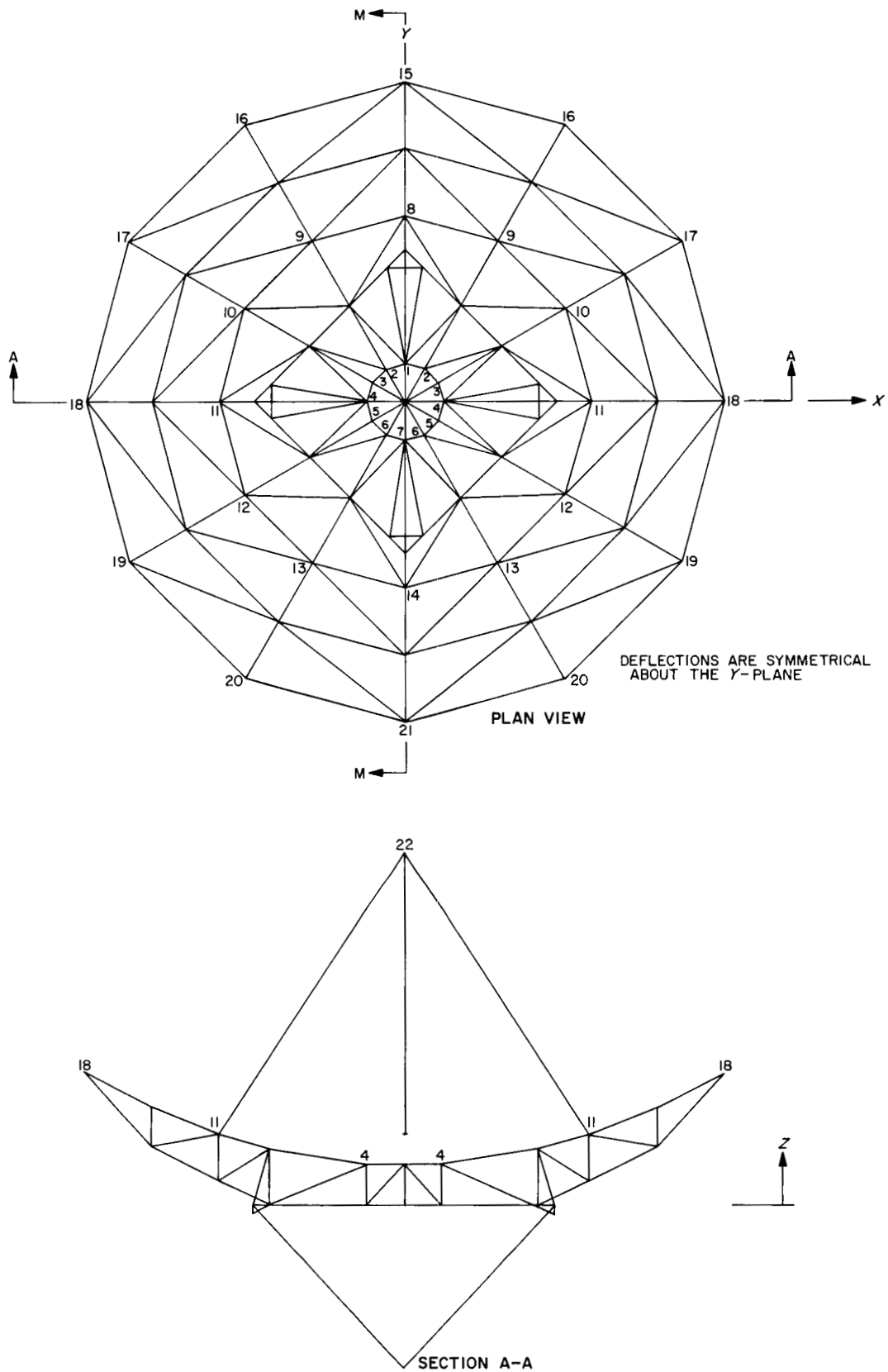


Fig. 1. Idealized reflector structure 85-ft HA-Dec antenna

It is important to note that the rms figure is based on the idealized structure assuming that:

- (1) There is no looseness in the joints of the structure.
- (2) Common joint bars intersect at a point: i.e., no bending moments in the bars.
- (3) Slightly curved bar members are assumed to be straight.
- (4) The initial field setting of the reflector panels is perfect.
- (5) Reflector panels contribute no errors to the surface accuracy.
- (6) Position of the RF feed introduces no errors in surface accuracy.

Further checks are planned to be made using the larger STAIR structural computer program and actual field data using optical tools and wire extensimeters.

Fig. 2 shows the orientation of the best fit paraboloid with respect to the original undeflected paraboloid. It appears that a deflection of the feedhorn would minimize the RF boresight error in elevation. For the idealized structure, Y-motion of the feed position from the original point must be about 1.00 in. for the boresight error to be zero at horizontal look. This 1.00 in. will be the sum of the deflections of the feed support connections to the dish structure (0.60 in., see Table 1) plus the deflection of the feedhorn on the feed support itself. The 1.00 in. was calculated by assuming that the RF reflection angle off the vertex of the paraboloid is approximately 90% of the angle of incidence.

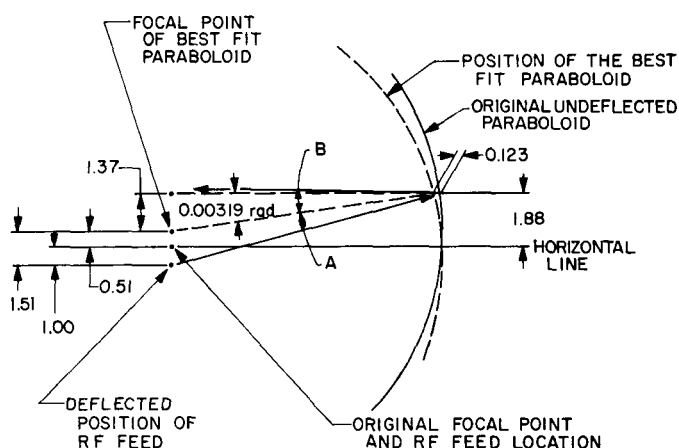


Fig. 2. 85-ft HA-Dec horizontal-look RF ray tracing

2. Extension of Work with the Hydrostatic Bearing Computer Program

Abstract. Further work with the computer program for the analysis of hydrostatic bearings (Ref. 3), which was developed by the Franklin Institute under contract with JPL, has been directed toward investigating the effects of various grid spacing and truncation constants used in the numerical solution of the Reynolds equation; and in correlating results from the digital program, using a constant film height, with the results of work done at Franklin Institute on the same problem using resistance paper and analog techniques (Refs. 4 and 5). The conclusions of the present work are that modifications to the program to permit more iterations in the Reynolds equation solution are desirable, particularly for smaller grid sizes. Fair correlation was found between digital and analog analysis of bearing systems with constant film height. Collateral work is being done at the Franklin Institute under an extension of their original contract to include the effect of velocity on the pressure pattern.

a. Grid and truncation studies on rectangular pad.

A pad of the basic proportions shown in Fig. 3 was used. This permitted using grid intervals of $L/64$, $L/32$ and $L/16$ where L is the length in the x -direction, while maintaining the same relative proportions and placement of the recesses. Analyses were made with truncation constants in the iteration routine of 0.001, 0.0001, and 0.00001 for each grid interval and for uniform film height and for tilts of 0.5 and 1.0. All runs were made for bearings with fixed flow to each recess.

The various input factors and the resulting output data are given in Table 2.

No significant difference was found in the convergence characteristics for the uniform film height and tilted cases as indicated by the number of iterations required for convergence. The 300 iterations available within the program did not produce answers for the 0.00001 truncation constant on the finer meshes ($L/32$ and $L/64$). The final pressures and loads for the finer meshes do not appear to represent any approach to an asymptote, indicating a lack of convergence within the available number of iterations.

b. Analog correlation. The analog studies (Ref. 4) were based on a square pad with four symmetric recesses as shown in Fig. 4. For this configuration, pressure coefficients, p_f , and flow coefficients, q_f , were plotted as a function of the ratio a/l which defines the relative size

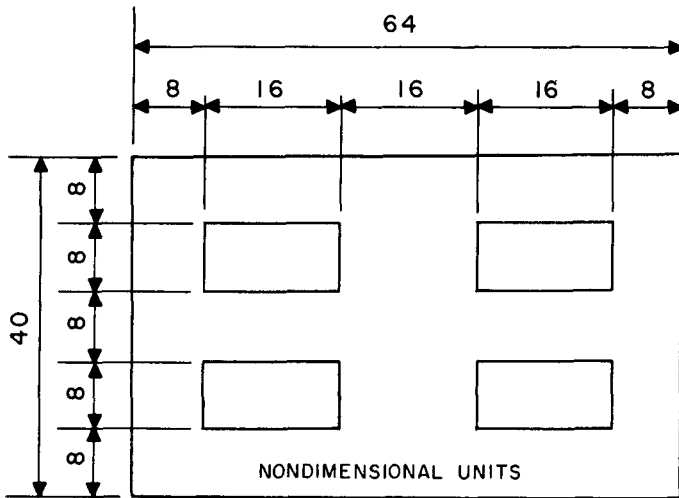


Fig. 3. Pad configuration—convergence studies

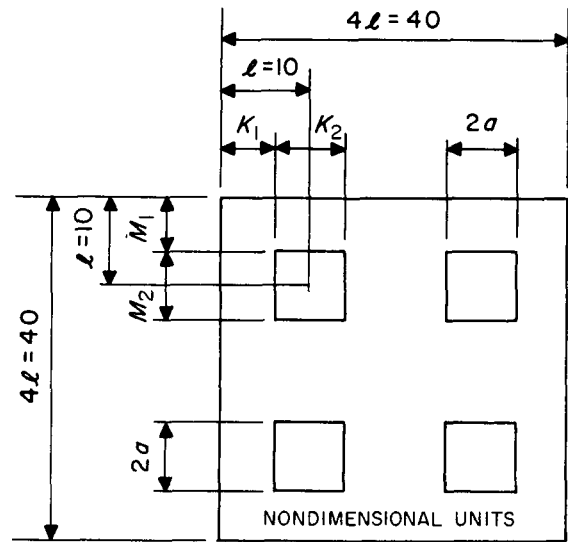


Fig. 4. Configuration for analog comparison

of the recesses. Using these coefficients, the actual recess pressure for a real bearing is:

$$p_s = p_l \frac{w}{16l^2}, \quad (1)$$

and the actual flow:

$$Q = q_l \frac{w}{16l^2} \cdot \frac{h^3}{12\mu}, \quad (2)$$

Table 2. Program output data for various grid sizes, tilts, and truncation constants

Run No.	Grid interval	Tilt	Iterations	Truncation constant	Total load	Total flow	Pressures at grid points under sill								
							1	2	3	4	5	6	7	8	Recess 9
425	L/16	0	53	0.00001	0.1840	4.0	0				0.0871				0.1750
422	L/16		37	0.0001	0.1838		0				0.0871				0.1751
419	L/16		20 (typical)	0.001	0.1809		0				0.0875				0.1759
413	L/32		104	0.0001	0.1902		0		(typical)	0.0462	0.0726		0.1393		0.1861
410	L/32		40	0.001	0.1902		0			0.0505	0.1012		0.1523		0.2037
404	L/64		249	0.0001	0.1962		0	0.0247	0.0494	0.0741	0.0990	0.1239	0.1489	0.1740	0.1991
401	L/64		63	0.001	0.2199		0	0.0337	0.0675	0.1018	0.1367	0.1721	0.2081	0.2446	0.2812
426	L/16	0.5	52/54	0.00001	0.1379	4.0	0				0.1227				0.2324
423	L/16		36/38	0.0001	0.1377		0				0.1227				0.2325
420	L/16		20/21	0.001	0.1358		0				0.1233				0.2336
414	L/32		100/107	0.0001	0.1447		0		0.0677		0.1316		0.1921		0.2494
411	L/32		39/42	0.001	0.1430		0		0.0734		0.1427		0.2084		0.2708
405	L/64		240/260	0.0001	0.1478		0	0.0366	0.0722	0.1067	0.1403	0.1730	0.2049	0.2359	0.2661
402	L/64		63	0.001	0.1592		0	0.0490	0.0968	0.1437	0.1899	0.2356	0.2807	0.3251	0.3685
427	L/16	1.0	51/55	0.00001	0.1227	4.0	0				0.1596				0.2800
424	L/16		35/39	0.0001	0.1285		0				0.1597				0.2801
421	L/16		19/22	0.001	0.1209		0				0.1606				0.2817
415	L/32		97/110	0.0001	0.1327		0		0.0953		0.1774		0.2489		0.3113
412	L/32		39/45	0.001	0.1309		0		0.1027		0.1912		0.2683		0.3359
406	L/64		?	0.0001	0.1367		0	0.0532	0.1024	0.1482	0.1908	0.2305	0.2677	0.3025	0.3350
403	L/64		63	0.001	0.1469		0	0.0713	0.1376	0.1999	0.2587	0.3145	0.3674	0.4174	0.4645

where w is the total load, h is the film height, and μ is the viscosity.

To obtain comparable data from the digital program, a pad with a total of 40 grid points in each direction, as shown in Fig. 4, was considered.

For this arrangement,

$$M_1 = K_1 = l - a,$$

$$M_2 = K_2 = 2a,$$

$$a/l = K_2/20.$$

Eight computer runs were made based on a uniform film height, constant flow to each recess, 0.0003 truncation and the following geometric values:

Run	a	K_1, M_1	K_2/M_2	a/l
501	1	9	2	0.1
502	2	8	4	0.2
503	3	7	6	0.3
504	4	6	8	0.4
505	5	5	10	0.5
506	6	4	12	0.6
507	7	3	14	0.7
508	8	2	16	0.8

The digital program output is in the form of dimensionless load and flow coefficients:

$$W = \frac{2}{L^2(p_r - p_a)}, \quad (3)$$

$$QQ = \frac{Q \cdot 12\mu}{(p_r - p_a)c^3}, \quad (4)$$

where:

L = length in the x -direction

p_r = reference pressure (usually 1.0)

p_a = ambient pressure (usually 0)

Q = actual flow

c = units in which film height is measured

The flow and pressure coefficients equivalent to the analog data which can be developed from these are:

$$p_f = \frac{p_s/p_r}{W} \quad (5)$$

$$q_f = \frac{QQ}{W} \quad (6)$$

where P_s is the dimensionless recess pressure from the output data.

The comparison of the digital and analog results is shown in Fig. 5. The flow coefficients are almost identical while a rather significant difference exists between the pressure coefficients at the lower values of a/l .

After some discussion with H. Rippel of The Franklin Institute, who did the original analog work, further runs were made for the ratio $l/a = 2$, using various truncation

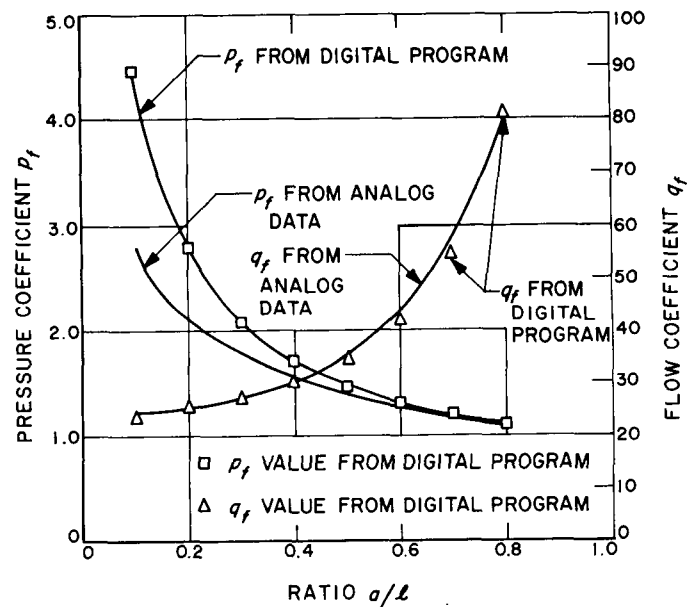


Fig. 5. Flow coefficient q_f and pressure coefficient p_f as a function of pad geometry

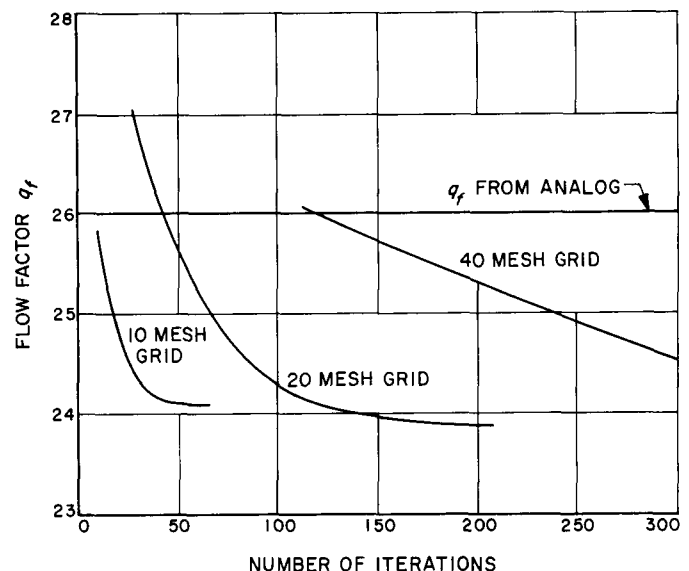


Fig. 6. Flow coefficient q_f versus number of iterations

constants and varying the grid interval from the original $L/40$ to $L/20$ and $L/10$. The resulting values of q_f , p_f and W are shown in Table 3 and are plotted as functions of the number of iterations in Figs. 6, 7, and 8. These curves offer an interesting insight into the convergence characteristic of the program.

For these cases, both the $L/10$ and $L/20$ interval runs have reasonably approached an asymptote within the allowable 300 iterations. For the $L/40$ interval runs, the W and q_f curves have not yet started to flatten out within 300 iterations, while the p_f curve is just beginning to.

Table 3. Summary of digital/analog comparison runs (5000 series)

Run No.	X-grid	Truncation constant	Iterations to converge	Total load	Q (I, I)	Sill grid point pressures						$p_f = \frac{1}{4W(I)} = p_s/W$
						$q_f = \frac{QQ}{W}$	0	$\frac{1}{4}$	$\frac{1}{2}$	$\frac{3}{4}$	Recess p_s	
5111	10	3×10^{-3}	13	0.1549	4.0829	25.82	0		0.1345		0.3243	2.095
5121	10	1×10^{-3}	23	0.1625	4.1309	24.62	0		0.1343		0.3142	1.935
5131	10	3×10^{-4}	33	0.1648	4.1406	24.27	0		0.1336		0.3112	1.890
5141	10	1×10^{-4}	43	0.1656	4.1433	24.15	0		0.1333		0.3102	1.875
5151	10	3×10^{-5}	54	0.1658	4.1441	24.13	0		0.1333		0.3099	1.869
5161	10	1×10^{-5}	63	0.1659	4.1443	24.12	0		0.1333		0.3098	1.868
5211	20	3×10^{-3}	27	0.1478	3.4133	27.06	0	(typical) 0.0739	0.1588	0.2665	0.4060	2.750
5221	20	1×10^{-3}	36	0.1507	3.5939	26.54	0	0.0720	0.1528	0.2524	0.3791	2.518
5231	20	3×10^{-4}	78	0.1619	3.7960	24.71	0	0.0684	0.1433	0.2223	0.3424	2.115
5241	20	1×10^{-4}	120	0.1658	3.8251	24.12	0	0.0675	0.1409	0.2275	0.3338	2.012
5251	20	3×10^{-5}	166	0.1672	3.8326	23.92	0	0.0671	0.1401	0.2250	0.3310	1.980
5261	20	1×10^{-5}	208	0.1675	3.8345	23.88	0	0.0670	0.1399	0.2255	0.3302	1.970
5411	40	3×10^{-3}	55	0.1777	2.2183	22.50	0	0.0875	0.2066	0.3886	0.6524	3.672
5421	40	1×10^{-3}	55	0.1777	2.2183	22.50	0	0.0875	0.2066	0.3886	0.6524	3.672
5431	40	3×10^{-4}	112	0.1534	3.2391	26.07	0	0.0756	0.1634	0.2778	0.4311	2.810
5441	40	1×10^{-4}	257	0.1610	3.6302	24.84	0	0.0694	0.1462	0.2404	0.3613	2.245
5451	40	3×10^{-5}	301	0.1630	3.6636	24.53	0	0.0687	0.1446	0.2371	0.3553	2.180
5461	40	1×10^{-5}	301	0.1630	3.6636	24.53	0	0.0687	0.1446	0.2371	0.3553	2.180

Notes:

1. Total flow = 4.0 for all cases (QQ).
2. Sill grid point pressures are along centerline of recess. 5100 series are averaged since centerline is between two grids.

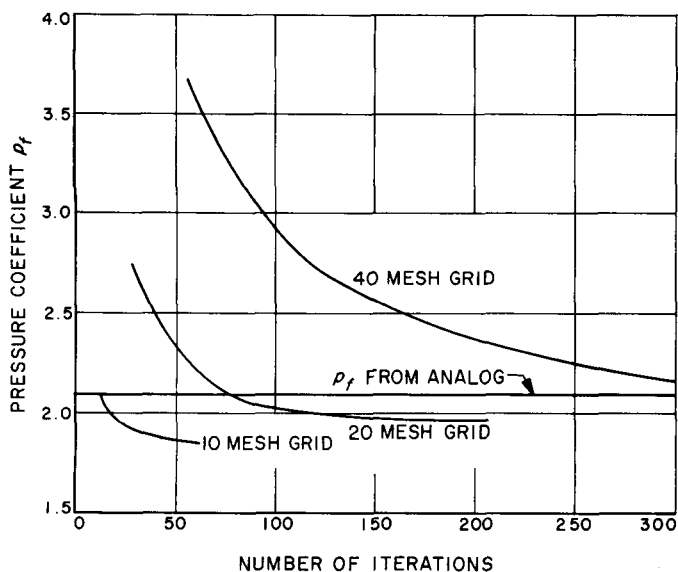


Fig. 7. Pressure coefficient p_f versus number of iterations

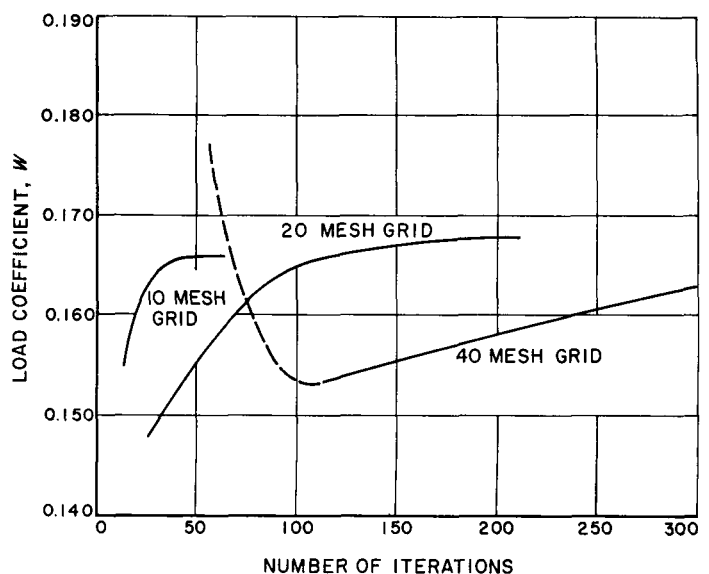


Fig. 8. Load coefficient W versus number of iterations

Oddly, with more runs, the q_f value from the digital data falls below the analog data, while the p_f values from the digital program begin to approach the analog results. From these curves it appears that, with sufficient iterations, correlation within 10% will be obtained in the values of q_f and p_f . It is also noted that larger grid intervals yield lower pressure and higher flow coefficients.

Conclusions. The following conclusions are drawn from these studies:

- (1) The correlation between digital and analog results is fair. A modification of the program to permit 1000 iterations, now in the checking stage, will permit further study of this, particularly for the smaller grid intervals.
- (2) Raising the present limit of 300 iterations is desirable for the upper limits of grid points (44×66). The program has been modified by The Franklin Institute, as noted above, to permit 1000 iterations.
- (3) The truncation constant should be related to the number of grid points, because a constant which will produce good meaning approaching an asymptote in results for a large grid interval (few points) is completely unsatisfactory for a small interval (many points). This change is included in the modification being checked out.

d. Other work. The Franklin Institute, under an extension of their original contract, is modifying the original program to include the effect of the velocity of the pad with respect to the runner. For the static case originally analyzed the Reynolds flow equation, which is solved numerically over the pad area, is in the form

$$\frac{\partial}{\partial z} \left(h^3 \frac{\partial p}{\partial x} \right) + \frac{\partial}{\partial y} \left(h^3 \frac{\partial p}{\partial y} \right) = 0. \quad (7)$$

When the relative velocity is included, this equation becomes

$$\frac{\partial}{\partial x} \left(\frac{h^3}{12\mu} \frac{\partial p}{\partial x} \right) + \frac{\partial}{\partial y} \left(\frac{h^3}{12\mu} \frac{\partial p}{\partial y} \right) = \frac{1}{2} U \frac{dh}{dx}. \quad (8)$$

Eq. (8) may be written in dimensionless form as

$$\frac{\partial}{\partial X} \left(H^3 \frac{\partial P}{\partial X} \right) + \frac{\partial}{\partial Y} \left(H^3 \frac{\partial P}{\partial Y} \right) = \frac{1}{2} \Lambda \frac{\partial H}{\partial X}, \quad (9)$$

where

$$\Lambda = \frac{6\mu v (p_r - p_a)}{c^2 l^3},$$

$$X = x/l,$$

$$Y = y/l,$$

$$H = h/c,$$

$$P = \frac{p - p_a}{p_r - p_a}$$

and

$$l = \text{length in } x\text{-direction}$$

$$c = \text{unit in which film height } h \text{ is measured}$$

$$p_a = \text{ambient pressure}$$

$$p_r = \text{reference pressure}$$

The solution of the expanded equation [Eq. (9)] consists of adding a solution for the nonhomogeneous (right-hand member) to the solution for the original homogeneous equation (at the expense of doubling computer running time). The extended program has been modified to permit 1000 iterations instead of 300, and to make certain changes in the output data presentation. The modified program is now being checked on the computer at JPL.

References

1. "STAIR (Structural Analysis Interpretive Routine)", Lincoln Laboratory, Lexington, Massachusetts.
2. Utku, S. and Barondess, S. M., "Computation of Weighted Root Mean Square of Path Length Changes Caused by the Deformations and Imperfections of Rotational Paraboloidal Antennas," Technical Memorandum No. 33-118, Jet Propulsion Laboratory, Pasadena, California.
3. Hinkle, J. G. and Castelli, V., "A Computer Solution for Hydrostatic Bearings with Variable Film Thickness," The Franklin Institute Final Technical Report, F-B2015, January 11, 1963.
4. Loeb, A. M., "Determination of the Characteristics of Hydrostatic Bearings Through the Use of the Electric Analog Field Plotter," *American Society of Lubrication Engineers Transactions*, Vol. 1, p. 1, April 1958.
5. Loeb, A. M. and Rippel, H. C., "Determination of Optimum Proportions for Hydrostatic Bearings," *American Society of Lubrication Engineers Transactions*, Vol. 1, October 1958.